MATERIALS SCIENCE

Torsional refrigeration by twisted, coiled, and supercoiled fibers

Run Wang[1]*, Shaoli Fang[2]*, Yicheng Xiao[1], Enlai Gao[2,3], Nan Jiang[2,4], Yaowang Li[5], Linlin Mou[1], Yanan Shen[1], Wubin Zhao[1], Sitong Li[1], Alexandre F. Fonseca[6], Douglas S. Galvão[6], Mengmeng Chen[1], Wenqian He[1], Kaiqing Yu[1], Hongbing Lu[7], Xuemin Wang[7,8], Dong Qian[7], Ali E. Aliev[2], Na Li[2,9], Carter S. Haines[2], Zhongsheng Liu[1], Jiuke Mu[2], Zhong Wang[2], Shougen Yin[10], Márcio D. Lima[11], Baigang An[12], Xiang Zhou[13], Zunfeng Liu[1]†, Ray H. Baughman[2]†

Higher-efficiency, lower-cost refrigeration is needed for both large- and small-scale cooling. Refrigerators using entropy changes during cycles of stretching or hydrostatic compression of a solid are possible alternatives to the vapor-compression fridges found in homes. We show that high cooling results from twist changes for twisted, coiled, or supercoiled fibers, including those of natural rubber, nickel titanium, and polyethylene fishing line. Using opposite chiralities of twist and coiling produces supercoiled natural rubber fibers and coiled fishing line fibers that cool when stretched. A demonstrated twist-based device for cooling flowing water provides high cooling energy and device efficiency. Mechanical calculations describe the axial and spring-index dependencies of twist-enhanced cooling and its origin in a phase transformation for polyethylene fibers.

Compared with conventional vapor-compression refrigerators, a solid that changes entropy when deformed could possibly provide higher efficiency; lower cost, weight, and volume; and more convenient miniaturization. An ordinary rubber band is an example, which was reported in 1805 to heat when stretched and to cool when stretch is released (*1*). Alternative materials for refrigeration are electrocaloric (*2*–*6*) and magnetocaloric (*6*, *7*), meaning they provide cooling because of changes in electric or magnetic fields, respectively. Although these solid-state cooling mechanisms have been widely investigated for diverse materials, none yet meets the performance needs for wide-scale applications. In fact, thermoelectrics are the only solid-state coolers that have been commercialized, and these coolers are expensive and have low energy conversion efficiencies.

Efficiencies of ~60% of the Carnot efficiency can be obtained for vapor-compression refrigerators (*8*, *9*), which is a mature technology that typically uses gases whose release can powerfully contribute to global warming. No alternative technology presently achieves this same efficiency. On the other hand, theoretical efficiencies of ~84% of the Carnot efficiency have been predicted for tensile deformation cycles of a NiTi shape memory alloy (*9*). Realization of close to this efficiency could have enormous consequences if the needed cycle life of vapor-compression refrigerators could be obtained, given that so much of global energy consumption goes to cooling.

Refrigeration materials that undergo cooling because of any type of mechanical deformation are called mechanocaloric, and those that cool because of changes in uniaxial stress (*5*, *6*, *9*–*15*) or hydrostatic pressure (*6*, *15*–*17*) are more specifically called elastocaloric and barocaloric, respectively (*6*). In this study, we demonstrate cooling by a change in yarn or fiber twist, which we call twistocaloric cooling. We call coolers that use twist changes for refrigeration "twist fridges."

Twist-based cooling using single natural rubber fibers

Vulcanized natural rubber (NR) fibers (*18*) (figs. S1 to S10) provide a prototypical twistocaloric material. Twisting these fibers causes coil nucleation and propagation, decreasing intercoil separation, and ultimately nucleation of supercoils (Fig. 1A). For isometric strains (i.e., constant strains during twist) of 100, 250, 300, and 450%, fracture occurs before completion of supercoiling, initiation of supercoiling, completion of coiling, and initiation of coiling, respectively. Unless otherwise stated, (i) stresses, strains, and twist densities are relative to the cross-sectional area or length of the nondeformed fiber (called the parent fiber), and (ii) a tensile strain rate of 42 cm/s and a twisting and untwisting rate of 50 turns/s were used for NR fibers having a nondeformed length of 3.0 cm. Here and elsewhere, tensile strain changes are made either while a fiber or yarn is torsionally tethered or for the nontwisted state.

Twistocaloric surface temperature changes occur inhomogeneously for coiled and supercoiled fibers. Hence, maximum and average surface temperature changes (ΔT_{max} and ΔT_{avg}, respectively) are reported. Surface temperatures were measured using a thermal camera, whose accuracy was established by comparison with thermocouple measurements in a temperature-controlled oven on fibers with different twist states (*18*).

The temperature swing on stretch and stretch release (between heating and cooling temperatures) is important for remotely optically readable strain sensors or mechanothermochromic fibers. For 300% isometric strain, this swing in surface-average temperature was 3.3°, 6.5°, and 7.7°C for highly twisted, coiled, and partially supercoiled fibers, respectively, compared with 2.4°C for a nontwisted fiber (Fig. 1B). The maximum surface temperature swing (fig. S11B) for this modest applied strain was 5.4°, 10.5°, and 12.9°C for the highly twisted, coiled, and partially supercoiled fibers, which is up to 5.4 times that for the nontwisted NR fiber. However, when released from strains >300%, nontwisted NR fibers provided greater surface cooling. Hence, these twisted NR fibers are not very useful for refrigerators that solely use large-magnitude stretch and release.

Examples of cooling by untwist are shown in Fig. 1, C to E; figs. S13 to S18; and movie S1. When twist is released from a supercoiled NR fiber having 100% isometric strain, the maximum (–15.5°C) and average (–12.4°C) surface cooling exceed that for 600% stretch release from a nontwisted fiber (–12.2°C) (Fig. 1B). By releasing twist and then stretch (Fig. 2, A and B), even higher maximum (–16.4°C) and average (–14.5°C) cooling was obtained. Hence, a twist-based cooler at 100% strain can be two-sevenths of the maximum length of the above stretch-based cooler and still provide 2.3°C higher surface-average cooling. Figure S34A and movie S2 illustrate the use of a thermochromic dye–coated NR fiber as a mechanothermochromic material whose color responds to changes in inserted twist.

The heating and cooling during stretch and stretch release of a nontwisted fiber are

[1]State Key Laboratory of Medicinal Chemical Biology, College of Pharmacy, Key Laboratory of Functional Polymer Materials, Nankai University, Tianjin 300071, China. [2]Alan G. MacDiarmid NanoTech Institute, University of Texas at Dallas, Richardson, TX 75080, USA. [3]Department of Engineering Mechanics, School of Civil Engineering, Wuhan University, Wuhan, Hubei 430072, China. [4]Shenzhen Geim Graphene Center, Tsinghua Shenzhen International Graduate School, Shenzhen 518055, China. [5]School of Life Sciences, Tsinghua University, Beijing 100084, China. [6]Applied Physics Department, State University of Campinas, Campinas, SP 13081-970, Brazil. [7]Department of Mechanical Engineering, University of Texas at Dallas, Richardson, TX 75080, USA. [8]Department of Mechanical Engineering, Georgia Southern University, Statesboro, GA 30458, USA. [9]Materials Science, MilliporeSigma, Milwaukee, WI 53209, USA. [10]Institute of Materials Physics, Tianjin University of Technology, Tianjin 300384, China. [11]Nano-Science and Technology Center, Lintec of America, Richardson, TX 75081, USA. [12]School of Chemical Engineering, University of Science and Technology Liaoning, Anshan 114051, China. [13]Department of Science, China Pharmaceutical University, Nanjing, Jiangsu 211198, China.
*These authors contributed equally to this work.
†Corresponding author. Email: ray.baughman@utdallas.edu (R.H.B.); liuzunfeng@nankai.edu.cn (Z.L.)

approximately independent of fiber diameter (fig. S11A). Also, NR fibers having different diameters but the same elongation have approximately the same dependence of ΔT_{max} and ΔT_{avg} on the product of twist density and stretched fiber diameter (fig. S17). The maximum surface cooling on twist release was essentially the same whether twist insertion was done isometrically (for constant tensile strain) or isobarically (for constant tensile load), as long as the percent stretch obtained after isometric twist release was identical (fig. S19). The NR fiber showed stable heating and cooling during isometric twisting and untwisting up to 15 turns/cm for 750 cycles (fig. S21).

Volume-average cooling for twisted NR fibers

The volume-average cooling upon untwisting a NR fiber was obtained from the cooling energy of this fiber in a water-containing plastic tube (fig. S44A). This cooling energy is the sum of the products of gravimetric heat capacity, mass, and temperature decrease for the water, plastic tube, and NR fiber after internal thermal equilibration of the system (fig. S44B). The volume-average cooling upon untwisting a NR fiber was obtained by dividing the derived cooling energy by the heat capacity and mass of the NR fiber (*18*). To minimize loss of cooling energy to surrounding air (fig. S12) by decreasing the temperature change of the water, a mass of water 4.63 times that of the NR fiber was used. This small loss of cooling energy was corrected by fitting the long-term temperature dependence of water and container to a standard heat-loss equation (*19*) and then adding these temperature corrections to the observed curves, so that the loss-corrected temperature curves reach long plateaus (*18*). The temperature changes for these plateaus were used to obtain the cooling energy and thereby the dependence of volume-average temperature change on twist density change.

Figure 1D compares the surface-average and volume-average temperature changes for isometric twist insertion and release from a 100% stretched NR fiber. For the high twist density most important for applications, where the twist removal time (1.5 s) exceeds the calculated radial thermal equilibration time (0.96 s) (*18*), the volume-average cooling is 11.3°C and the ratio of volume-average to surface-average temperatures reaches 0.91. This is consistent with nearly complete equilibration in the radial direction.

Although the maximum twistocaloric specific cooling energy obtained (19.4 J/g) is lower than reported for releasing 600% stretch from a nontwisted NR fiber (21.6 J/g) (*20*), the stretch needed for this torsional cooling is much smaller (100%). At 100% strain, stretch-based cooling would only be 4.2% of that delivered by twistocaloric cooling (*18*).

Coefficients of performance for twisted NR fibers

Using the above volume-average cooling on isometric twist release, the coefficient of performance (COP) for NR twist fridges was obtained. The COP can be described as the ratio of the cooling energy (the product of the volume-average cooling, the gravimetric heat capacity, and the mass of the fiber) to either the input mechanical energy or the net energy consumed during a mechanical cycle (called COP_{HC} and COP_{FC}, for a half cycle and a full cycle, respectively) (*6*). COP_{HC} is useful when device simplicity or miniaturization is more important than increasing efficiency by recapturing part of the input mechanical energy.

Using the stretch release–induced cooling of the nontwisted fiber (Fig. 1B), the volume-average cooling during twist release (Fig. 1D), and mechanical measurements (figs. S7 and S10B), the COPs were obtained as a function of volume-average cooling (Fig. 2C and fig.

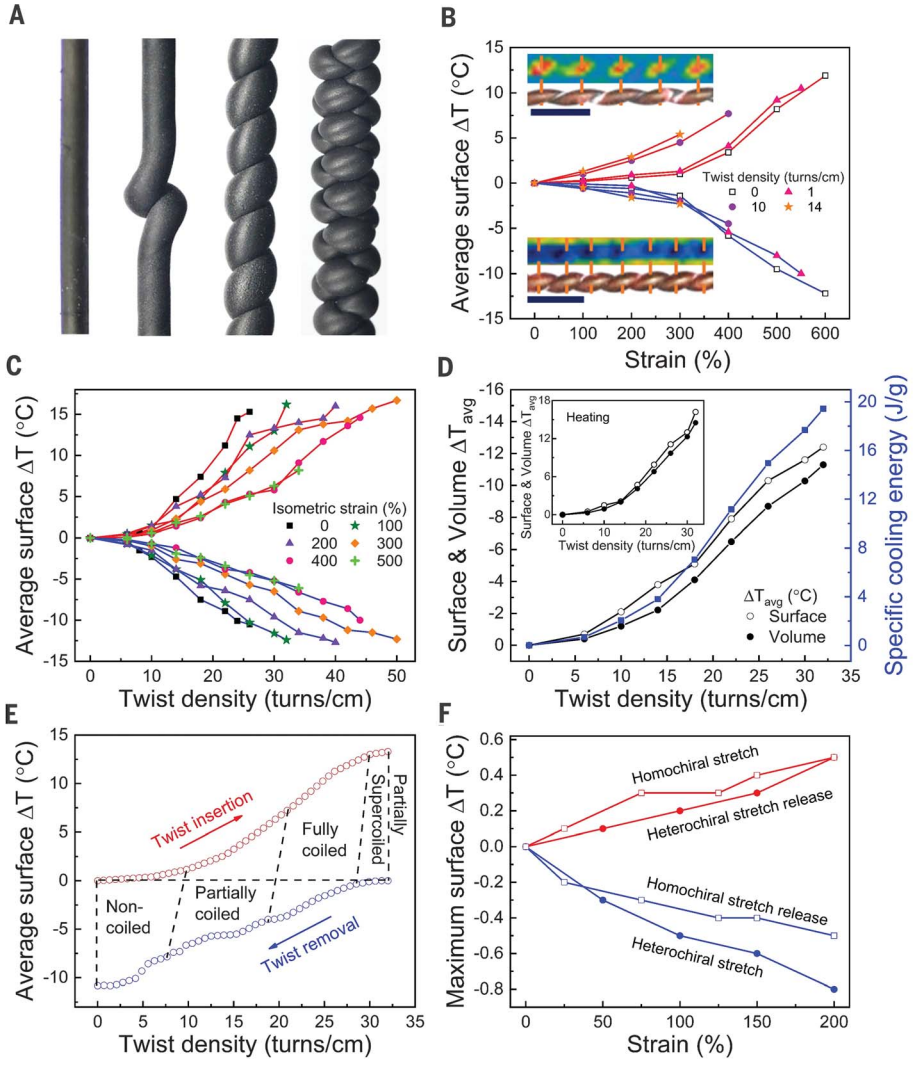

Fig. 1. Twist-based mechanocaloric performance for single rubber fibers. (**A**) Photographs of twisted, partially coiled, fully coiled, and fully supercoiled 2.5-mm-diameter NR fibers at 100% strain. The background was digitally removed. (**B**) Surface-average temperature changes versus strain for NR fibers having 0, 1, 10, and 14 turns/cm of twist (nontwisted, highly twisted, fully coiled, and partially supercoiled, respectively, in the nonstretched state). Insets show thermal and optical photographs after 100% stretch (top) and after stretch release (bottom) for a coiled NR fiber (18 turns/cm). Scale bars: 0.5 mm. (**C**) Surface-average temperature changes of a NR fiber during isometric twist and untwist at different tensile strains. (**D**) Surface-average cooling, volume-average cooling, and specific cooling energy for isometrically untwisting a NR fiber at 100% strain. Inset shows corresponding results for volume-average and surface-average heating. (**E**) Surface-average temperature changes for isometrically twisting and untwisting a NR fiber at 200% strain, when measured continuously during an increasing twist and a decreasing twist scan. (**F**) Twistocaloric temperature changes versus strain for heterochiral and homochiral coiled NR fibers. In the experiments corresponding to (B) to (F), 2.2-mm-diameter NR fibers were used.

S43). The COP_{FC} and COP_{HC} for cooling, either by twist release or by releasing twist and then stretch, are much higher than for cooling by stretch release from the nontwisted fiber when the volume-average cooling is above −0.4°C (Fig. 2C and fig. S43). For the highest volume-average cooling obtained for releasing stretch from a nontwisted fiber (−12.2°C), isometric untwist (−11.3°C), and releasing twist and then stretch (−12.1°C), the COP_{FC} values are 3.8, 8.3, and 8.5, respectively (Fig. 2C), and the COP_{HC} values are 1.9, 5.2, and 5.3, respectively (fig. S43).

The intrinsic efficiency of a material, which is the maximum theoretical efficiency for a refrigerator, is the ratio of COP_{FC} to the COP of a Carnot cycle (COP_{Carnot}). COP_{Carnot} is $T_C/(T_H - T_C)$, where T_C and T_H are the minimum and the maximum temperatures in the cycle, respectively. These material efficiencies for cooling during isometric untwisting and during releasing twist and then stretch are much higher than for cooling during stretch release from a nontwisted fiber, for both full-cycle and half-cycle processes (fig. S43, C and D). For the highest volume-average cooling for stretch release from a nontwisted fiber, isometric untwisting, and releasing twist and then stretch, the full-cycle intrinsic material efficiencies were 0.32, 0.63, and 0.67, respectively.

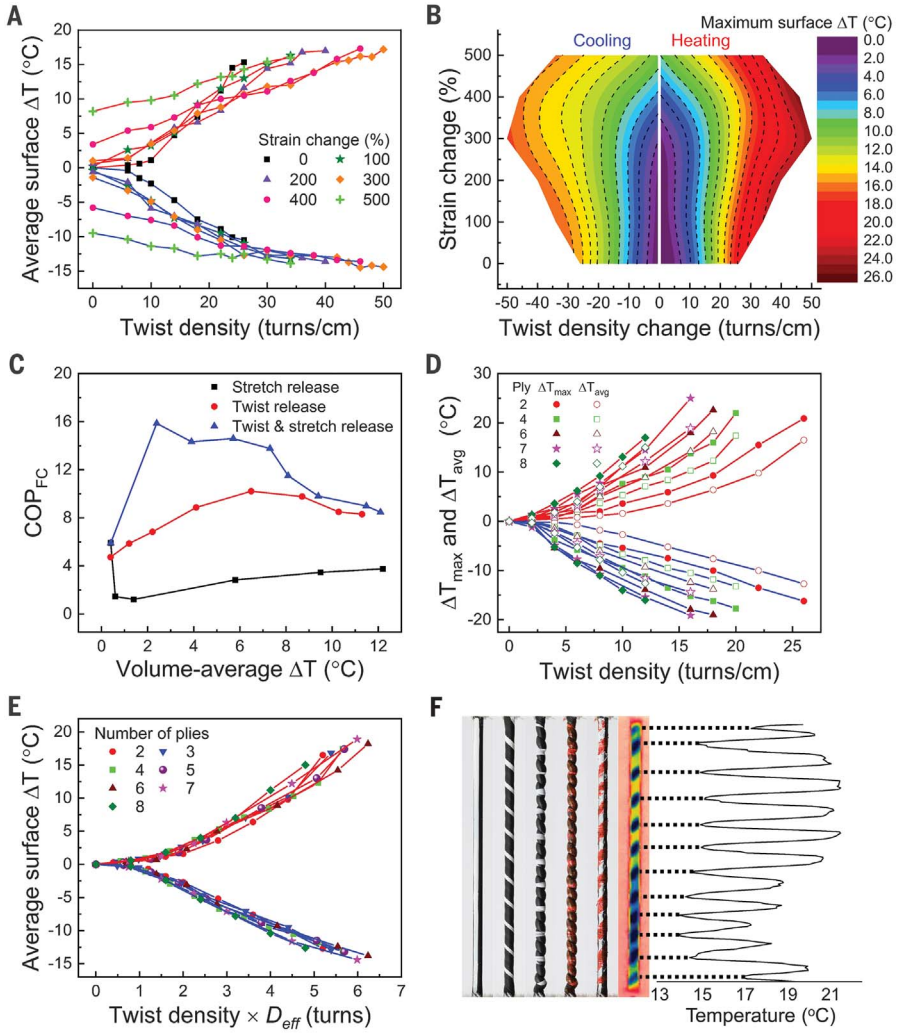

Fig. 2. Mechanocaloric performance of single and plied NR fibers during twist and stretch. (**A**) Average and (**B**) maximum surface temperature changes of a NR fiber during sequential stretch and then isometric twisting and during sequential isometric untwisting and then stretch release. (**C**) The COP_{FC} versus volume-average cooling for releasing up to 600% strain from a nontwisted fiber (black), isometric untwisting a fiber at 100% strain (red), and isometric untwisting at 100% strain followed by stretch release (blue). (**D**) The maximum and surface-average temperature changes versus twist density for plying and unplying NR fibers at 100% strain. (**E**) The surface-average temperature changes of (D) versus the product of twist density and the effective fiber diameter. In the experiments corresponding to (A) to (E), 2.2-mm-diameter NR fibers were used. (**F**) Photographs of an initially nontwisted, 3-cm-long, 3-mm-diameter NR fiber that was (from left to right) stretched to 100% and painted with a white line along its length; highly twisted; fully coiled; painted red on the coil's exterior; and then fully untwisted. The thermal image and temperature profile (right) show the fiber immediately after removing 12 turns/cm of inserted twist.

Twist-based cooling by plying NR fibers

To demonstrate scalability, cooling was measured while isometrically unplying multiple NR fibers. Unplying seven-ply 2.2-mm-diameter NR fibers (Fig. 2, D and E) produced higher maximum (−19.1°C) and average (−14.4°C) surface cooling than for 600% stretch release from a nontwisted fiber (−12.2°C) (Fig. 1B) or for isometric untwisting of a 100% stretched single fiber (−15.5°C maximum and −12.4°C average) (Fig. 1C and fig. S15). Unplying from isometric strains around 100% produced the highest twistocaloric cooling (figs. S23 and S24).

Guided by the correspondence between twistocaloric cooling for single fibers having the same stretch, and a similar product of twist density and stretched fiber diameter (fig. S17), we found that the twistocaloric cooling associated with isometric fiber plying approximately depends on the product of the twist density of plying and the effective diameter of the bundle ($D_{eff} = n^{0.5} \times D_s$, where n is the number of fibers and D_s is the stretched fiber diameter) (Fig. 2E).

Spatial and temporal dependencies of twistocaloric temperature changes for NR fibers

Spatially complex surface temperature changes occur for twistocaloric processes for coiled or supercoiled fibers (Fig. 2F and fig. S20). Like for a bent cantilever, the inside of a coiled fiber is compressed and the outside is stretched, causing the coil's exterior to undergo the highest temperature change during coil formation and removal. Painting the exterior of a coiled fiber enabled demonstration that these maximum strained regions have the highest cooling after fiber untwisting. The periodicity of these regions on the surface of the untwisted fiber (5.6 mm) is much longer than the average coil period of the fully coiled fiber (2.5 mm).

The peak surface cooling increases with increasing distance from the site where coiling nucleates (fig. S20), because coiling stretches noncoiled fiber regions and thereby decreases the spring index (the ratio of the average coil diameter to the diameter of the fiber within the coil) of later-introduced coils. The sharp change in maximum surface cooling upon complete removal of coiling (fig. S17A) disappears when measuring average cooling (fig. S17B), indicating that the effects of bending approximately average to zero. Because the number of coils is strain invariant, the separations between temperature peaks during both stretching and releasing are identical to the intercoil separations (Fig. 1B, inset).

Twistocaloric cooling by self-coiled polyethylene and nylon fibers

Twistocaloric cooling was also investigated for polymers used for fishing line and sewing thread. These polymers were made elastically deformable by isobarically twisting until the fiber coils, as is done to make powerful thermally driven artificial muscles (*21*). These self-coiled fibers are called homochiral because fiber twist and coiling have the same handedness.

Initial experiments used 0.41-mm-diameter, 65-pound test, braided polyethylene (PE) fishing line (fig. S25A). Spring indices from 1.4 to 0.5 were obtained by inserting 6.5 to 7.3 turns/cm of twist under isobaric loads of 37.1 to 74.2 MPa, respectively. When releasing 22.7% strain, maximum and average surface cooling of −5.1°C and −3.2°C, respectively, were obtained for a spring index of 0.8 (Fig. 3A and fig. S25). For comparison, the temperature change upon stretch release of nontwisted polyethylene yarn was below ±0.1°C, and the highest reported elastocaloric cooling for a nonelastomeric polymer is −2.5°C for a poly(vinylidene fluoride-trifluoroethylene-chlorotrifluoroethylene) terpolymer (*15*), which is a relaxor ferroelectric (*2*).

The highest temperature swing between maximum heating and cooling (12.9°C, for a spring index of 0.8) was obtained for 22.7% stretch and stretch release, which is a much higher per-strain change (0.57°C per percent) than for a nontwisted NR fiber (0.04°C per percent for 600% strain). This high sensitivity is useful for mechanothermochromic indicators (movie S3). No degradation in performance occurred during the investigated 2500 stretch-release cycles to 13% strain (fig. S26). The twistocaloric cooling for self-coiled, high-strength polyethylene yarn at 10°C ambient temperature is smaller than for ambient temperatures of 25° and 40°C (fig. S25). In contrast, the stretch-release–induced cooling for a nontwisted NR fiber at 10°C is higher than for either higher or lower ambient temperatures (*22*).

Twistocaloric cooling was also observed during stretch release for coiled, single-filament nylon 6 fishing line with parent diameters (*D*) of 0.2, 0.4, and 0.6 mm. To ensure the same spring index (1.0), these fibers were coiled using the same isobaric stress and the same twist number (twist density times *D*). These homochiral fibers, having progressively larger diameters, provided progressively increasing maximum cooling (−1.3°, −1.9°, and −2.1°C) and average cooling (−0.8°, −1.2°, and −1.8°C) upon stretch release (fig. S28).

The strain dependence of twistocaloric cooling generally increases with decreasing spring index for coiled, high-strength polyethylene yarn (fig. S25), low-strength polyethylene (fig. S27), and nylon 6 fibers (fig. S28). Similarly, for coiled polymer muscles (*21*), higher heating is needed to cause a given stroke for a smaller spring-index muscle. The origin in both cases is the stretch-induced twist change per fiber length, whose magnitude is spring-index dependent.

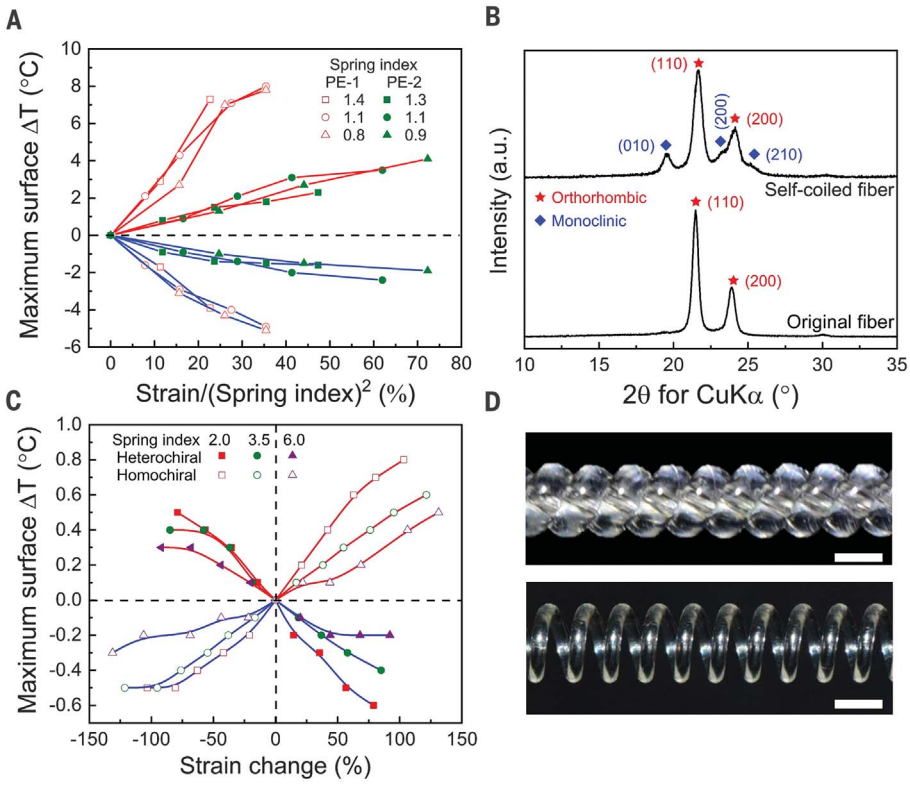

Fig. 3. Twistocaloric performance for coiled polyethylene and nylon 6. (**A**) The maximum changes in surface temperature versus the ratio of tensile strain to the square of spring index, for high-strength and low-strength polyethylene fibers (PE-1 and PE-2, respectively). (**B**) XRD for nontwisted and self-coiled PE-1 fibers. (**C**) Twistocaloric temperature changes versus strain for homochiral and heterochiral coiled nylon 6 fibers having different spring indices. (**D**) Optical images of a self-coiled, 0.6-mm-diameter nylon 6 fiber (top) and a thermally annealed (180°C for 1 hour), mandrel-coiled, 0.6-mm-diameter nylon 6 fiber (bottom). Scale bars: 1.0 mm (top) and 2.0 mm (bottom).

Theoretical results (*18*) (fig. S39) show that the stretch-induced twist change per fiber length, divided by the percent stretch of a coiled fiber, should approximately depend on the inverse square of spring index. This dependence arises because both the strain needed to pull out one coil and the fiber length per coil linearly increase with coil diameter. In agreement, the observed twistocaloric temperature changes for self-coiled polyethylene and nylon 6 fibers or yarns are approximately proportional to the ratio of percent stretch to the square of the spring index (Fig. 3A and fig. S40). This dependency is predicted only for the case where different-spring-index yarns have approximately the same initial coil bias angle. Owing to the difficulty of controlling this coil bias angle for later-described mandrel-coiled fibers, deviations from these theoretical results are observed.

Origin of twistocaloric cooling of polyethylene fibers

Because the above polyethylene and nylon 6 fibers are crystalline, it is challenging to explain the origin of the entropy decrease caused by stretching the coiled fiber. One possible explanation for polyethylene is the known deformation-driven orthorhombic-to-monoclinic phase conversion (fig. S41) (*23*–*26*). Using molecular dynamics calculations at 300 K (*18*), we predict that the entropy of the orthorhombic phase is 0.097 J K^{-1} g^{-1} higher than for the monoclinic phase, which agrees with the entropy difference calculated more than 30 years ago (*26*) from vibrational spectra (~0.12 J $K^{-1}g^{-1}$). Our predicted free energy difference resulting from this entropy change (29.1 J/g) and the specific heat capacity (*27*) of polyethylene (1.56 J $K^{-1}g^{-1}$) provides a predicted −18.7°C cooling if coil stretch caused complete conversion from the orthorhombic to monoclinic phase.

X-ray diffraction (XRD) measurements for polyethylene show that self-coiling results in partial conversion of orthorhombic to monoclinic phase. Thermally annealing the coiled yarn (120°C for 2 hours) largely reverses this transformation (Fig. 3B and fig. S42B) but barely affects twistocaloric cooling (fig. S42A). Stretching the coiled yarn to 20% strain reversibly increases the amount of monoclinic phase from 5.0 to 11.4% (table S2). Using this

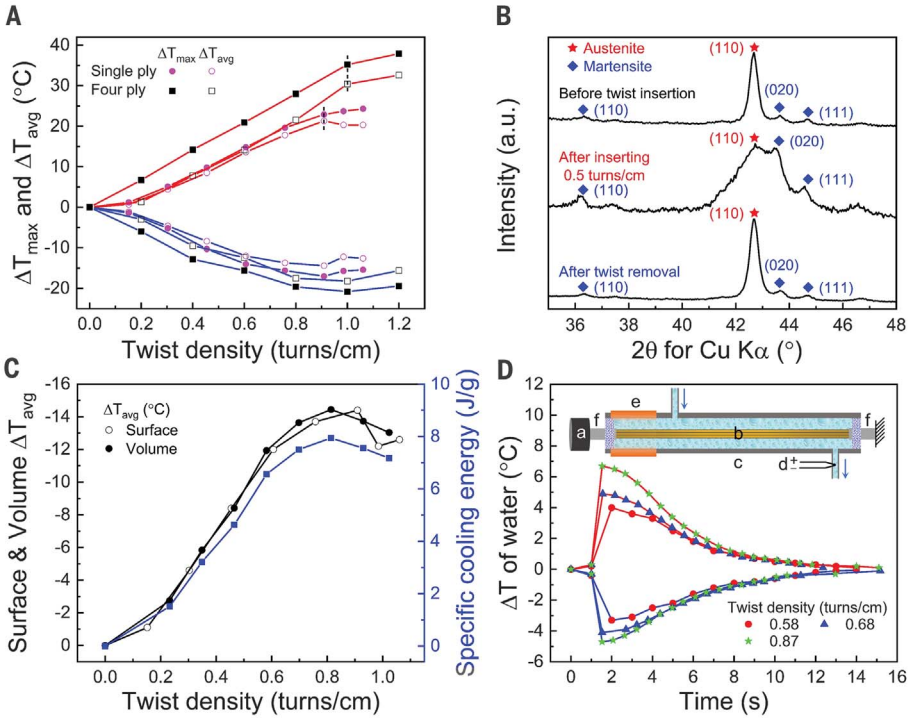

Fig. 4. Twistocaloric performance for twisted and plied NiTi wires. (**A**) The twist-induced maximum and surface-average temperature changes for a single NiTi wire and four-ply wires at 0% nominal strain. The dashed vertical lines indicate where buckling occurs. (**B**) XRD for a NiTi wire before twist insertion, after twist insertion, and after twist removal. (**C**) Surface-average cooling, volume-average cooling, and specific cooling energy for untwisting a 0.7-mm-diameter NiTi wire at 0% strain. (**D**) The time dependence of outlet water temperature change after isometric twist insertion and twist removal for a three-ply, 0.6-mm-diameter NiTi wire at a water flow rate of 0.04 ml/min using the device in the inset. This device contains (a) a motor, (b) NiTi wires, (c) a polypropylene tube containing flowing water, (d) a thermocouple, (e) a rubber tube, and (f) epoxy resin that seals the tube ends.

percent change of monoclinic phase and the −18.7°C cooling for 100% orthorhombic-to-monoclinic phase conversion, a volume-average cooling of −1.2°C is predicted for 20% strain release, which is identical to the measured surface-average cooling for this strain release. This suggests that monoclinic-to-orthorhombic phase conversion substantially contributes to twistocaloric cooling. The entropy change contribution from the amorphous phase is apparently small, which is consistent with the negligible change in amorphous scattering profile and with the unchanged ratio of the integrated diffraction intensity of the amorphous phase to the total diffraction intensity for the crystalline phases (from 0.49 to 0.50 during 20% stretch).

Twistocaloric cooling by stretching heterochiral fibers

Whereas stretch increases fiber twist for a homochiral coil, stretch causes fiber untwist for a heterochiral coil, which enables reversal of the temperature changes produced by stretch and stretch release. A heterochiral NR coil was made by wrapping a self-coiled 2.2-mm-diameter NR fiber onto a mandrel to provide a spring index of 2.5 (*18*). This mandrel was retained during twistocaloric measurements to prevent twist cancellation in the rubber fiber.

This heterochiral NR coil provides an inverse mechanocaloric effect. For 200% strain, the maximum surface cooling during stretch was −0.8°C, and the maximum surface heating upon stretch release was +0.5°C (Fig. 1F and fig. S22A). For comparison, stretching and releasing the same strain from an identical spring index homochiral coil caused maximum surface temperature changes of +0.5° and −0.5°C, respectively (Fig. 1F and fig. S22B).

An inverse twistocaloric effect was also found for heterochiral coils of nylon 6 and polyethylene, which can be thermally set to maintain their coiled shape without retention of a mandrel. Stretching heterochiral coils of nylon 6 and polyethylene, with spring indices of 2.0, induces cooling of −0.6° and −0.3°C, respectively, and stretch release produces heating of +0.5° and +0.5°C, respectively (Fig. 3C and figs. S31 and S32). For comparison, stretching identical spring index homochiral coils of nylon 6 and polyethylene produces a maximum heating of +0.8° and +1.4°C, respectively, and stretch release produces a maximum cooling of −0.5° and −0.6°C, respectively (Fig. 3C and figs. S29 and S30). When a heterochiral nylon 6 fiber was stretched to 90%, which is beyond the coil's yield stress, the coil irreversibly deformed to form segments having short (1.0 mm) and long (2.8 mm) intercoil periods, which cooled and heated during stretch, respectively (fig. S33).

Twistocaloric cooling by twisting and plying NiTi wires

Large, reversible temperature changes also result from twist insertion and removal from a single NiTi shape memory wire, and from plying and unplying these wires. The investigated 0.7-mm-diameter $Ni_{52.6}Ti_{47.4}$ wires had a martensite-to-austenite transition from −29.0° to 15.0°C during heating, and an austenite-to-martensite transition from 13.5° to −44.6°C during cooling (fig. S35B).

Twistocaloric cooling resulted from isometrically untwisting a single NiTi wire (−17.0°C maximum and −14.4°C average surface temperature changes) at 0% strain and at a twist rate of 50 turns/s (Fig. 4A and figs. S36 and S37). Unplying a four-ply bundle of NiTi wires produced even higher cooling (−20.8°C maximum and −18.2°C average surface temperature changes), compared with the −17.0°C elastocaloric cooling provided by an identical NiTi wire (table S1). This twistocaloric cooling was stable over 1000 cycles of twisting and untwisting up to 0.6 turns/cm (fig. S38). XRD results demonstrate reversible austenite-to-martensite conversion during twisting and untwisting a NiTi wire (Fig. 4B). Because this conversion is incomplete, there is an opportunity to increase twist-induced cooling by optimizing the NiTi composition and the operating temperature range of the cooler.

The calculated time for internal thermal equilibration of a 0.7-mm-diameter NiTi wire was 2.5 ms (*18*), which is much faster than the untwist process at 15 turns/s (65 to 455 ms). In agreement, the optically measured surface-average cooling upon untwisting a NiTi wire is close to the volume-average cooling (Fig. 4C) derived from the calorimetric specific cooling energy of this wire (*18*) (fig. S45). The anomalous behavior at very high twist, where cooling slightly decreases, is likely due to the onset of wire buckling. The maximum specific cooling energy (7.9 J/g) for untwisting the NiTi wire (Fig. 4C) is similar to literature results for stretch-released NiTi wires and sheets (5.0 to 9.4 J/g) and for stretch release of the present wires (9.4 J/g) (*18*).

A device that enabled one cycle of refrigeration was demonstrated for the cooling of a stream of water (Fig. 4D and figs. S46 and S47). Flowing ambient-temperature water over a three-ply NiTi wire cable, while removing 0.87 turns/cm of plying, cooled the water by

up to −4.7°C; higher water cooling (−7.7°C) resulted from adding thermal insulation, increasing the water channel diameter, and increasing the water flow rate (*18*). Integrating the cooling until the water stream returned to ambient temperature provided a specific cooling energy of 6.75 J/g (table S3), indicating that much of the cooling energy of the NiTi wire has effectively chilled the water. The twist-produced temperature changes of a thermochromic paint–coated NiTi wire provided visible indication of torsional rotation (fig. S34B and movie S4).

Summary

Twist release from fibers or fiber plies resulted in high cooling for materials as different as NR and NiTi. The material cooling efficiency was doubled (to 65%) and cooler length was reduced by a factor of two-sevenths by replacing elastocaloric cooling by twistocaloric cooling for NR fibers. A NiTi-based twist-fridge cooled flowing water by up to −7.7°C in one cycle.

Twist induced by stretch release from coiled polyethylene fishing line resulted in surface cooling that was more than 50 times higher than that obtained by releasing stretching from the nontwisted fiber. Depending on the relative chiralities of fiber and coil, polymers were engineered to cool either during stretch or stretch release. The spatial periodicity of surface temperature changes of coiled fibers can be an asset for remotely readable tensile and torsional strain sensors and for color-changing fibers for fabrics that dynamically respond to body movement.

REFERENCES AND NOTES

1. J. Gough, *Mem. Lit. Phil. Soc. Manchester 1 (2nd Series)* **288**, 288–295 (1805).
2. R. Ma *et al.*, *Science* **357**, 1130–1134 (2017).
3. B. Neese *et al.*, *Science* **321**, 821–823 (2008).
4. E. Defay *et al.*, *Nat. Commun.* **9**, 1827 (2018).
5. M. Trček *et al.*, *Philos. Trans. R. Soc. London Ser. A* **374**, 20150301 (2016).
6. X. Moya, S. Kar-Narayan, N. D. Mathur, *Nat. Mater.* **13**, 439–450 (2014).
7. T. Gottschall *et al.*, *Nat. Mater.* **17**, 929–934 (2018).
8. A. Chauhan, S. Patel, R. Vaish, C. R. Bowen, *MRS Energy Sustain.* **2**, E16 (2015).
9. J. Cui *et al.*, *Appl. Phys. Lett.* **101**, 073904 (2012).
10. J. Tušek, K. Engelbrecht, L. P. Mikkelsen, N. Pryds, *J. Appl. Phys.* **117**, 124901 (2015).
11. J. Tušek *et al.*, *Nat. Energy* **1**, 16134 (2016).
12. Y. Liu *et al.*, *Adv. Mater.* **26**, 6132–6137 (2014).
13. Y. Li *et al.*, *ACS Appl. Mater. Interfaces* **10**, 25438–25445 (2018).
14. S. Qian *et al.*, *Philos. Trans. R. Soc. London Ser. A* **374**, 20150309 (2016).
15. Y. Yoshida, K. Yuse, D. Guyomar, J. F. Capsal, G. Sebald, *Appl. Phys. Lett.* **108**, 242904 (2016).
16. I. Takeuchi, K. Sandeman, *Phys. Today* **68**, 48–54 (2015).
17. A. M. G. Carvalho, W. Imamura, E. O. Usuda, N. M. Bom, *Eur. Polym. J.* **99**, 212–221 (2018).
18. Materials and methods are available as supplementary materials.
19. T. L. Bergman, F. P. Incropera, D. P. DeWitt, A. S. Lavine, *Fundamentals of Heat and Mass Transfer* (Wiley, ed. 7, 2011).
20. S. L. Dart, R. L. Anthony, E. Guth, *Ind. Eng. Chem.* **34**, 1340–1342 (1942).
21. C. S. Haines *et al.*, *Science* **343**, 868–872 (2014).
22. Z. Xie, G. Sebald, D. Guyomar, *Phys. Lett. A* **381**, 2112–2116 (2017).
23. R. J. Young, P. B. Bowden, *Philos. Mag.* **29**, 1061–1073 (1974).
24. P. A. T. Olsson *et al.*, *Phys. Rev. Mater.* **2**, 075602 (2018).
25. R. Androsch, M. L. Di Lorenzo, C. Schick, B. Wunderlich, *Polymer* **51**, 4639–4662 (2010).
26. H. Tadokoro, *Polymer* **25**, 147–164 (1984).
27. Y. Jin, B. Wunderlich, *J. Phys. Chem.* **95**, 9000–9007 (1991).

ACKNOWLEDGMENTS

Funding: Support from China was provided by the National Key Research and Development Program of China (grant 2017YFB0307000), the National Natural Science Foundation of China (grants U1533122 and 51773094), the Natural Science Foundation of Tianjin (grant 18JCZDJC36800), the Science Foundation for Distinguished Young Scholars of Tianjin (grant 18JCJQJC46600), the Fundamental Research Funds for the Central Universities (grant 63171219), and the State Key Laboratory for Modification of Chemical Fibers and Polymer Materials, Donghua University (grant LK1704). A.F.F. and D.S.G are fellows of the Brazilian Agency CNPq (grants 311587/2018-6 and 307331/2014-8, respectively) and acknowledge support from São Paulo Research Foundation (FAPESP) (grants 2018/02992-4 and FAPESP/CEPID 2013/08293-7, respectively). Support at the University of Texas at Dallas was provided by the Air Force Office of Scientific Research grant FA9550-18-1-0510, the Robert A. Welch Foundation grant AT-0029, the National Science Foundation (grants CMMI-1661246, CMMI-1636306, CMMI-1726435, and CMMI-1727960), and the Louis Beecherl Jr. Endowed Chair. **Author contributions:** R.W., S.F., Zu.L., and R.H.B. conceived of and initiated the project. All authors contributed to experimental design, planning, and execution; data analysis; and manuscript writing. E.G., A.F.F., D.S.G., H.L., X.W., D.Q., and R.H.B. did the theory. **Competing interests:** R.W., S.F., A.E.A., N.L., C.S.H., M.D.L., J.M., Z.W., Zu.L., and R.H.B. are listed as the inventors on a provisional U.S. patent application (patent filing no. 62/909,018) describing twistocaloric coolers. **Data and materials availability:** All data needed to evaluate the conclusions in the paper are present in the paper or the supplementary materials.

SUPPLEMENTARY MATERIALS

science.sciencemag.org/content/366/6462/216/suppl/DC1
Materials and Methods
Supplementary Text
Figs. S1 to S47
Tables S1 to S3
References (*28*–*41*)
Movies S1 to S4

8 April 2019; accepted 18 September 2019
10.1126/science.aax6182

Science

Torsional refrigeration by twisted, coiled, and supercoiled fibers

Run Wang, Shaoli Fang, Yicheng Xiao, Enlai Gao, Nan Jiang, Yaowang Li, Linlin Mou, Yanan Shen, Wubin Zhao, Sitong Li, Alexandre F. Fonseca, Douglas S. Galvão, Mengmeng Chen, Wenqian He, Kaiqing Yu, Hongbing Lu, Xuemin Wang, Dong Qian, Ali E. Aliev, Na Li, Carter S. Haines, Zhongsheng Liu, Jiuke Mu, Zhong Wang, Shougen Yin, Márcio D. Lima, Baigang An, Xiang Zhou, Zunfeng Liu and Ray H. Baughman

Science **366** (6462), 216-221.
DOI: 10.1126/science.aax6182

Twisting is cool

Rubber bands that are stretched and held in an extended shape for a while will extract heat from their surroundings as they are allowed to relax, owing to a reversal of stress-induced crystallization, which is an exothermic process. Wang *et al.* examine the potential for solid-state cooling of twisted fibers, along with configurations such as supercoiling, for materials including natural rubber, polyethylene, and nickel-titanium fibers. The cooling is related to the change in entropy of the material as it is mechanically deformed.

Science, this issue p. 216

science.sciencemag.org/content/366/6462/216/suppl/DC1

Supplementary Materials for

Torsional refrigeration by twisted, coiled, and supercoiled fibers

Run Wang*, Shaoli Fang*, Yicheng Xiao, Enlai Gao, Nan Jiang, Yaowang Li, Linlin Mou, Yanan Shen, Wubin Zhao, Sitong Li, Alexandre F. Fonseca, Douglas S. Galvão, Mengmeng Chen, Wenqian He, Kaiqing Yu, Hongbing Lu, Xuemin Wang, Dong Qian, Ali E. Aliev, Na Li, Carter S. Haines, Zhongsheng Liu, Jiuke Mu, Zhong Wang, Shougen Yin, Márcio D. Lima, Baigang An, Xiang Zhou, Zunfeng Liu†, Ray H. Baughman†

*These authors contributed equally to this work.
†Corresponding author. Email: ray.baughman@utdallas.edu (R.H.B.); liuzunfeng@nankai.edu.cn (Z.L.)

Published 11 October 2019, *Science* **366**, 216 (2019)
DOI: 10.1126/science.aax6182

This PDF file includes:

Other Supplementary Material for this manuscript includes the following:
(available at science.sciencemag.org/content/366/6462/216/suppl/DC1)

Movies S1 to S4 (.mov)

Table of Contents

Materials and Methods

1. Fibers used for twistocaloric coolers

Because of their convenient availability and attractive performance as materials for twistocaloric coolers, the present work on elastomers primarily exploited vulcanized natural rubber (NR) fibers purchased from Tianjin Zhixin Rubber Products Co., Ltd. The used solid NR fibers had diameters of 2.0, 2.2, 3.0, 4.0, 5.0, and 7.0 mm. According to this supplier, these vulcanized rubbers were made by curing the following relative gravimetric chemical amounts at 160°C for 30 minutes: natural rubber (100); stearic acid (2); zinc oxide (5); an antioxidant, N-(1,3-dimethylbutyl)-N'-phenyl-p-phenylenediamine (1); sulfur (1.2); and an accelerator, N-cyclohexyl-2-benzothiazole sulfonamide (1.2). Although the black colored fibers contained about 2 wt% carbon black, no significant effect of this additive on mechanocaloric performance was observed. In order to ensure highly reversible elasticity to high strains, the commercially purchased NR fibers were trained at the beginning of experiments by ~10 cyclic deformations to 600% strain.

Other commercially available elastomeric fibers evaluated as twistocaloric coolers include styrene-ethylene-butadiene-styrene copolymer (SEBS, Kraton Co., Ltd.), ethylene propylene diene monomer rubber (EPDM, Wuxi PLK Seal Material Co., Ltd.), Spandex (20D, Huafeng Spandex Co., Ltd.), thermoplastic polyurethane (TPU, Zhejiang Shengli Pioneer Line Co., Ltd.), and polydimethylsiloxane (PDMS, Hangzhou Bald Advanced Materials Co., Ltd.). The SEBS elastomer was evaluated as a composite that contained 83% liquid wax (Liquid Wax #5 from ExxonMobil). Other materials investigated for twistocaloric coolers include nickel titanium (NiTi) wire (Baohong Metal Material Co., Ltd.), ultra-high-molecular-weight polyethylene fishing line (high-strength polyethylene yarn, 65 lb, Power Pro., Innovative Textiles, Inc.), monofilament polyethylene fishing line (low-strength polyethylene fiber, Nantong Ntec Monofilament Technology Co., Ltd.), and nylon 6 fishing line (STRONG & STRETCHY Model 0.2, 0.4 and 0.6 from Crystal String). Table S1 compares the maximum and average surface temperature changes during isometric twist insertion and twist removal at 0% strain and during stretch and stretch release of non-twisted fibers. Higher cooling resulted from combining stretch release and twist release.

In some experiments, a thermochromic paint was coated on a single NR fiber and NiTi wire to provide visual indication of the twistocaloric temperature changes that occur during twist insertion and twist removal. This paint comprised a thermochromic dye mixture in a rubber binder (5 wt% plasticized SEBS, comprising 14% SEBS and 86% liquid wax, that was dissolved in 95 wt% cyclohexane). For the NiTi wires, the selected paint composition changes color from orange to yellow at 31°C and from orange to dark green at 15°C. At room temperature, the thermochromic layer is orange, after twist-induced heating it is yellow, after equilibration to room temperature it becomes orange, after twist-induced cooling it is dark green, and it returns to orange after equilibration to room temperature. This thermochromic paint contains dyes: Orange-Yellow 31 mixed with Green-Yellow 15 (from Jinhua Lijin Technology Co., Ltd.). For the NR fibers, the selected paint composition changes color from orange to yellow at 22°C and from orange to dark green at 15°C. This thermochromic paint contains dyes: Orange-Yellow 22, mixed with Green-Yellow 15 (from Jinhua Lijin Technology Co., Ltd.).

In another experiment, a thermochromic paint (cholesteric liquid crystal, Shenzhen Color Technology Co., Ltd.) was coated on a high-strength, self-coiled polyethylene fishing line to provide visual indication of the twistocaloric temperature changes that occur during stretch and stretch release. This paint has a cholesteric thermochromic range from 21 to 26°C, during which

it provides the following color changes: red (21°C), orange (22°C), yellow (23°C), green (24°C), blue (25°C), and purple (26°C).

2. Spectroscopic and thermal analysis of natural rubber fibers

Fourier transform infrared (FTIR) spectra were obtained using a Bruker Tensor 37 FTIR spectrometer. In the FTIR spectra of a NR fiber (Fig. S1), strong asymmetric and symmetric stretching of methylene groups were observed near 2911 and 2844 cm^{-1}, respectively, and the stretching mode of methyl groups ($-CH_3$) occurred at ~2956 cm^{-1}. The band at 1083 cm^{-1} is attributed to symmetrical stretching vibrations in the two C−S bonds in C−S−C groups (*28, 29*).

Thermogravimetric analysis (TGA) curves for the NR fibers (Fig. S2) were obtained using a thermogravimetric analyzer (Netzsch model TG209). These results show that the NRs are stable with respect to weight loss at a scan rate of 20°C/min until ~350°C. The TGA measurements for carbon-black-containing NR samples show that the weight percent of carbon black is below 2.0%.

The heat capacities of NR fibers were measured using a differential scanning calorimeter (DSC, model Q2000–V24.1, TA Instruments Inc.). The quasi-isothermal modulated DSC mode was applied for precise control of heat flow and for measurement of the glass transition temperature (–65°C). Figure S3 shows the heat capacity of a 2.2-mm-diameter NR fiber that was measured between −20°C and +50°C. The obtained heat capacity at 25°C was 1.72 ± 0.1 $JK^{-1}g^{-1}$.

Elemental analysis of the NR fibers were obtained using an elemental analyzer model vario EL cube (Elementar). The weight percentages of C, H, N and S in the carbon-black-containing NR fibers were 85.30%, 12.60%, 0.53%, and 1.10%, respectively.

3. Fabrication of twistocaloric coolers

Twistocaloric coolers were made by inserting twist either isobarically (meaning under constant load) or isometrically (meaning at constant length). An eighty-step servo motor (#80AEA07530-SC3, Huatian Technology Co., Ltd.) was used for twist insertion, since it provided reliable output of the degree of twist insertion. During isobaric twist insertion, the fiber was vertically suspended with a twist-inserting motor providing the top support, with a weight attached to its bottom end, and a bar at fiber bottom contacting pins to prevent end rotation.

Twist was inserted isometrically or isobarically until a desired twisted state was obtained, which was one in which the fiber was either below the twist level needed to produce coiling, at a twist level that produced partial or complete coiling, or at the very high twist level that caused coils to coil upon themselves to produce supercoiled fibers. Some of these configurations were not obtainable for all fiber types due to fiber rupture at a high twist level. Unless otherwise indicated, twist density is normalized with respect to the length of the non-twisted, non-stretched fiber.

When starting from the same diameter precursor fiber, inserting a given amount of twist will produce either a twisted fiber, a partially coiled fiber, a fully coiled fiber, or a partially supercoiled fiber depending upon whether the applied load is low or high. Use of a high load stabilizes the non-coiled state or partially coiled state. Reducing the applied load on a fiber after twist insertion can transform a twisted fiber to a partially or fully coiled fiber. Similarly, increasing the applied load on a partially or fully supercoiled fiber can result in a coiled fiber. As another complication, these transformations are hysteretic: the fiber structure obtained by inserting T_w twist and removing ΔT_w twist is not generally identical to the structure obtained if the initially inserted twist were $T_w - \Delta T_w$.

4. Characterization methods for fiber mechanical properties

Tensile stress-strain curves for non-twisted, twisted, partially coiled, fully coiled and partially supercoiled NR fibers that were torsionally tethered were measured on an Instron 5566 machine.

Here and elsewhere, unless otherwise indicated, stresses (σ) are nominal values that were obtained by normalizing the applied force to the cross-sectional area of a non-twisted and non-stretched fiber. In other important examples, we use measured forces and the weight per initial length of the fiber to derive gravimetric stresses.

The apparatus illustrated in Fig. S4 was used to measure the torque of a NR fiber during isometric twist insertion and twist removal. Torque was applied to a 2.2-mm-diameter NR fiber by attaching it to a 3.0-mm-diameter axle (which was supported by two metal bearings), around which a fiber holding the load "d" was wrapped. The load was placed on a balance, so that the force used for applying the torque to the 3.0-mm-diameter axle was the difference between the weight of the load and the reading recorded by the balance. Twist insertion increased this difference and twist removal decreased it. Hence, electronically outputted readings from the balance enabled torque measurements. Several cycles of twist insertion and twist removal were performed until reversible readings from the balance were obtained.

5. Characterization methods for mechanocaloric cooling

Five kinds of mechanical deformations were applied to a fiber in order to characterize twistocaloric cooling: 1) isometric twist, followed by isometric untwist; 2) successive stretch and then isometric twist, followed by successive isometric twist release and then stretch release; 3) isobaric twist, followed by isobaric untwist; 4) stretch and isobaric twist, followed by isobaric twist release and then stretch release; and 5) stretch and release of a twisted or coiled fiber that was torsionally tethered to prohibit fiber untwist. The length of the used twistocaloric fibers before stretch or twist was inserted was typically ~3 cm. Unless otherwise indicated, the rate of twist insertion and twist removal was 50 turns/s, and the rate of stretch and stretch release was 42 cm/s.

Temperature increases resulting from twist or stretch insertion and temperature decreases resulting from twist or stretch removal were measured using a thermal camera (FLIR T440). The reliability of temperature measurements using the thermal camera was established by comparing temperatures measured using the thermal camera and a thermal couple in ambient temperature air and in a furnace. Based on these measurements, the thermal emissivity of the presently used black NR fibers was 0.90. The temperature derived by thermal imaging was not significantly affected by the degree of twist in the imaged fiber. More specifically, good agreement was obtained between temperatures measured using the thermal camera for a non-twisted NR fiber (28.9°C at fiber midpoint), a coiled NR fiber (28.9°C at fiber midpoint), and the temperature measured using a thermal couple when the fibers were in ambient temperature air (28.8°C). Additionally, we found good agreement for measured surface temperature for different diameter NR fibers and for temperature measurements at different lateral viewing angles with respect to the fiber surface. The average surface temperature change (ΔT_{avg}) and the maximum surface temperature change (ΔT_{max}) along a software-generated centerline were obtained using the software of the FLIR T440 thermal camera.

Using the same approaches as used above for determining the emissivity of black NR fibers, an emissivity of 0.90 was obtained for the commercial obtained NiTi wires. These wires were duller in surface appearance than ordinary metal wires, perhaps because of the utilized wire drawing process. For high-strength polyethylene yarns, low-strength polyethylene fibers, and nylon 6 fibers, the experimentally measured thermal emissivities were 0.95, 0.95 and 0.96, respectively.

Supplementary Text

6. The mechanical properties of non-twisted, highly-twisted, fully-coiled, and partially-supercoiled natural rubber fibers

6.1. The strain dependence of the Poisson's ratio of a natural rubber fiber

The dependence of the Poisson's ratio of a NR fiber on the applied strain is next evaluated. To accomplish this, high-resolution photographs were obtained during fiber stretch and image analysis software was used to obtain the fiber diameter (d) as a function of fiber length (l) from these photographs. The Poisson's ratio (ν) for true strain was calculated from these results using the following equation:

$$-\mathrm{d}\log d/\mathrm{d}\log l = \nu, \qquad \text{(S1)}$$

The average Poisson's ratios over 10% increments of true strain (and its standard deviation for 5 successive measurements of fiber diameter) were derived from a plot of log d as a function of log l. As shown in Fig. S5A, the measured Poisson's ratio for the rubber fiber was close to 0.5 up to the maximum investigated engineering strain (500%), which means that little volume change occurs during such extreme stretch.

The observed Poisson's ratio of 0.5 implies that the NR fiber behaves like an incompressible solid. This explains our observation (Fig. S5B) that the diameter of the non-coiled NR fiber is independent of twist density during isometric twist insertion. In order to avoid the onset of coiling, these measurements were conducted on a 2.2-mm-diameter NR fiber that was stretched to a strain of 100%.

6.2. Stress-strain curves and the dependence of the gravimetric tensile modulus of a natural rubber fiber on twist density for different amounts of isometric strain during twist insertion

Figure S6A provides gravimetric engineering stress-strain curves for NR fibers that were isometrically twist-inserted at 0% strain. The strain is normalized to the 3-cm initial length of the twist-inserted fiber, the stress is gravimetric (based on the measured force and the initial mass per length), and the strain rate was 5 mm/min. These results show that the stress-strain curves are highly hysteretic and that twist insertion dramatically increases the high-strain tensile modulus. The results of Fig. S6B show that the engineering stress-strain curves for the commercially obtained NR fibers having different diameters are quite similar.

Figure S7 shows gravimetric stress-strain curves for non-twisted, highly-twisted (1 turns/cm), fully-coiled (10 turns/cm), and partially supercoiled (14 turns/cm) 2.2-mm-diameter, 3-cm-long NR fibers, which were obtained during loading and unloading NR fibers at a strain-rate of 42 cm/s. The NR fibers were thermally equilibrated before stretch release. Note that the hysteresis of the stress-strain curves dramatically decreases for the fully coiled and partially supercoiled fibers, compared to the results for non-twisted and highly-twisted fibers.

Figure S8 shows the dependence of gravimetric modulus on twist density. To obtain these results, a non-twisted fiber was stretched to 100%, 200%, 300%, and 400%, and then twist was inserted. This gravimetric modulus was obtained by varying the length of the twisted fiber by ±10%, relative to the above stretched lengths. Note that the gravimetric modulus slowly increases with increase in twist density for the low twist density region, and increases dramatically for high twist densities. All fibers underwent at least partial coiling during twist insertion. However, fibers having 300% and 400% stretch did not complete coiling. Discontinuities in modulus appear at 14 and 24 turns/cm for the fibers having 100% and 200% stretch, respectively, which correspond to the twist needed to complete coiling. The discontinuities in modulus at 22 and 34 turns/cm for the fibers having 100% and 200% stretch, respectively, correspond to the onset of supercoiling.

6.3. Stress generation during isometric twist and untwist of natural rubber fibers

Measurements were conducted to determine the relationship between gravimetric stress generation during isometric twist insertion and twist removal and the structure of the NR fiber. Figure S9 shows the variation of gravimetric stress during isometric twisting/untwisting at a strain of 0% (Fig. S9A), 100% (Fig. S9B), and 200% (Fig. S9C), where these strains are respect to the length of the non-twisted NR fiber. The speed of twist insertion and twist removal was 1.7 turns/s, and the initial diameter of the non-twisted fiber was 2.0 mm. The twist range of highly-twisted, partially-coiled, fully-coiled, and partially-supercoiled states of the NR fiber are labeled in the figure using different colors. It can be seen for a fiber with 0% isometric strain (Fig. S9A) that twist insertion causes the fiber to elongate until the beginning of coiling, and therefore generate a stress that is opposite to the stretching direction. Similarly, for all applied isometric strains, twist insertion in twisted and fully coiled states causes the gravimetric stress to decrease.

6.4. The effects of structural transitions on the torque for twist insertion and removal in a natural rubber fiber

The torque during isometric twist insertion and during isometric twist release was characterized for a 2.2-mm-diameter, 3-cm-long parent NR fiber by using the apparatus shown in Fig. S4. Figure S10A shows the relationship between this torque and the structure of this NR fiber for a twist insertion and twist removal rate of 1.7 turns/s. During twist insertion at an isometric strain of 100%, the torque initially increased nearly linearly with increasing twist density to reach a torque of 0.34 mN·m at a twist density of 5.1 turns/cm. Coiling was initiated at a twist density of 5.1 turns/cm, where there is the start of a plateau region. Towards the end of coil insertion, the torque abruptly increased (likely due to increased local tensile strain in regions where coils are introduced). After the end of complete fiber coiling, there is a short region where torque slightly increases because of increasing twist insertion in existing coils. Upon further twist insertion in the fully coiled fiber, the applied torque dramatically increases as supercoiling is initiated and propagates.

The torque during twist removal dramatically decreased from 1.69 to 0.31 mN·m as the twist density decreased from 32 to 22 turns/cm, which can be compared to the about 18.6 turns/cm where supercoiling is eliminated. Afterward, the torque underwent a slow average decrease to 0.21 mN·m as the twist density decreased to 3.7 turns/cm, where the coils were completely removed. The torque decreased quasi-linearly from 0.13 to about 0.002 mN·m as the twist density decreased from 3.7 to 0 turns/cm during removal of all fiber twist.

7. Twistocaloric measurements for a single natural rubber fiber

7.1 The strain and time dependence of temperature changes produced by stretching and releasing a natural rubber fiber

Figure S11A shows the surface temperature changes during fiber stretch and stretch release for non-twisted NR fibers having diameters between two and five millimeters. The original pristine samples were 3 cm long and stretch and stretch release were at 42 cm/s. These results indicate that these fibers have similar properties and that diameter-dependent thermal transport does not dominate. Figure S11B shows the strain dependence of maximum surface temperature changes on stretch and stretch release for 2.2-mm-diameter NR fibers having different amount of inserted twist.

Figure S12A shows the time dependence of the surface temperature that results in a room temperature environment (25.8°C) when a non-twisted, 2.2-mm-diameter NR fiber is stretched to 300% strain in 0.28 s, and then allowed to equilibrate with an environment of room-temperature still air. The initial stretch increased fiber surface temperature to 26.6°C, corresponding to a ΔT of

+0.8°C, and in the following 27 s the temperature of the fiber's surface decreased to close to room temperature. Figure S12A also shows the time dependence of the tensile stress on this fiber during the measured temperature changes. Figure S12C shows, on a magnified time scale, the dependence of temperature and stress on time. Note that there is a short time delay in temperature increase during stretch (in which the temperature increased from 26.4°C to 26.6°C from 6.78 s to 7.18 s), which can be attributed to the time required for heat release due to stretch-induced crystallization of the NR fiber (*30*). The strain in the thermally equilibrated NR fiber was subsequently released within 0.28 s, which caused the fiber temperature to decrease to 24.2°C, corresponding to a ΔT of −1.6°C (Fig. S12, B and D).

7.2. The time and twist-rate dependence of temperature changes for isometric twist insertion and twist removal for a natural rubber fiber

The following experiments show that twist removal from a NR fiber having 200% isometric strain can provide much higher maximum cooling than removal of 300% stretch from a non-twisted fiber (Section 7.1). For operation in room temperature still air (25.8°C), Fig. S13A shows the time dependence of temperature for a 2.2-mm-diameter NR fiber having 200% isometric strain that was twist inserted in 1.5 s to provide a twist density of 30.0 turns/cm. This twist insertion caused the maximum temperature of the fiber surface to increase to 41.4°C, corresponding to a ΔT_{max} of +15.6°C. Then the twisted NR fiber was held for ~170 s, during which the fiber equilibrated to room temperature (25.8°C). Next, the inserted twist in the NR fiber was removed in 1.5 s, which caused the fiber's minimum surface temperature to decrease to 14.4°C, corresponding to a temperature change of −11.4°C. Finally, the NR fiber was again allowed to equilibrate to room temperature. The insets of Fig. S13A show, on a magnified time scale, the temperature changes that result from insertion and removal of 30 turns/cm of twist, respectively.

Figure S14 compares the cooling obtained by twist release at 50 turns/s using a motor (which took ~1.2 s) with the faster twist release that was enabled by using a torsional bearing (which took ~0.6 s). These results indicate that decreasing the twist removal time from 1.2 s to 0.6 s did not significantly affect the average surface temperature decrease.

7.3. The strain dependence of twistocaloric surface temperature changes of a natural rubber fiber during isometric twist insertion and twist removal

Figure S15 shows the maximum surface temperature increase during twist insertion and the maximum surface temperature decrease during twist removal as a function of the isometric strain and the twist density change (relative to the non-twisted fiber) for a 2.2-mm-diameter NR fiber. These results indicate that the temperature changes increase monotonically with increasing twist density at constant strain. The observed maximum heating during isometric twist insertion was +20.5°C, and the observed maximum cooling during isometric twist removal was –15.5°C, which were obtained for inserting or removing 32 turns/cm of twist at 100% strain. These maximum temperature changes resulting from isometric twisting/untwisting processes are higher than those that result from stretch/release processes (+11.9°C for heating and –12.2°C for cooling) for a non-twisted NR fiber (Fig. 1B).

Figure S16 shows the average and maximum surface temperature changes for different applied strains as a function of the product of twist number (the product of twist density and fiber diameter) and λ_s, where λ_s is the extension ratio (the ratio of the stretched length to the non-deformed length). The results in Fig. S16 indicate that both the average and maximum temperature changes increase monotonically with increasing twist density at constant strain. The maximum average surface temperature increase (+16.7°C) was obtained during isometric insertion of 50

turns/cm of twist at 300% strain, and the maximum average surface temperature decrease (−12.7°C) was obtained during removal of 40 turns/cm of twist at 200% strain. These maximum values for average surface temperature changes resulting from isometric twisting/untwisting processes are higher than those that result from stretch/release processes for a non-twisted NR fiber (+11.9°C for heating and −12.2°C for cooling, Fig. 1B).

Separate curves were obtained for the twist dependence of both the maximum and average surface temperature changes that are produced by isometric twist insertion at different levels of isometric strain (Fig. S15 and Fig. 1 C, respectively). However, the curves for cooling more closely coincide when inserted twist is replaced by the product of twist number and the extension ratio (Fig. S16). The effect of this normalization can be rationalized by noting that the stretch process and the twist process compete for producing changes in total fiber entropy. Multiplication of the twist number by the extension ratio might compensate the temperature decrease for the lower entropy change available when the fiber is elongated.

Figure S17 shows the dependence of maximum and average surface temperature changes on the product of twist density and the stretched fiber diameter (D_s) for different diameter parent NR fibers. The isometric stretch during twist density changes was 100%. If different diameter parent rubber fibers had identical properties, and the diameter dependence of thermal loss during heating after twist insertion and cooling after twist removal could be ignored (as well as the time for radial thermal equilibration), these curves should superimpose. The approximate coincidence of curves for fibers having different diameters indicates that the net effect of these different factors does not importantly affect the correlation between twistocaloric temperature changes and the product of twist density and stretched fiber diameter.

7.4. Twistocaloric temperature changes of a natural rubber fiber for isobaric twist insertion and twist removal and for these processes combined with stretch release

We next evaluated the cooling that results from isobaric twist insertion and twist removal, as an alternative to the isometric twist insertion and twist removal processes of Section 7.3. As shown in Fig. S18A, the maximum cooling obtained for isobaric twist removal was −8.4°C, which was obtained for 0.57 MPa stress and removal of an inserted twist of 30 turns/cm. This cooling is much lower than the maximum cooling obtained for the isometric untwist process shown in Fig. S15, which resulted in −15.5°C of cooling for removal of 32 turns/cm of twist at 100% strain.

Figure S18B shows that combining successive fast isobaric twist release and then fast stretch release increased the maximum surface cooling of a NR fiber. The highest cooling resulting from the present processes of isobaric untwist and stretch release was −12.4°C, which was obtained for 1.34 MPa applied stress and a twist density of 44 turns/cm. This cooling was higher than for either pure stretch release (−12.2°C, Fig. 1B) or pure isobaric twist release (−8.4°C, Fig. S18A). However, this cooling was lower than the maximum surface cooling obtained for isometric twist release followed by stretch release (Fig. 2B), which provided –16.4°C cooling for the combined release of 50 turns/cm of inserted twist and 300% strain.

Figure S19 compares, for 2.0-mm-diameter NR fibers having the same inserted twist and strained length, the maximum surface cooling during isometric twist removal when the twisted state was obtained by isometric twist insertion or by isobaric twist insertion. Heating was measured during isobaric twist insertion for a first fiber while this fiber was under 0.70 MPa stress. A second, non-twisted fiber was stretched for isometric measurements by applying the same elongation as obtained in the twisted state for the isobarically loaded NR fiber. This strain for isometric measurements increased with increasing twist up to the initiation of coiling, at a strain of 228% and 14.3 turns/cm of inserted twist, and then decreased. Afterwards, heating during isometric twist

insertion was measured for the second fiber. Finally, the cooling during twist release was measured isometrically for both fibers. Figure S19 shows that the obtained maximum surface cooling on twist release is essentially the same for both fibers, whether twist insertion was done isometrically or isobarically, as long as the percent stretch obtained after twist release is identical.

7.5. Periodic temperature variations along the length of a natural rubber fiber due to insertion and removal of fiber coiling

We found that rapidly isometrically inserting sufficient twist to produce coiling results in small periodic variations in temperature along the fiber length. Likewise, we also observed small periodic temperature variations along the fiber length when this twist was rapidly isometrically removed from the thermally equilibrated coiled fiber. Interestingly, even though the present experiments of twist insertion and twist removal were conducted at the same isometric strain with the same twist density change, the observed periods for this twist-heated fiber and the twist-release-cooled fiber are different.

In these experiments on a 2.0-mm-diameter, 3-cm-long parent NR fiber having a strain of 200%, 30 turns/cm of twist was isometrically inserted (to produce a fully coiled fiber) and the same twist was isometrically removed to produce a non-twisted fiber. The time duration of both twist insertion and twist removal was 1.8 s. Movie S1 was recorded during and after twist insertion and twist removal. Figure S20, A to C show (1) the absence of temperature variation along the stretched, non-twisted NR fiber that was equilibrated to room temperature, (2) the spatial periodicity of temperature along the NR fiber immediately after twist insertion to produce the fully coiled state, and (3) the spatial periodicity of temperature along the NR fiber immediately after twist removal to produce the non-twisted state. Figure S20D plots the temperature along the length of: the stretched, non-twisted NR fiber that was equilibrated at room temperature (black curve), the NR fiber just after twist insertion to provide the fully coiled state (red curve), and just after complete twist removal from the fully coiled fiber that had been equilibrated at room temperature (blue curve). The non-twisted NR fiber showed a uniform temperature along the rubber fiber, except at near fiber ends (where the end connections might have interfered with thermal camera measurements). Just after twist insertion to produce the fully coiled state, the NR fiber showed a temperature distribution containing 44 periods (corresponding to a wavelength of 1.8 mm). In contrast, immediately after twist removal the NR fiber showed a periodic temperature distribution along its length that contained 21 periods (corresponding to a wavelength of 4.5 mm).

Figure S20E provides photographs of the non-twisted (top) and twist-released NR fiber (bottom), as well as a fully coiled NR fiber (middle). The fully coiled fiber contains 44 coils, which is the same as the number of thermal fluctuations for the coiled fiber (with 1.8 mm wavelength). The longer periodicity for the untwisted fiber is more fundamental, and reflects the differing stress on the inner and outer surfaces of a coiled fiber.

Note that the local average temperature for the coiled fiber and the untwisted coiled fiber changes monotonically on going from left to right in the Fig. S20D plots. Excluding regions near fiber ends (to avoid likely artifacts due to connections at fiber ends), the average gradient in local average temperature along the coiled fiber is about 0.18°C/cm for twist insertion and about −0.1°C/cm after twist removal. This small temperature gradient might be a result of the observed nucleation of coiling at the right-hand end of the fiber and the observed initiation of coil removal at the same end. More specifically, the heating during insertion of each coil and the cooling upon removal of each coil will depend upon the local tensile strain, and this tensile strain will increase with increasing number of inserted coils and decrease with increasing number of removed coils.

7.6. The effect of cycles of isometric twist insertion and twist release on twistocaloric heating and cooling of a natural rubber fiber

Figure S21 shows that the maximum surface temperature changes (+4.8°C for heating and −6.7°C for cooling) and the average surface temperature changes (+2.6°C for heating and −3.6°C for cooling) were maintained for 750 cycles of isometric insertion and removal of 15 turns/cm of twist at 100% strain.

7.7. Twistocaloric cooling during elongation of a heterochirally coiled natural rubber fiber

In all previous reports of elastocaloric effects in rubbers, or in any other polymer, stretch causes the polymer to heat and stretch relaxation causes cooling. In the following work, we demonstrate an example of a rubber fiber that cools during stretch.

In order to obtain this unusual behavior, we elastically stretched a doubly-coiled (i.e., supercoiled) rubber fiber that has a heterochiral structure, meaning that the handiness of the self-coiled rubber fiber (with the same handiness of twist and coiling) is opposite to the handiness of coiling on the mandrel. The mandrel used to provide this structure comprised a 0.6-mm-diameter, non-twisted nylon 6 monofilament fishing line that was wrapped around an identical non-deformed nylon 6 fiber to form a spring, which was thermally set at 220°C for one hour in vacuum. The heterochiral coiled NR fiber was prepared by wrapping a 2.2-mm-diameter, 30-cm-long, S-direction self-coiled NR fiber in the Z direction around the above S-coiled nylon 6 mandrel spring. This opposite chirality of the natural rubber and nylon 6 coils was used to avoid inter-penetration of the rubber and nylon 6 coils, which would interfere with uniform elongation of the coiled NR fiber. As the rubber spring was elongated, the nylon spring simultaneously elongated by sliding on the core nylon 6 fiber. The spring index (*SI*) of the resulting heterochiral NR fiber (which is defined as $(D_1–D_0)/D_0$, where D_1 is the outer diameter of the NR supercoil and D_0 is the outer diameter of the NR coil within the supercoil) was 2.5. For comparison with twistocaloric measurements for the heterochiral supercoiled NR fiber, a homochiral supercoiled NR fiber was analogously prepared.

The maximum surface temperature changes for the heterochiral and homochiral fibers are shown in Fig. S22. For a supercoil elongation of 200%, the cooling of the heterochiral NR fiber during stretch (−0.8°C) and the heating during release of this stretch (+0.5°C) were maximized for a heterochiral NR fiber having 30 turns/cm of S-twist. For comparison, the heating of the homochiral NR fiber during 200% stretch (+0.5°C) and the cooling during release of this stretch (−0.5°C) were maximized for a homochiral supercoiled NR fiber having 10 turns/cm of Z-twist.

8. Twistocaloric temperature changes during isometric twist insertion to cause plying and isometric twist removal to eliminate plying of natural rubber fibers

Figure S23 shows the maximum and surface-average temperature changes of 2.2-mm-diameter NR fibers during twist insertion to cause plying and twist removal to eliminate plying for isometrically applied strains of 0, 100, and 300%. For removal of the twist of plying at 100% strain, the maximum surface temperature changes of two-, three-, four-, five-, six-, seven-, and eight-ply NR fibers were −16.2, −17.0, −17.7, −17.7, −19.0, −19.1, and −16.0°C, respectively. The corresponding changes in average-surface temperature during removal of plying at 100% strain for two-, three-, four-, five-, six-, seven-, and eight-ply NR fibers were −12.7, −12.9, −13.2, −13.2, −13.8, −14.4, and −12.6°C, respectively. Insertion of a much higher or lower isometric strain than 100% resulted in lower twistocaloric cooling during untwist to eliminate plying. Cooling could be slightly increased if fiber unplying was followed by release of tensile stretch, though the curves of Fig. 1B for a non-twisted single NR fiber indicate that the additional cooling would be only −0.4, −0.6, and −1.4°C for the isometric plying processes at 100, 200, and 300% strains, respectively.

Using the results of Fig. S23, Fig. S24 shows the dependences of twistocaloric temperature changes on the product of twist density and the effective ply diameter, which were obtained by using isometric twist insertion to ply two, four, six, seven, and eight NR fibers. The effective ply diameter (D_{eff}) is $n^{0.5}\times D_s$, where n is the number of plies and D_s is the diameter of each stretched fiber before plying.

9. Twistocaloric heating and cooling during tensile strain changes for self-coiled non-elastomeric polymers

9.1. Heating and cooling for a self-coiled, high-strength, braided polyethylene fishing line

Since we observed different twistocaloric properties for different types of polyethylene fibers and yarns, it is important to first comment on their structures. A 0.41-mm-diameter, 30-cm-long polyethylene fishing line (65 lb fishing line from Power Pro., Innovative Textiles, Inc.) was used for the present experiments. This fishing line, shown in Fig. S25A, is multifilament, and comprises four braided fibers. For comparison with later described low-strength polyethylene fibers (which have a strength of 252 MPa and a modulus of 1.0 GPa), the present braided yarn has a strength of 3.37 GPa and a modulus of 43.0 GPa. The high-strength polyethylene yarn is called PE-1 and the low-strength polyethylene fiber is called PE-2.

Thirty-cm-long lengths of these high-strength braided yarns were fully coiled by twist insertion to produce different spring index coils. As earlier indicated, this spring index is defined as $(D_1-d)/d$, where D_1 is the outer diameter of the polymer coil and d is the diameter of the polymer yarn within the coil (as measured optically). By inserting 6.5, 6.7, 7.0, and 7.3 turns/cm of twist under loads of 37.1, 52.0, 59.4, and 74.2 MPa, respectively, fully-coiled yarns having spring indices of 1.4, 1.1, 0.8, and 0.5, respectively, were obtained from 30-cm-long precursor yarns. Under these respective loads, the lengths of these coiled yarns were 8.5, 10.5, 14.6, and 16.0 cm, respectively.

Figure S25, B and C show, for a stretch and stretch release rate of 42 cm/s and an ambient temperature of 25°C, the tensile strain dependence of heating during stretch and cooling during stretch release that results for coiled yarns having different spring indices. Note that the yarn stretch that can be inserted without causing yarn damage (44.4, 42.8, 22.7, and 16.8%) decreases with decreasing spring index (1.4, 1.1, 0.8, and 0.5, respectively). For these yarns having spring indices of 1.4, 1.1, 0.8, and 0.5, the maximum surface temperature changes during stretch were +7.3, +8.0, +7.8, and +6.9°C, respectively, the maximum surface temperature changes during stretch release were –3.9, –4.9, –5.1, and –4.8°C, respectively, the average surface temperature changes during stretch were +6.0, +6.2, +5.8, and +5.4°C, respectively, and the average surface temperature changes during stretch release were –2.9, –3.5, –3.2, and –2.8°C, respectively. The ratio of the maximum surface temperature changes to the percent inserted stretch increases in magnitude with decreasing spring index (0.16, 0.19, 0.34, and 0.41°C/% for heating and –0.09, –0.11, –0.22, and –0.29°C/% for cooling, for yarns having spring indices of 1.4, 1.1, 0.8, and 0.5, respectively). Also, the ratio of the average surface temperature changes to the percent inserted stretch increases in magnitude with decreasing spring index (+0.13, +0.14, +0.26, and +0.32°C/% for heating and –0.07, –0.08, –0.14, and –0.17°C/% for cooling for yarns having spring indices of 1.4, 1.1, 0.8, and 0.5, respectively).

Figure S25, D and E show, for a stretch and stretch release rate of 42 cm/s, the tensile strain dependence of heating during stretch of the coiled yarn and cooling during stretch release that results for these coiled yarns that were elastically deformed at different ambient temperatures. These coiled yarns have a spring index of 1.1. For these yarns tested at ambient temperatures of

10, 25, and 40°C, the maximum surface temperature changes during stretch were +6.9, +8.0, and +9.7°C, respectively, the maximum surface temperature changes during stretch release were –3.6, –4.9, and –4.5°C, respectively, the average surface heating during stretch were +3.6, +6.2, and +6.6°C, respectively, and the average surface cooling during stretch release were –2.7, –3.5, and –3.3°C, respectively. No degradation in performance occurred during the investigated 2500 stretch/release cycles to 13% strain (Fig. S26).

In contrast to the case for stretched homochiral rubber fibers, the dependences of temperature changes on strain changes for both heating and cooling are high for high-strength polyethylene yarn at low strains. In addition, it is important to note that the twistocaloric cooling per strain change was highest for low spring index yarns. While this trend will also be seen in the data of the next sections for low-strength polyethylene and nylon 6 fibers, the range of spring indices that could be investigated was smaller. The reason is that high tensile stresses during coiling must be used to obtain very small spring indices, and these weaker fibers fail during twist insertion under these tensile stresses.

9.2. Heating and cooling for a self-coiled low-strength polyethylene monofilament fiber

For the present experiments, 30-cm-long monofilament polyethylene fishing line (Nantong Ntec Monofilament Technology Co., Ltd.) was used. For comparison with the above described high-strength polyethylene yarns (which have a strength of 3.37 GPa and a modulus of 43.0 GPa), the present monofilament fibers have a strength of 0.252 GPa and a modulus of 1.0 GPa. While the high-strength polyethylene yarns were made by an expensive gel spinning process (*31*), the present fibers were melt-spun.

The polyethylene monofilament fiber was fully self-coiled by twist insertion to produce different spring index coils. Figure S27 shows, for a stretch and stretch release rate of 42 cm/s, the tensile strain dependences of heating during fiber stretch and cooling during stretch release that result for these coiled fibers having different spring indices (but the same 0.4-mm diameter for the fiber before twist insertion). For these fibers having spring indices of 0.9, 1.1, and 1.3, the maximum surface temperature changes during stretch were +4.1, +3.5, and +2.3°C, respectively; the maximum surface temperature changes during stretch release were –1.6, –2.4, and –1.9°C, respectively; the average surface temperature changes during stretch were +2.6, +2.3, and +1.7°C, respectively; and the average surface temperature changes during stretch release were –1.2, –1.4, and –1.3°C, respectively. Note that the coils with the lower spring indices provided higher maximum cooling and maximum heating than do the highest spring index coils. However, since fabrication of fibers having very low spring indices requires the application of high loads during twist insertion, the low strength of this fiber meant that the lowest spring index that could be fabricated was 0.9, as compared to the spring index of 0.5 for the high-strength polyethylene yarn of the last section.

9.3. Heating and cooling for a self-coiled, monofilament nylon 6 fishing line fiber

The next experiments evaluate twistocaloric heating and cooling for coiled monofilament nylon 6 fibers. Before twist insertion to provide self-coiling, the fibers were 30 cm in length and had diameters of 0.2, 0.4, and 0.6 mm. The fibers were coiled under the same applied stress (15.6 MPa, normalized to the diameter of the non-twisted fibers), which provided a spring index of 1.0. The 0.4-mm-diameter fiber was also coiled under different applied stresses (11.7, 15.6, and 19.5 MPa, normalized to the diameter of the non-twisted fiber), which provided spring indices of 1.2, 1.0, and 0.9, respectively.

Figure S28, A and B show, for a stretch and stretch release rate of 42 cm/s, the tensile strain dependence of heating during fiber stretch and cooling during stretch release that results for these

coiled fibers having different spring indices. For these fibers having spring indices of 1.2, 1.0, and 0.9, the maximum observed heating during stretch were +4.0, +4.2, and +3.8°C, respectively; the average observed heating during stretch were +1.9, +2.3, and +1.8°C, respectively; the maximum observed cooling during stretch release were –1.6, –1.9, and –1.4°C, respectively; and the average observed cooling during stretch release were –0.9, –1.2, and –1.3°C, respectively. Note that these maximum magnitude temperature changes (obtained for different strain levels) are similar for the different spring index fibers, and that the strain dependence of cooling during stretch release is little affected by spring index. This insensitivity of twistocaloric temperature changes to spring index likely arises from the small variation in spring index. However, the strain dependence of heating during stretch does depend upon spring index.

Figure S28, C and D show the strain dependence of twistocaloric temperature changes during stretch and stretch release for different-diameter nylon 6 fibers having a spring index of 1.0. The maximum surface temperature changes were +4.3, +4.2, and +1.6°C for stretch and –2.1, –1.9, and –1.3°C for stretch release for fibers having diameters of 0.6, 0.4, and 0.2 mm, respectively. The average surface temperature changes were +2.5, +2.3, and +0.9°C for stretch and –1.8, –1.2, and –0.8°C for stretch release for fibers having diameters of 0.6, 0.4, and 0.2 mm, respectively. This decreased measured heating and cooling as the fiber diameter decreases is likely a result of increasing thermal losses to the environment (before temperature measurement) as fiber diameter decreases (because of increased surface to volume ratio) or of differences in the degree of thermal equilibration within the fiber, although differences in the mechanical properties of the different diameter parent fibers might also be a factor.

9.4. Comparison of mechanocaloric temperature changes during isometric twist insertion and removal at 0% strain and during stretch and stretch release of non-twisted fibers

The results in Table S1 for stretch-based and twist-based cooling cycles for the NiTi wire can be compared with results in the literature for NiTi wires. A 0.7-mm-diameter $Ni_{48.9}Ti_{51.1}$ wire (which was optimized for elastocaloric cooling during stretch release by composition choice, training cycles, and the used ambient temperature) provided –21°C cooling (*10*) when operated at 49°C. A 3-mm-diameter NiTi wire generated −17°C of cooling when operated at 22°C ambient temperature (*9*). When operating at an ambient temperature of 26°C, the presently used 0.7-mm-diameter NiTi wires provided –17.0°C of cooling during stretch-release (for the non-twisted NiTi wire) and maximum and average surface cooling of –17.0°C and –14.4°C, respectively, for isometric twist removal from the twist-containing, non-stretched NiTi wire.

One possible explanation for the wide variation in the mechanocaloric heating and cooling of different elastomers is that the temperature changes caused by stretch and stretch release (or isometric twist insertion and twist release) in an elastomer are proportional to the mechanical strain energy density changes during these processes and inversely proportional to the elastomer's heat capacity. The measured gravimetric work inputs during stretching the non-twisted fiber to close to failure stress (at the strain rate used for elastocaloric measurements) are 6.32, 5.10, 4.19, 0.676, 6.89 and 1.42 J/g, respectively, for the NR, Spandex, EPDM, SEBS, TPU, and PDMS fibers. The heat capacities of the NR, Spandex, EPDM, SEBS, TPU, and PDMS fibers are 1.72, 1.32, 1.83, 1.17, 1.60, and 1.10 $JK^{-1}g^{-1}$, respectively. The elastocaloric temperature changes during stretch are +11.9, +6.6, +2.3, +0.2, +4.3, and +1.6°C and the elastocaloric temperature changes during stretch release are −12.2, −7.1, −2.6, −0.3, −1.2, and −0.6°C, respectively, for these fibers. When these temperature changes are normalized to the ratio of input mechanical energy to heat capacity, the temperature change ratios for the NR, Spandex, EPDM, SEBS, TPU, and PDMS fibers are 3.24, 1.71, 0.99, 0.34, 1.00, and 1.24 on heating and 3.32, 1.83, 1.12, 0.52, 0.28, and 0.40 on

cooling. Hence, such normalization reduces the range of observed elastocaloric temperature changes for these elastomers from factors of 59.5 on stretch and 40.7 on stretch release for the measured temperature changes to factors of 9.5 on stretch and 11.9 on stretch release for the normalized temperature changes.

10. The spring-index dependence of twistocaloric heating and cooling upon stretch and stretch release for thermally-set, mandrel-coiled homochiral non-elastomeric polymers

10.1. The dependence of twistocaloric heating and cooling on coil spring index for a low-strength polyethylene monofilament fiber

Homochiral mandrel-coiled polyethylene (PE) fibers with different spring indices were produced by wrapping a S twisted PE fiber (with 0.4-mm-diameter and 40-cm-length before twisting) in the S direction around steel rods (0.4, 1.0 and 2.0 mm in diameter), and then annealing these coiled fibers under vacuum at 100°C for 1 hour. The present experiments utilized the low-strength polyethylene fibers (Section 9.2), rather than the higher-performing high-strength polyethylene yarn (Section 9.1), since we could not thermally set mandrel-coiled high-strength polyethylene yarns to provide a structure that was reversibly deformable when removed from the mandrel.

Figure S29 provides measurements of the temperature changes during a stretch-release process for these homochiral coiled PE fibers having different spring indices. The observed maximum heating during stretch was +1.4, +0.9 and +0.7°C, and the maximum cooling during stretch release was −0.6, −0.4 and −0.3°C, for the fibers having spring indices of 2.0, 3.5 and 6.0, respectively. Note for these mandrel coiled PE fibers, where large variations of spring index were obtained, that the lowest spring index fiber provided the highest heating during stretch and the highest cooling during stretch release, which agrees with the results for self-coiled polymer fibers in Section 9.

10.2. The dependence of twistocaloric heating and cooling on coil spring index for a homochiral, mandrel-coiled nylon 6 fishing line fiber

Homochiral, mandrel-coiled nylon 6 fishing line fibers having different spring indices were produced by wrapping a S-twisted nylon 6 fishing line (with 0.4-mm-diameter and 40-cm-length before twisting) in the S direction around steel rods (0.4, 1.0, and 2.0 mm in diameter), and then annealing these coiled fibers under vacuum at 180°C for 1 hour. Figure S30 provides measurements of the temperature changes during fiber stretch and stretch release for these homochiral coiled nylon 6 fibers having different spring indices. The observed maximum heating for the highest strain level during stretch was +0.8, +0.6 and +0.5°C and the maximum cooling for the highest stretch release was −0.5, −0.5 and −0.3°C for the fibers having spring indices of 2.0, 3.5 and 6.0, respectively. Like described above (Section 10.1) for mandrel-coiled polyethylene, the cooling during stretch release was largest for the lowest spring index fiber. While the cooling at strains up to 80% was highest for the lowest spring index fiber, the cooling for fibers having 3.5 and 2.0 spring indices became equal for strains above about 80%.

11. Strain-inverted twistocaloric temperature changes, which provide cooling upon stretch and heating upon stretch release, for heterochiral non-elastomeric polymers

11.1. The dependence of twistocaloric heating and cooling on spring index for a heterochiral, coiled nylon 6 monofilament fiber

Although the homochiral, coiled high-strength polyethylene yarn provided higher twistocaloric temperature changes than did homochiral, coiled nylon 6 fiber, we could not

thermally set the structure of a coiled heterochiral, high-strength polyethylene yarn. Consequently, the present measurements for a heterochiral fiber are for the nylon 6 fiber.

Heterochiral, coiled nylon 6 monofilament fishing line with different spring indices was produced by wrapping a S-twisted nylon 6 fishing line (with 0.4-mm-diameter and 40-cm-length before twisting) in the Z direction around steel rods (0.4, 1.0 and 2.0 mm in diameter), and then annealing these coiled fibers under vacuum at 160°C for 1 hour. Figure S31A provides measurements of the temperature changes during fiber stretch and stretch release for these heterochiral, coiled nylon 6 fibers having different spring indices. The observed maximum cooling during stretch was −0.6, −0.4 and −0.2°C and the maximum heating during stretch release was +0.5, +0.4 and + 0.3°C for the fibers having spring indices of 2.0, 3.5 and 6.0, respectively.

Figure S31B shows the effect of thermal setting temperature on the maximum twistocaloric heating and cooling for a heterochiral, coiled nylon 6 fiber having a spring index of 2.0. The maximum observed cooling during stretch was −0.3, −0.6, and −0.4°C, and the maximum observed heating during stretch release was +0.4, +0.5, and +0.3°C for the heterochiral, coiled nylon 6 fiber with thermal setting temperatures of 140, 160, and 180°C, respectively.

11.2. The dependence of twistocaloric heating and cooling on coil spring index for a heterochiral, coiled, low-strength polyethylene monofilament fiber

Heterochiral, coiled PE fibers having different spring indices were prepared by twisting low-strength PE fibers (0.4 mm in diameter and 40 cm in length) in the S direction to just before coiling, which involved inserting 6.0 turns/cm of twist, and then wrapping the twisted PE fiber in the Z direction around steel rods having different diameters (0.4, 1.0, and 2.0 mm). The coiled PE fibers were then thermally set, so that twist was retained even after release of torsional and tensile tethering. This was accomplished by annealing the mandrel-coiled PE fibers in vacuum at 100°C for 1 hour. The obtained spring indices were 2.0, 3.5, and 6.0, and the corresponding lengths of the coiled fibers were 70, 40 and 30 mm, respectively.

Figure S32A provides the temperature changes on stretch and stretch release for these heterochiral, coiled PE fibers having different spring indices. Since the thermally-set twist-containing polymer fibers do not undergo snarling during stretch release to zero stress, the indicated strains are relative to the non-loaded length of the coiled fibers. Note that the maximum reversible stretch of the coiled fiber decreased from 80% and 77% to 54% as the spring index decreased from 6.0 and 3.5 to 2.0. The observed maximum temperature decreases during stretch to the maximum reversible strains were −0.1, −0.2, and −0.3°C, and the maximum temperature increases during stretch release were +0.1, +0.4, and +0.5°C for the heterochiral, coiled PE fibers having spring indices of 6.0, 3.5, and 2.0, respectively. Figure S32B shows the twistocaloric temperature changes for a heterochiral, coiled PE fiber having a spring index of 2.0, which utilized different thermal setting temperatures. The time for thermal setting was one hour. The observed temperature decreases during stretch were −0.2, −0.3 and −0.2°C and the temperature increases during stretch release were +0.2, +0.5 and +0.3°C for the heterochiral, coiled PE fibers with thermal setting temperatures of 80, 100, and 120°C, respectively.

To our knowledge, the present results for heterochiral polyethylene, nylon 6, and rubber fibers provide the first examples of a solid material that cools when stretched. Figure S32 shows that the cooling resulting from high stretch and the heating resulting from high stretch release for a heterochiral coiled PE fiber do not monotonically increase with increasing stretch or stretch release. Note that two processes are occurring during the elongation of a heterochiral PE fiber. These processes are twist decrease during stretch (which causes cooling) and fiber elongation (which causes heating). In contrast, stretching a homochiral, coiled NR fiber causes both up-twist and

elongation of the fiber within the coils, so the entropy change of both processes contribute in the same direction to provide twistocaloric temperature changes during both the heating on coil stretch and the cooling on stretch release.

While the cooling during stretch of a heterochiral, coiled PE fiber is much smaller than can be obtained by stretch release of a NR fiber from much larger strains, the cooling obtained for reversible stretch of the heterochiral PE fiber to 100% strain is comparable to that here reported for stretch release from this strain for NR fibers having 0, 1, 10, and 14 turns/cm of twist (−0.4, −0.5, −1.0, and −0.7°C, respectively).

Figure S33 shows thermal and optical images for irreversible large stretch of a nylon 6 heterochiral coiled fiber having a low initial spring index (2.0), and therefore a limited elastic deformation range. Since the spring index is small for a heterochiral, mandrel-coiled fiber, 90% strain resulted in inhomogeneous deformation. As a result of irreversible plastic deformation, portions of the tightly-coiled, heterochiral fiber transformed to loosely-coiled segments, which were not removed upon strain release. While the tightly-coiled fiber regions cool by −0.3°C during stretch, the plastically deformed loosely-coiled segments heat by +0.6°C during stretch.

12. Using twistocaloric temperature changes for causing color changes

A 7.0-mm-diameter NR fiber was stretched to 200% strain and then coated with a mixture of commercial thermochromic dyes (Orange-Yellow 22 and Green-Yellow 15, Jinhua Lijin Technology Co., Ltd.). Figure S34A shows the color changes that result from isometrically inserting 6.4 turns/cm of twist in this fiber at 50 turns/s, allowing thermal equilibration to room temperature, removing this twist at 50 turns/s, and then again allowing equilibration to room temperature. Figure S34A shows that the color changes are from orange for the initial non-twisted fiber, to yellow after twist insertion, to orange for the fully coiled fiber after thermal equilibration to room temperature, to dark green after twist removal, and then to orange for the non-twisted fiber equilibrated to room temperature. For comparison, the color of the dye on the rubber fiber changes from orange at 15.0°C to yellow at 23.0°C, and then to dark green at 8.3°C. Movie S2 shows the color changes during these twist insertion and twist removal processes.

The twist-produced temperature changes of a NiTi wire were used to provide visible indication of torsional rotation (Fig. S34B). Figure S34B demonstrates this twist-induced color change by coating a NiTi wire with a thermochromic paint that changes color from orange-to-yellow at 31°C, and from orange-to-green at 15°C. Twist-induced heating changes the color from orange at room temperature to yellow, and untwist-induced cooling changes the color from orange to green (Movie S4).

13. Twistocaloric temperature changes for single ply and multi-ply NiTi shape memory metal wires

While NiTi shape memory wires have been highly investigated as a material for practical elastocaloric cooling, the use of twist insertion and twist removal to provide twistocaloric temperature changes has apparently not been investigated. We here show that large reversible temperature changes result from twist insertion and twist removal from a single NiTi shape memory wire, and by plying and unplying NiTi shape memory wires. The investigated wires were 0.7-mm-diameter NiTi wires having a composition $Ni_{52.6}Ti_{47.4}$, which were purchased from Baohong Metal Material Co., Ltd. These wires had a martensite-to-austenite finish transition temperature of 15.0°C and an austenite-to-martensite start transition temperature of 13.5°C for increasing and decreasing temperatures, respectively.

Figure S35A shows the stress-strain curves for a 3-cm-long, 0.7-mm-diameter NiTi wire at an elongation rate of 5 mm/min. The stress-strain curve for NiTi wire can be divided into different regimes: an elastic region at small strain (~1.8%), a plateau region to ~6% (where the austenite is converted to martensite on increasing strain), and a plateau region on decreasing strain (where the martensite is converted to austenite) that ends at ~1.6% strain.

Figure S36A shows the twist dependence of temperature changes during twist insertion and twist removal for a 0.7-mm-diameter single NiTi wire at 0% strain. All twistocaloric experiments on NiTi wires were conducted at an ambient temperature of about 26.0°C, which means that the non-deformed wires are largely in the austenite phase. Like the case later described for plying NiTi wires, the twist insertion and twist removal processes for a single NiTi wire are only partially isometric, since the length of the wires increases during the twist insertion process. This eventually results in reversible wire buckling, which is likely due to the lower density of the martensite phase that results from twisting or plying. The maximum values for heating (+24.3°C) and cooling (−17.0°C) and the average values for heating (+20.3°C) and cooling (−14.4°C) were obtained during isometric twist insertion of 1.06 turns/cm for heating and during twist removal of 0.9 turns/cm for cooling. For comparison, tensile elongation of the same NiTi wires increased temperature by +21.0°C. Subsequent removal of stretch caused −17.0°C of cooling.

Figure S36, B to D compare the twist dependence of twistocaloric heating and cooling for two-ply, three-ply, and four-ply NiTi wires. Like for the above case of twisting a single NiTi wire, our intension was to conduct these experiments isometrically using 0% stretch before twist insertion. However, since the plied wires elongated during plying, the length of the plied wires were longer than the non-plied wires. Hence, this experiment is only quasi-isometric. The results in this figure show that the maximum heating and cooling were larger for twist insertion and twist removal by plying (+37.9 and –20.8°C, for four-ply wires) than for twist insertion and twist removal for a single-ply wire. Figure S37 shows the dependence of average twistocaloric surface temperature changes on twist density for a 0.7-mm-diameter single NiTi wire. The average heating and cooling resulting from insertion and removal of 0.8 turns/cm of twist were +19.0 and –13.5°C, respectively. While the data in Fig. S36A are for a sequence of measurements where twist was cycled between 0 twist and a twist level that was progressively increased, the data of Fig. S37 show that essentially the same temperature changes were obtained if the maximum twist level was progressively increased or decreased in going between successive pairs of data points. Figure S38 shows that the maximum and average surface temperature do not significantly change during 1000 cycles of quasi-isometric twist insertion and twist removal up to 0.6 turns/cm of twist for a 0.7-mm-diameter NiTi wire.

14. Theoretical analysis

14.1 Calculation of the effect of spring index on the strain dependence of twistocaloric cooling for self-coiled polymer fibers

The dependence of stretch-induced temperature changes on coil spring index can be approximated by considering coil geometry. For a spring of length L, having N coils (with average coil diameter D_c) and a coil bias angle α' (Fig. S39), the length of the fiber (l) making up the spring is:

$$l = \pi D_c N/\cos(\alpha'), \quad \text{(S2)}$$

Furthermore, the strain required to stretch a coil by a given length increases with spring index. This can be understood by considering that the strain required to stretch a coil into a straight fiber corresponds to the fiber length l minus the initial coil length L, which also roughly increases with

D_c according to Eqn. S2. Since the twist generated per strain is inversely related to spring diameter and the fiber length increases with spring diameter, the twist change per fiber length, $\Delta T_w/l$, follows an inverse square relationship to spring index (*SI*). More precisely, starting from Eqn. S3 of (*21*):

$$\Delta T_w = N\Delta L/l^2, \quad \text{(S3)}$$

the change in twist per filament length, $\Delta T_w/l$, depends on coil strain $\varepsilon = \Delta L/L$, such that:

$$\Delta T_w/l = \varepsilon NL/l^3, \quad \text{(S4)}$$

Substituting into Eqn. S4 the geometric constraints of Eqn. S2 and using $L = l\sin(\alpha')$, which is from coil geometry,

$$\Delta T_w/l = \varepsilon\sin(\alpha')\cos^2(\alpha')/(\pi^2 D_c^2 N), \quad \text{(S5)}$$

Since the spring index is $SI = D_c/d$, this equation becomes:

$$\Delta T_w/l = \varepsilon\sin(\alpha')\cos^2(\alpha')/(SI^2\pi^2 d^2 N), \quad \text{(S6)}$$

For coils with different spring indices, but having otherwise similar geometry and starting coil bias angle, Eqn. S6 shows that stretching a coil will generate a twist per fiber length that is inversely proportional to the square of coil spring index. This dependency of twistocaloric temperature changes on the ratio of strain to the square of spring index was not observed for mandrel coiled fibers, likely because of the large room for variation in initial coil bias angle when fabricating very large spring index fibers by mandrel coiling. This difference in initial bias angle results in different amounts of twist generated per coil strain, thus causing different observed surface temperatures. In agreement, the observed twistocaloric temperature changes for self-coiled polyethylene and nylon 6 fibers or yarns are approximately proportional to the ratio of percent stretch to the square of the spring index (Fig. 3A and fig. S40).

14.2 Calculation of the entropy difference between the orthorhombic and monoclinic phases of polyethylene

The entropy difference between the orthorhombic and monoclinic phases of polyethylene at 300 K was calculated using molecular dynamics (MD) simulations. The structures simulated are shown in Fig. S41. The space groups for the orthorhombic and monoclinic phases were Pnam and C2/m, respectively, and the chain axis direction in both cases is the *c*-axis (*24*). The unit cell parameters used to build the structures are from the literature (*24, 26*).

The structures were initially equilibrated at 300 K for 500 ps under NPT conditions (where the number of particles, pressure, and temperature are constant), which allows the overall structure to be fully relaxed (i.e., energy minimized). Afterwards, we ran an additional 100 ps at 300 K under NPT conditions. We then collected the values of the structural entropy, according to the below formulas. This was done every 50 fs to obtain averages over 100 ps. Using a time step of 0.5 fs, we used the computational package LAMMPS (*32*) to integrate the equations of motion of the system. After 500 ps at 300 K, the predicted unit cell parameters for the monoclinic phase were a = 8.34 Å, b = 4.78 Å, c = 2.56 Å, and β = 108°, and those for the orthorhombic phase were a = 7.44 Å, b = 4.97 Å, and c = 2.56 Å.

Based on an entropy calculation derived by Piaggi and Parrinello (*33*), entropy values (s_i) were calculated from the following set of equations:

$$s_i = -2\pi\rho k_B \int_0^{r_m} [g_i(r)\ln g_i(r) - g_i(r) + 1] r^2 dr, \quad \text{(S7)}$$

where k_B is the Boltzmann constant, $g_i(r)$ is the radial distribution function of atom i, r_m is cutoff distance up to which $g_i(r)$ should be calculated, and ρ is the density of the system. $g_i(r)$ is computed using:

$$g_i(r) = \frac{1}{4\pi\rho r^2}\sum_j \frac{1}{\sqrt{2\pi\sigma^2}} e^{-(r-r_{ij})^2/(2\sigma^2)}, \quad \text{(S8)}$$

where the sum in *j* goes through the neighbors of atom *i*, and σ is a parameter used to control the smoothness of the function. We obtained additional averaging, in order to provide improved distinction between ordered and disordered environments, using

$$s_i = \frac{\sum_j s_j + s_i}{N+1}, \quad \text{(S9)}$$

where the sum *j* goes over the neighbors of atom *i* and *N* is the number of neighbors defined by another cutoff distance.

Using σ = 0.05 and cutoff distance of 4.5 Å, we calculated that the entropy of the orthorhombic phase of polyethylene at 300 K is 0.097 $JK^{-1}g^{-1}$ higher than for the monoclinic phase. This calculated entropy difference is consistent with the entropy difference (0.12 $JK^{-1}g^{-1}$) calculated over thirty years ago by Todokoro (*26*) from the vibrational frequencies of the two phases (ΔS = 0.12 $JK^{-1}g^{-1}$).

15. Evidence of orthorhombic to monoclinic phase conversion induced by coiling pristine polyethylene fibers and by a stretch cycle for thermally annealed, coiled polyethylene

As shown in Fig. 3B and Table S2, self-coiling a high-strength polyethylene fiber results in partial conversion of the orthorhombic phase to the monoclinic phase. Annealing this self-coiled fiber for 2 hours at 120°C results in nearly complete conversion of the monoclinic phase to the orthorhombic phase. The results of Fig. S42A show that the cooling resulting from the release of tensile strain is similar for the annealed and non-annealed samples. Figure S42B shows that stretch converts some of the orthorhombic phase to the monoclinic phase and that stretch release reverses this transformation for the thermally annealed sample. These X-Ray diffraction patterns were obtained by using an Ulitma IV diffractometer from Rigaku Co., Ltd., and averaging meridional scans.

16. Comparison of the coefficients of performance for twist-based and purely tensile mechanocaloric cooling of natural rubber fibers

Figure S43, A and B compare the coefficients of performance (COP_{HC} and COP_{FC}) for NR fibers that provide cooling during stretch release, twist release, and the combination of twist and stretch release. The COP_{HC} and COP_{FC} are the ratios of the specific cooling energy to the input gravimetric mechanical work for a half cycle and the overall gravimetric work for a full cycle, respectively. This specific cooling energy is the product of the temperature change on cooling and the gravimetric heat capacity, which for the present NR fibers is 1.72 $JK^{-1}g^{-1}$ (Fig. S3). These mechanical energies were calculated from the measured stress-strain curves for tensile stretch and release (Fig. S7) and for torque versus rotation angle for twist insertion and twist release (Fig. S10B). The specific cooling energies, which are the numerators of the COPs, were obtained using the data of Fig. 1B for stretch-release of a non-twisted fiber and the volume-average temperature changes of Fig. 1D. The COP_{FC} and COP_{HC} based on volume-average cooling are plotted versus volume-average cooling in Fig. 2C and Fig. S43, respectively.

For volume-average cooling higher than −0.4°C, Figure S43, A and B show that the COP_{HC} and COP_{FC} for both isometric twist release and for combination of isometric twist release and stretch release at 100% strain are much higher than for stretch release from a non-twisted NR fiber.

Figure S43, C and D compare intrinsic efficiencies for NR fibers that provide cooling during stretch release, isometric twist release, and combined isometric twist release and stretch release. The intrinsic material efficiencies are the ratios of COP (either COP_{HC} or COP_{FC}) to the COP of a Carnot cycle (COP_{Carnot}). The COP_{Carnot} is the maximum theoretical efficiency for a refrigerator, which is defined as $T_C/(T_H - T_C)$, where T_C and T_H are the minimum and the maximum temperatures in the Carnot refrigeration cycle, respectively. Figure S43C shows that the intrinsic material

efficiencies for cooling during isometric twist release and combined isometric twist release and stretch release reach 0.39 and 0.42, respectively, versus 0.16 for stretch release, when the energy recaptured during strain release is ignored. Considering the full cycle, by using COP_{FC}, Fig. S43D shows that the intrinsic material efficiencies for cooling during isometric twist release and combined isometric twist release and stretch release reach 0.63 and 0.67, respectively, versus 0.32 for stretch release.

Note that the COP_{HC} and the COP_{FC}, as well as the corresponding intrinsic material efficiency, will depend upon the rates of strain insertion, which are presently 42 cm/s and 50 turns/s for both strain insertion and strain removal. Since stress relaxation occurs for NR fibers, there is an additional complication for the COP_{FC} in that the recoverable mechanical energy depends on the time required for thermal equilibration after strain insertion. The same times for thermal equilibration were used for all measurements, including the measurements of mechanical energies. The COP_{FC} can also be affected by the present approximation that the strain energy recoverable upon strain release is independent of the maximum strain applied.

17. Experimental determination of the ratio of surface-average temperature change to volume-average temperature change upon removing twist from a natural rubber fiber or a NiTi wire

The volume-average temperature changes for isometrically twist-released NR fibers were experimentally derived by calorimetrically measuring the cooling energy produced by releasing fiber twist within a water-filled tube. By dividing the derived cooling energy by the gravimetric heat capacity of the NR fiber, the volume-average temperature change of this fiber before equilibration with its surrounding was obtained. Upon thermal equilibration within the NR fiber, this cooling energy is the sum of terms due to the temperature decreases of the water surrounding the NR fiber, the NR fiber, and the cooling of the tube that contains the water.

The following method was used to measure the cooling energy. A 2.2-mm-diameter NR fiber was inserted into the center of a vertically-suspended 6.5-cm-long polypropylene (PP) tube, which was sealed at the bottom using epoxy resin that torsionally tethered the bottom end of the NR fiber. The inner and outer diameters of the PP tube were 3.4 and 4.0 mm, respectively. The top end of the NR fiber was connected to an eighty-step servo motor. The PP tube was filled with water to a height of 6.4 cm, so 98.5% of the length of the stretched NR fiber was immersed in the water. In order to minimize loss of cooling energy to surrounding air, by decreasing the temperature change of the water, the mass of water was 4.63-times the mass of the NR fiber. Two thermal couples (K-type, 0.1 mm in diameter) were used to measure cooling temperatures. One was located between the NR fiber and the PP tube for measurement of temperature of the water and the NR fiber, and the second thermal couple was attached to the outer surface of the PP tube, so that the cooling of this tube could be measured. These measurements were conducted for an isometric strain of 100% and twist levels that produced coiled and partially supercoiled NR fibers.

The NR fiber was isometrically twisted and untwisted at 15 turns/s using the servo motor. For an illustrative experiment using the apparatus of Fig. S44A, which provided the cooling curves shown in Fig. S44B, the NR fiber had an initial twist density of 30.0 turns/cm, so complete twist removal required 6 seconds. Figure S44B shows the temperatures of the water and the PP tube decreased to a minimum, and then increased as the system slowly heated back to ambient temperature. The room temperature was 29.74°C. The water and the PP tube decreased to minimum temperatures of 29.04 and 29.13°C, corresponding to temperature decreases of −0.70 and −0.61°C, respectively. The corresponding results for heating curves, during and after twist insertion (Figure S44C), show that the temperatures of the water and the PP tube increased to a

maximum, and then decreased as the system slowly cooled back to ambient temperature. The room temperature was 29.53°C. The water and the PP tube increased to maximum temperatures of 30.35 and 30.24°C, corresponding to temperature increases of +0.82 and +0.71°C, respectively.

The cooling curves and heating curves were corrected for temperature changes due to heat exchange with the environment by using the following method. The long-term temperature dependence of water and container were separately fit to the following equation: $\Delta T(t) = \Delta T(0)\exp(-t/\tau)$, where $\Delta T(t)$ is the temperature with respect to the ambient temperature at elapsed time t and τ is the characteristic time constant for heat exchange (*19*). Correction of the observed temperature change curves for cooling by subtracting for the cooling curves (and adding for the heating curves) the temperature changes resulting from heat exchange with the environment resulted in the curves shown in Fig. S44 B and C. The plateau values correspond to the ambient-loss-corrected temperature changes. These plateau values for water and container were used for the following calculation of the cooling energy and heating energy of the twistocaloric material.

The specific cooling energy of the NR fiber, as a function of released twist density, was calculated using these loss-corrected temperature changes for the cooling of water and the PP tube. The cooling energy contribution (and the heating energy contribution) of the NR fiber that remains after equilibration with water was calculated by approximating that the volume-average temperature of the NR fiber equalled that of the water. This approximation has little effect on the derived specific cooling energy of the NR fiber, since the thereby-calculated residual cooling energy in the NR fiber was from 7.7% to 8.5% of the sum of the cooling energies in the water and in the PP tube. Also, the derived heating energy was little effected by this approximation, since the residual heating energy in the NR fiber was from 7.8% to 8.1% of the sum of the heating energies in the water and in the PP tube. Moreover, the internal thermal equilibration time predicted from the thermal diffusivity (0.05) of the 2.2-mm-diameter NR fiber is 0.96 s (*34*), while the duration of the time for equilibration with the water bath was about 30 s for cooling and 30 s for heating. The heat capacity used for these calculations for the NR fiber, the PP tube, and the water are 1.72, 1.80 (*35*), and 4.18 $JK^{-1}g^{-1}$, respectively.

The above time for adiabatic thermal equilibration ($t_a=0.08R^2/\alpha$, where R is the fiber radius and α is the thermal diffusivity in the radial direction) was calculated as the time to increase the ratio of volume-average temperature change to surface-average temperature change to F, where F is 90%. This time, which was derived using COMSOL5.4 software by approximating that the initial temperature change between fiber center and fiber surface linearly depends on the radial distance from fiber center. Since the thermal diffusivity used is for the non-deformed NR fiber, this equilibration time ignores the effects of torsional and tensile stain on thermal diffusivity in the radial direction.

By dividing the thereby derived specific cooling energy of the NR fiber by the heat capacity of this fiber, the volume-average cooling of the NR fiber was obtained as a function of twist density for isometric twist release at 100% strain. The thereby obtained twist dependence of the ratio of volume-average cooling to surface-average cooling is shown in Fig. 1D. The specific heating energy and the thereby derived dependence of heating during twist insertion (Fig. 1D inset) were analogously obtained as a function of inserted twist.

For the investigated parent natural rubber fiber diameter (2.2 mm) and the used weight ratio of water to natural rubber (4.63), the times for twist insertion and twist removal (and for internal thermal equilibration in the fiber's radial direction) are so short that the times for thermal equilibration with surrounding water determine the cycle rate capability of a twist fridge. Since the thermal equilibration time for heat transfer to the water are for the coiled fiber (or supercoiled fiber)

and the heat transfer time from the water are for the non-twisted fiber, heating and cooling curves (Fig. S44, B and C and corresponding plots for lower inserted twist) enable evaluation of the relative rates of heat transfer for the coiled, supercoiled, and non-twisted states. For this comparison, the mass of fiber and the mass of water per cooler length does not change, since the twist and untwist processes are isometric and the pre-twist stretch (100%) is kept constant. These equilibration times for heat transfer to the water, which range from approximately 30 s to 40 s for the present configuration, do not significantly differ for the fully coiled, partially supercoiled, and non-twisted states.

An apparatus that is nearly identical to that of Fig. S44A was used to measure the specific cooling energy of a NiTi wire during quasi-isometric twist removal. A 0.7-mm-diameter NiTi wire was placed in the center of a 6.5-cm long polypropylene (PP) tube that was sealed at the bottom, like shown in Fig. S44A. The inner and outer diameters of the PP tube were 2.0 and 4.0 mm, respectively. The NiTi wire was tethered at the bottom end and attached to the eighty-step servo motor at the top end. Then the PP tube was filled with water to a height of 6 cm. Twist was quasi-isometrically inserted and removed at near zero tensile strain at a rotation speed of 15 turns/s using the servo motor.

During twist removal, the temperatures of the water and the PP tube decreased to maximum cooling, and then slowly increased as the system equilibrated to the environmental temperature (Fig. S45). The specific cooling energy of the NiTi wire, as a function of released twist density, was obtained analogously to method used above for the NR fiber (from the plateaus in the loss-corrected cooling curves of the water and the PP tube). The approximation that the temperature of the NiTi equals that of the surrounding water (when the loss-corrected cooling curve reach plateau values) has little effect on the derived specific cooling energy of the NiTi wire, since the thereby-calculated residual cooling energy in the NiTi wire was from 6.3% to 7.1% of the sum of the cooling energies in the water and in the PP tube. Based on the thermal conductivity, heat capacity, and density of NiTi wire (*36*, *37*), a 0.7-mm-diameter NiTi wire will internally thermally equilibrate within 2.5 ms, while the time for twist release was between 65 and 455 ms. The heat capacities used for these calculations for the NiTi wire, the PP tube, and the water are 0.55, 1.80, and 4.18 $JK^{-1}g^{-1}$, respectively. This calculated time for radial thermal equilibration in the NiTi wire was obtained by the calculation method used in this section for NR fibers.

By dividing the thereby derived specific cooling energy of the NiTi wire by the gravimetric heat capacity of this wire (0.55 $JK^{-1}g^{-1}$), the volume-average cooling of the NiTi wire was obtained as a function of twist density for quasi-isometric twist release at near zero strain. The thereby obtained twist dependence of volume-average cooling is shown in Fig. 4C. As shown in this figure, the volume-average cooling is essentially identical to the surface-average cooling. This can be explained by the very high thermal conductivity of the NiTi wire, which enables essentially complete thermal equilibration within the wire volume during twist release at 15 turns/s. These measurements (Fig. 4C) provided a maximum specific cooling energy of 7.9 J/g on twist release, which is within the range of cooling energies that are derived from the reported cooling of NiTi wires and sheets from room temperature during stretch-release (5.0 to 9.4 J/g) (*10*, *38*, *39*,*40*, *41*).

18. Twist-removal-based refrigeration of flowing water using plied NiTi wires

18.1. Device for refrigeration of flowing water by untwisting plied NiTi wires

The apparatus illustrated in Fig. S46 was used for refrigeration of continuously flowing water by isometric twist removal from plied NiTi wires. Three-ply, 11.1-cm-long, 0.6-mm-diameter NiTi wires were inserted into a 10.3-cm long polypropylene (PP) tube. The inner and outer diameters

of the PP tube were 1.2 and 1.8 mm. One end of the NiTi wire was torsionally tethered using a clamp, and the other end of the NiTi wire was connected to an eighty-step server motor for twist insertion and twist removal. Both ends of the PP tube were sealed by a cyanoacrylate resin in order to prevent water leakage from this horizontally operated refrigerator. To enable plying and unplying of the NiTi wires, a 10-mm-length of the PP tube was removed, and replaced by a NR tube. The NR tube had inner and outer diameters of 1.5 and 3.0 mm. To provide inlet and outlet pipes for water flowing through the PP tube, two holes were drilled into the PP tube and 0.8-mm-diameter polyethylene tubes were inserted into the two holes and glued in place. A peristaltic pump (model AB55, Goso technology Co., Ltd.) was used for pumping water at a constant flow rate of 0.04 ml/s. Two thermal couples (K-type, 0.1 mm in diameter) were used for temperature measurements. The first thermal couple was inserted into the polyethylene outlet tube for the flowing water (1 mm away from the PP tube). The second thermal couple was attached to the exterior of the PP tube. Twist was isometrically inserted into the NiTi wires using the servo motor at a rotation speed of 50 turns/s. The temperatures of the water and the PP tube increased to a maximum value, and then decreased to room temperature. Then the inserted twist was isometrically removed using the servo motor at a rotation speed of 50 turns/s to form non-twisted NiTi wires. The temperatures of the water and the PP tube decreased, and then slowly equilibrated to room temperature. The specific cooling energy of the NiTi wires as a function of twist density could be obtained from the cooling of water and the cooling of the PP tube during twist removal from the NiTi wires.

18.2. The time dependence of the temperature of flowing water during water cooling by isometric twist removal from plied NiTi wires

Figure S47 shows the time dependence of outlet water temperature for a water flow rate of 0.04 mL/s in the apparatus of Fig. S46. Water heating and cooling were produced by isometrically twisting and untwisting three-ply, 0.6-mm-diameter NiTi wires to provide twist densities of 0.58, 0.68 and 0.87 turns/cm. During twist insertion, the outlet water temperature quickly increased to a peak value and then slowly cooled to room temperature, which indicated that the water flow was carrying the generated heat out of the system. A similar time dependence of water cooling was observed during the twist-release process. The maximum heating and cooling temperatures of flowing water (6.7°C and –4.7°C, respectively) were obtained by inserting the maximum twist (0.87 turns/cm) into the NiTi wires. While the rubber tube that was used in the device of Fig. S46 to enable twist of the NiTi wire is also a twistocaloric material, experiments in which the NiTi wire was replaced by a cotton yarn fiber showed that this rubber tube contributed at its peak only –0.07°C to water cooling. Adding thermal insulation to the water flow pipe of the cooler, increasing the water flow rate to 0.05 ml/s, and increasing the inner diameter of the polypropylene tube to 1.5 mm, increased the peak cooling temperature of the water to -7.7°C.

18.3. The dependence of the derived specific cooling energy due to unplying of NiTi wires on the ratio of water flow length to the total twisted NiTi wire length

We next investigated the dependence of the experimentally derived specific cooling energy from unplying NiTi wires on the ratio of water flow length (the separation between water inlet and water outlet) to the total twisted length of the NiTi wire. The water-flow length was kept constant (at around 5.5 cm) while the length of the twisted NiTi wire was varied. As shown by the results in Table S3, the ratio of flow length to plied wire length has little effect on the derived specific cooling energy and the thereby-derived volume-average cooling of the NiTi wires. As this ratio decreased from 61.6% to 35.4%, the specific cooling energy varied only between 6.60 and 6.88 J/g.

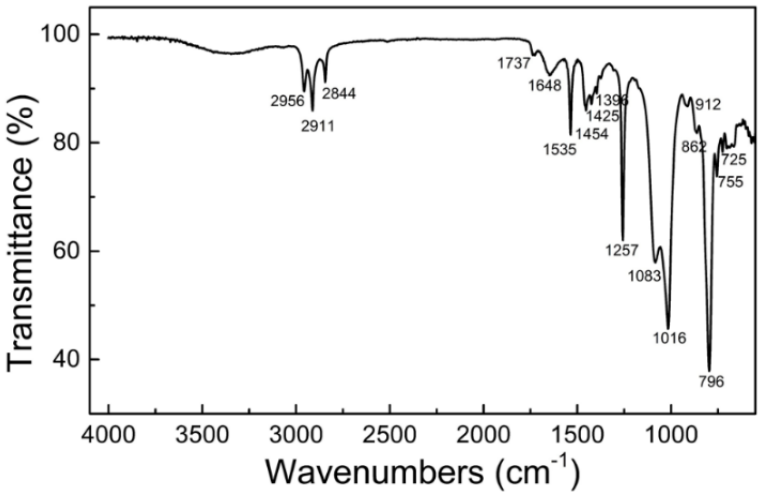

Fig. S1.
The FTIR spectrum of the carbon-black-containing natural rubber fiber.

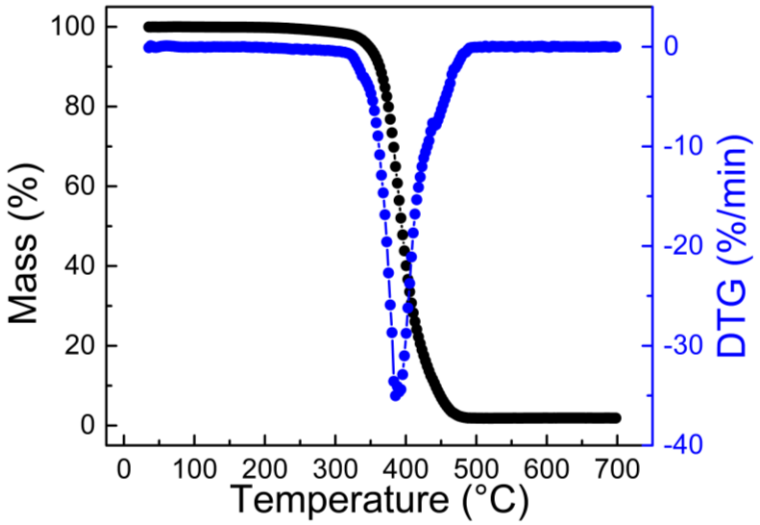

Fig. S2.
Thermogravimetric analysis (TGA) measurements for a 2.2-mm-diameter carbon-black-containing NR fiber when heated at 20°C/min in N_2 atmosphere. The mass of the NR fiber and the time derivative of this mass (DTG) are represented by black and blue curves and data points, respectively.

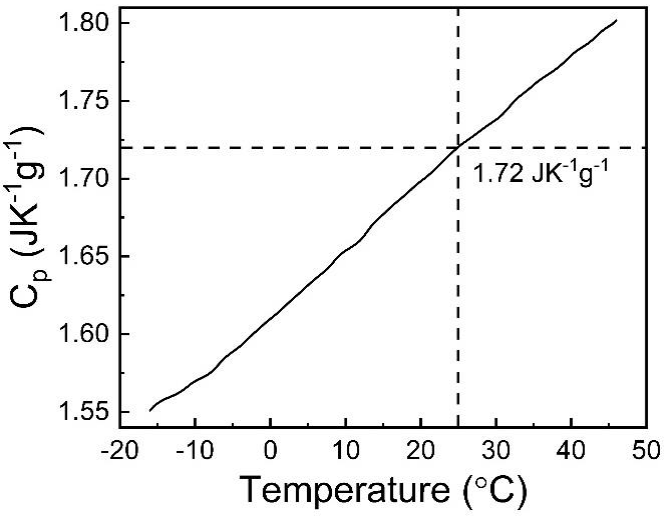

Fig. S3.

The temperature dependence of heat capacity for a 2.2-mm-diameter NR fiber, when measured at a heating rate of 1°C/min in N_2 atmosphere by using a temperature modulation amplitude of ± 0.5°C for the DSC measurements.

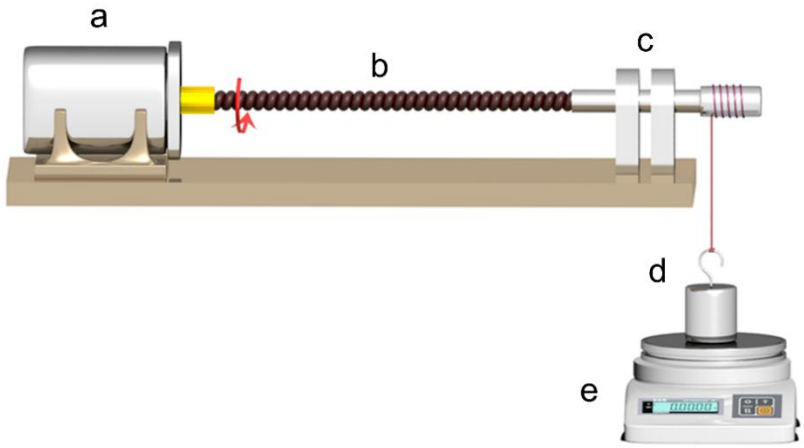

Fig. S4.

Schematic illustration of the apparatus for measuring torque as a function of twist density during isometric twist insertion and twist removal for a NR fiber. The components were (a) a servo motor; (b) a NR fiber; (c) a bearing-supported axle (connecting to the NR fiber) that prohibited fiber length change, about which was wrapped a thread that applied torque to the NR fiber; (d) a weight for providing torque; and (e) a balance for measuring the difference between the force provided by this weight and the force needed during twist and untwist.

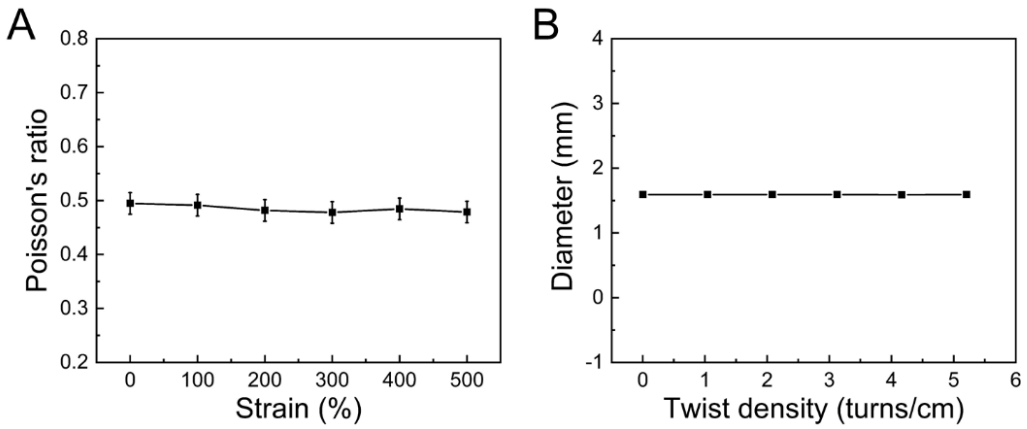

Fig. S5.

(**A**) The Poisson's ratio of a 2.2-mm-diameter NR fiber for different applied strains. (**B**) The independence of the diameter of a NR fiber on twist density for a 2.2-mm-diameter NR fiber that was isometrically stretched to 100% strain. These results imply that negligible volume change occurs during stretching or isometric twist insertion.

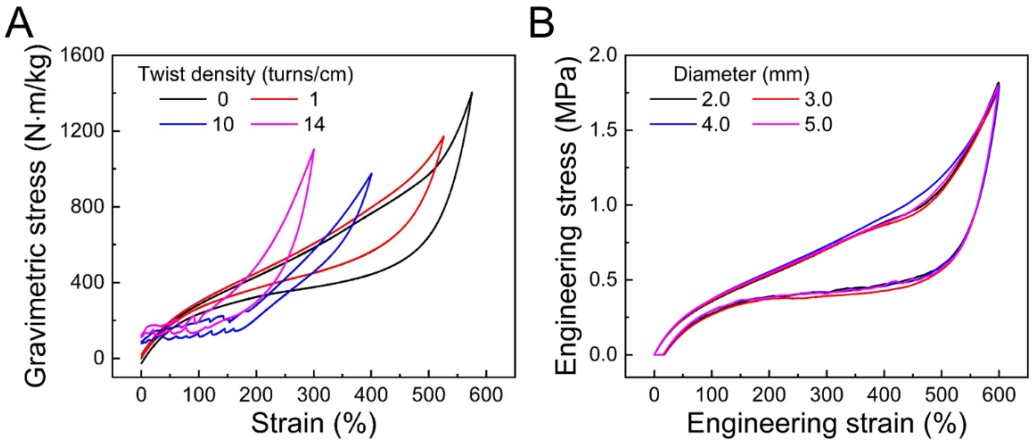

Fig. S6.

Stress-strain curves for (**A**) non-twisted, highly-twisted (1 turns/cm), fully-coiled (10 turns/cm), and partially supercoiled (14 turns/cm) 2.2-mm-diameter NR fibers. (**B**) Stress-strain curves for non-twisted NR fibers having diameters of 2.0, 3.0, 4.0, and 5.0 mm.

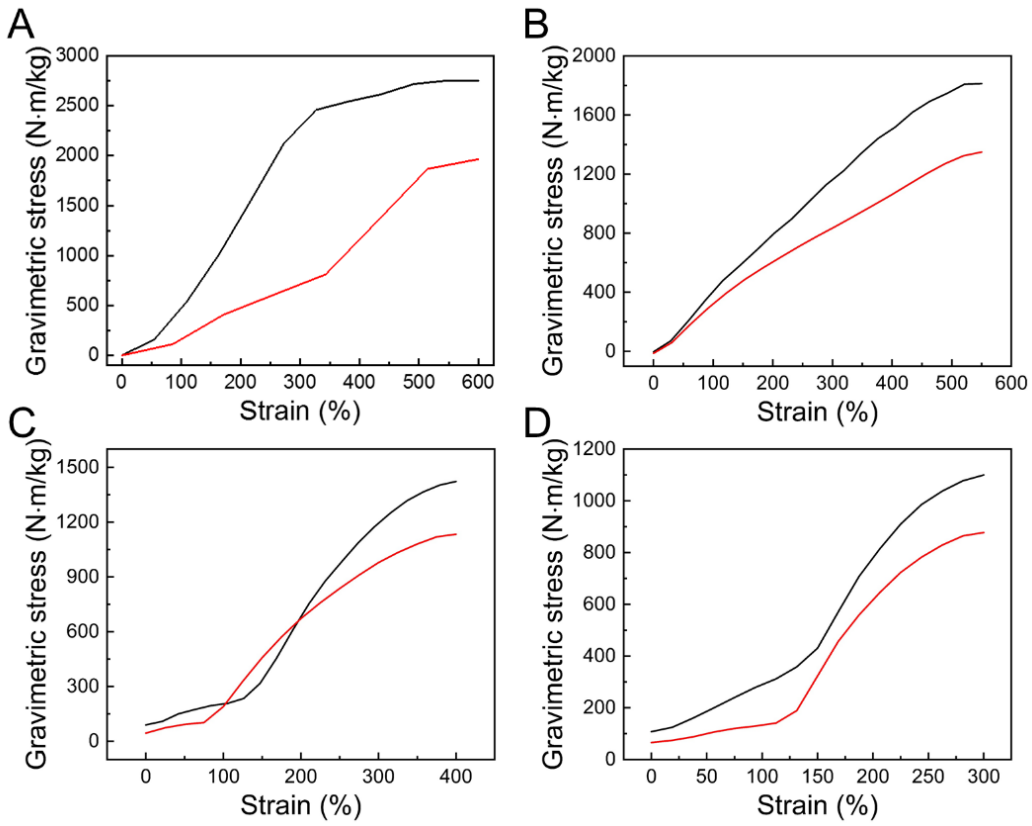

Fig. S7.

Gravimetric stress versus strain curves for (**A**) non-twisted, (**B**) highly-twisted (1 turns/cm), (**C**) fully-coiled (10 turns/cm), and (**D**) partially supercoiled (14 turns/cm) NR fibers, which were obtained during loading (black curve) and unloading (red curve) the NR fibers at a strain-rate of 42 cm/s. These fibers were obtained by isometrically inserting twist into 2.2-mm-diameter parent NR fibers that were 3-cm long. The input and output mechanical energies for these nearly adiabatic stretches and stretch releases, as a function of strain increase and strain decrease, were calculated from the above data. The applied stress at 0% strain is non-zero for the twist-containing fibers (B−D), since the above-reported strains are relative to the length of non-twisted fiber.

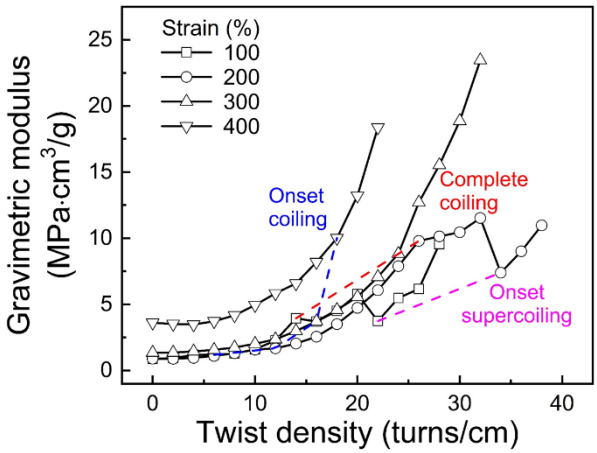

Fig. S8.

The dependence of the gravimetric tensile modulus of a 2.2-mm-diameter NR fiber on twist density for different amounts of strain during isometric twist insertion.

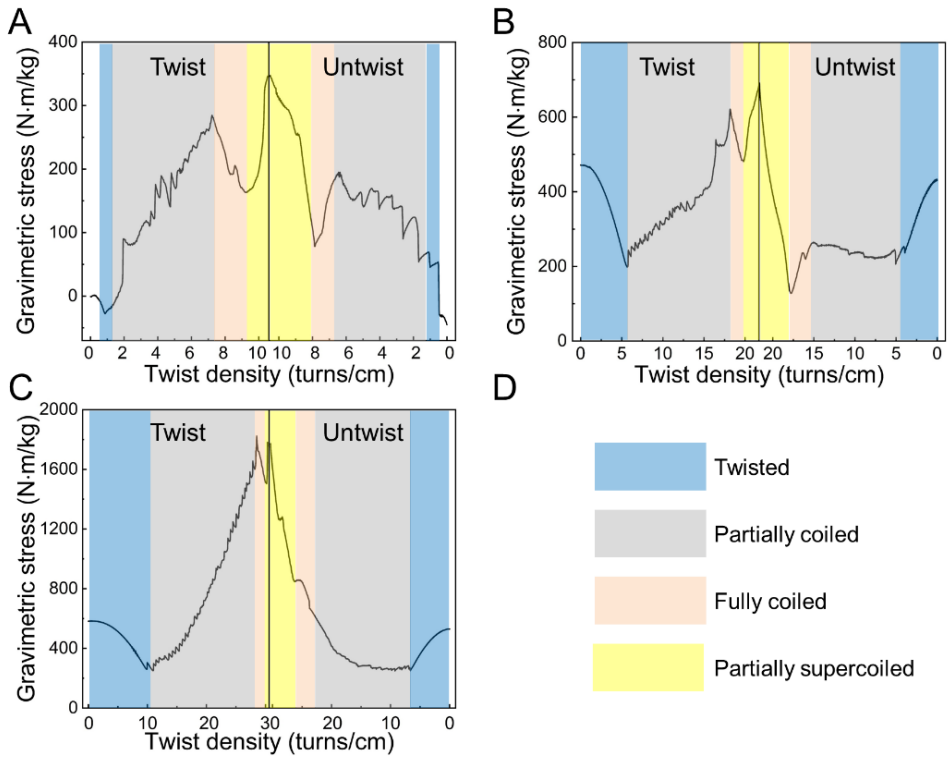

Fig. S9.

(**A**–**C**) Gravimetric tensile stress as a function of the degree of twist during isometric twist insertion and twist removal from a NR fiber that has been stretched to a strain of (**A**) 0%, (**B**) 100%, and (**C**) 200%. The speed of twist insertion and twist removal was 1.7 turns/s and the diameter of the pristine NR fiber was 2.0 mm. (**D**) The gray, yellow, blue, and red colors are for NR fibers with highly twisted, partially coiled, fully coiled, and partially supercoiled structures.

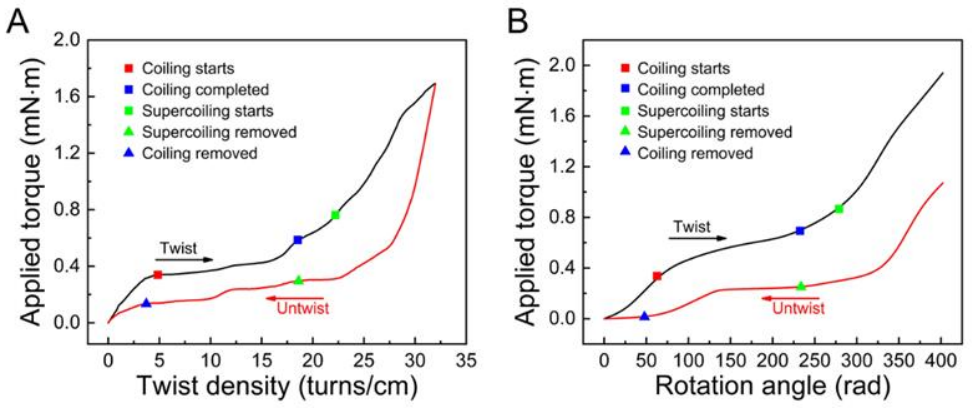

Fig. S10.

Torque on NR fibers during isometric twist insertion and twist removal at 100% strain, which was measured using the apparatus of Fig. S4. (A) The applied torque versus twist density during twist insertion (black line) and twist removal (red line) for a 2.2-mm-diameter, 3-cm-long parent NR fiber and a rotational speed of 1.7 turns/s. The red, blue, and green squares on the curves indicate, respectively, when coiling starts, is completed, and when supercoiling starts during twist insertion. The green and blue triangles during untwist indicate, respectively, when supercoiling is completely removed and when coiling is completely removed. (B) The torque on a 2.2-mm-diameter, 3-cm-long parent NR fiber during isometric twist insertion (black line) and twist removal (red line). The rotational speed for twist insertion and twist removal (50 turns/s) was 30-times that used in (A). Integration of the applied force corresponding to the applied torque over the twist angle range for twist insertion and twist removal provided the input mechanical energy and the recovered mechanical energy, respectively. Unlike the results in (A), where twist insertion was immediately followed by twist release, the NR fiber in (B) was allowed to equilibrate for 3.8 minutes before fiber untwist.

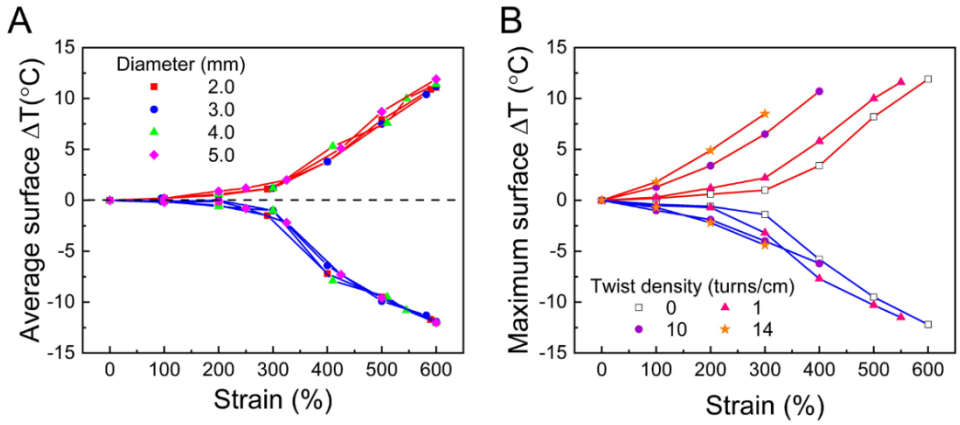

Fig. S11.

(**A**) The surface temperature changes during stretch and stretch release as a function of engineering strain for non-twisted NR fibers having parent diameters of 2.0, 3.0, 4.0, and 5.0 mm, respectively. (**B**) The maximum surface temperature changes versus percent fiber stretch for NR fibers having different amounts of inserted twist. In the initial non-stretched state, fibers having 1, 10, and 14 turns/cm of twist were highly twisted, fully coiled, and partially supercoiled, respectively.

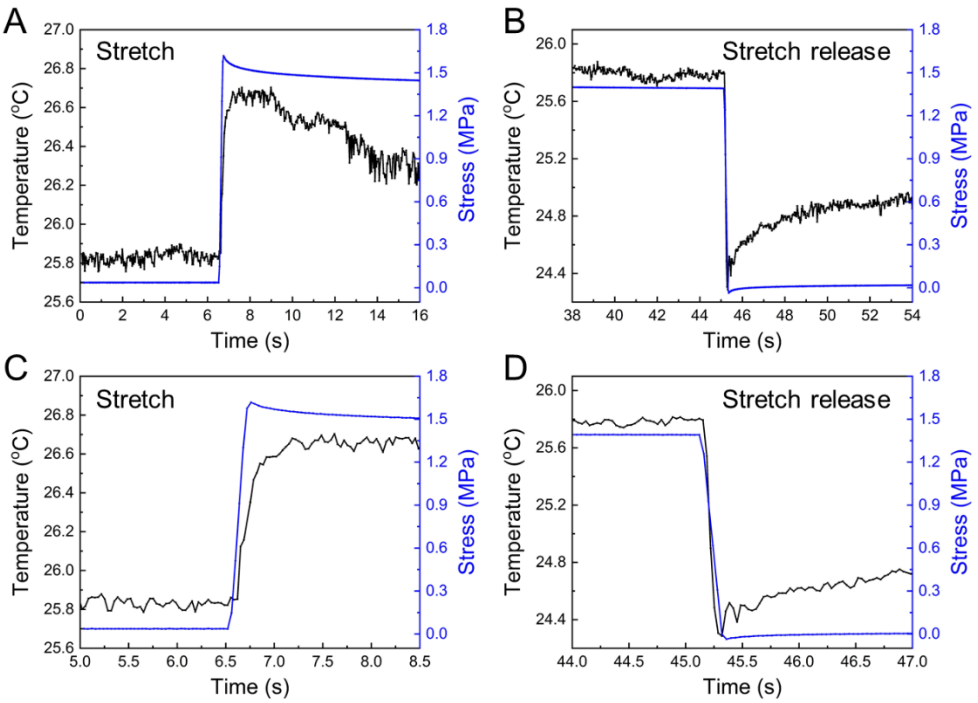

Fig. S12.

(**A, B**) The average surface temperature for a 2.2-mm-diameter parent NR fiber as a function of time during and after stretch and stretch release, respectively, by applying 300% strain, and the time dependence of the tensile stress that resulted from this strain. (**C**, **D**) Zoomed-in regions, for (A) and (B), showing the sharp temperature increase during stretch and the sharp temperature decrease during stretch release, respectively.

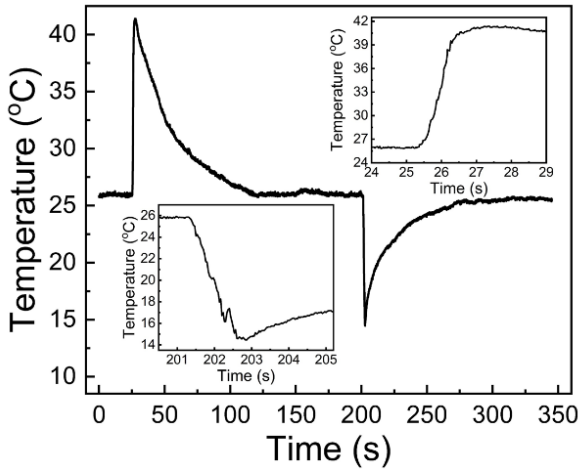

Fig. S13.

The time dependence of maximum surface temperature during and after twist insertion and the time dependence of minimum surface temperature during and after twist removal for a 2.2-mm-diameter NR fiber having an isometric strain of 200%. Insets: Expanded time-scale plots of these time dependencies (upper right and bottom left, respectively).

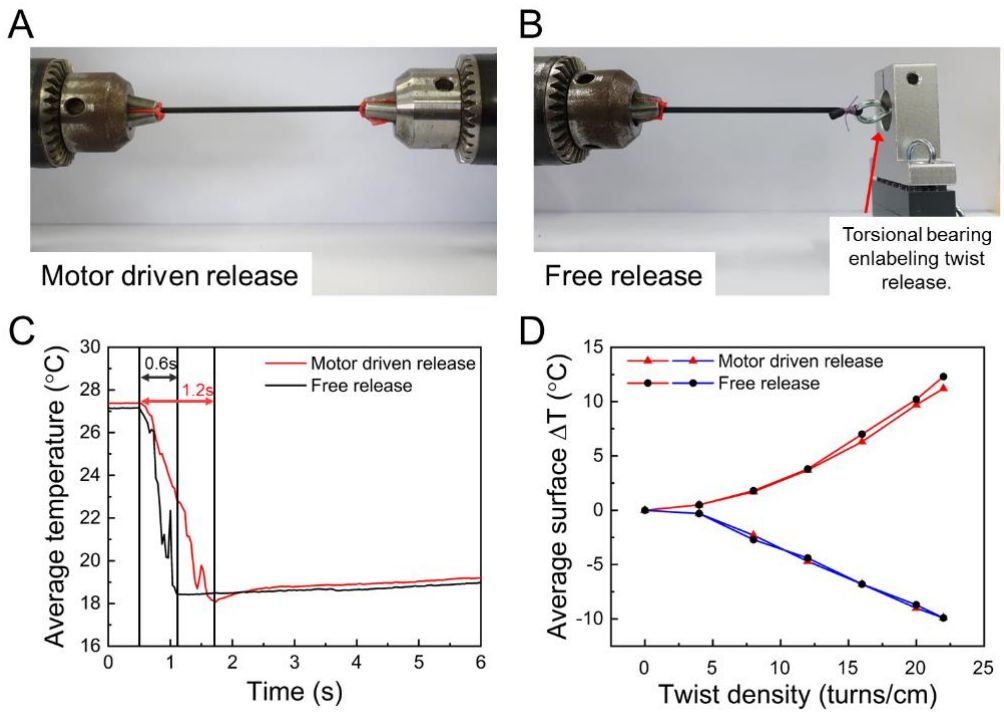

Fig. S14.

The effects of isometric twist release rate on the twistocaloric cooling of a 3-cm-long, 3-mm-diameter NR fiber that is stretched by 100%. (**A**) The apparatus used for motor-driven twist insertion and twist removal at a rotation speed of 50 turns/s. (**B**) The apparatus used for motor-driven twist insertion at a rotation speed of 50 turns/s and unconstrained twist removal using a torsional bearing at an average rotation speed of 100 turns/s. (**C**) The time dependence of average surface temperature during motor-controlled twist release and free twist release using a torsional bearing. The motor-controlled twist release took ~1.2 s, while the free release took ~0.6 s. (**D**) The dependence of average surface temperature changes on twist density during twist insertion and during twist release using the apparatus of (A) and (B). During twist insertion, coiling was initiated at a twist density of 4.0 turns/cm and was completed at a twist density of 10 turns/cm. During twist removal, coil removal was initiated at a twist density of 9.0 turns/cm and was completed at a twist density of 3.8 turns/cm.

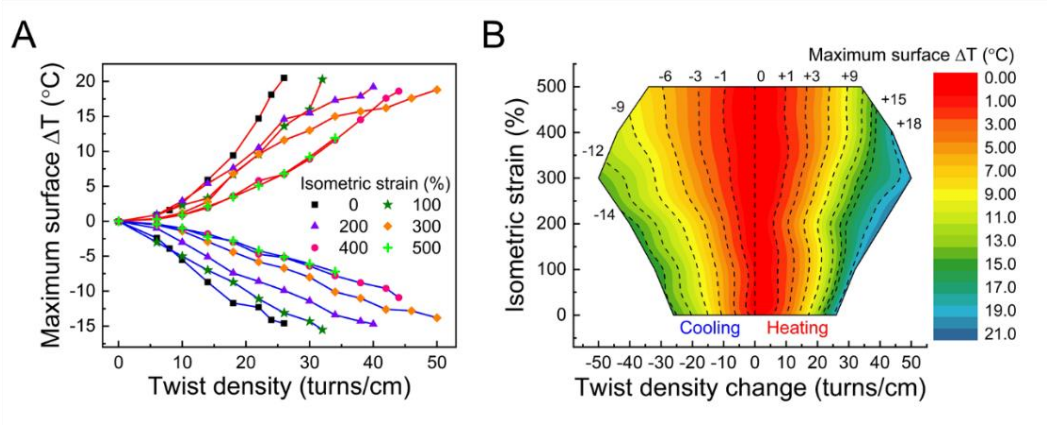

Fig. S15.

(**A**) The maximum surface temperature change of a 2.2-mm-diameter NR fiber during isometric twisting and untwisting at different tensile strains. (**B**) Contour plot showing maximum surface temperature changes (contour lines and colors) as a function of twist density and strain for a 2.2-mm-diameter NR fiber during isometric twist insertion and twist removal at different strains.

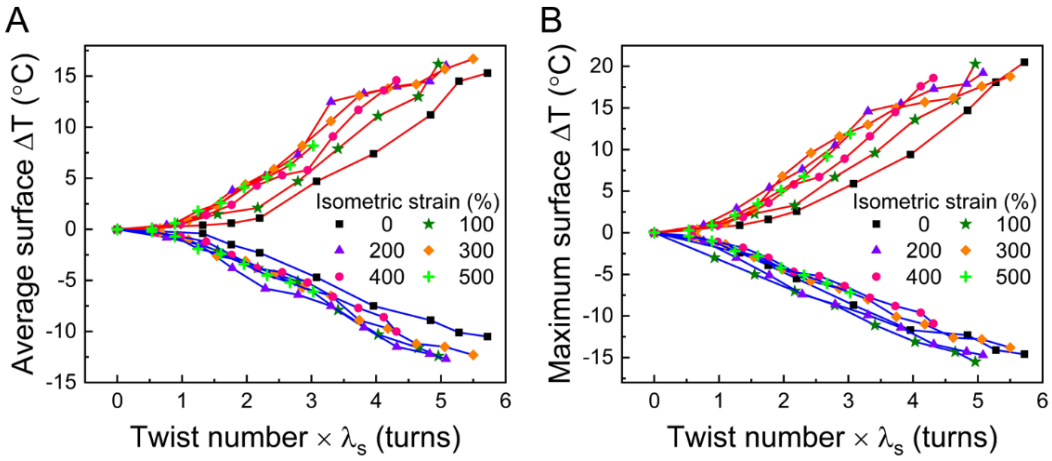

Fig. S16.

(**A, B**) The average (A) and maximum (B) surface temperature changes of a 2.2-mm-diameter NR fiber during isometric twist insertion and twist removal at different isometric strains as a function of the product of twist number and λ_s. λ_s is the extension ratio, which is the ratio of stretched length to non-deformed length.

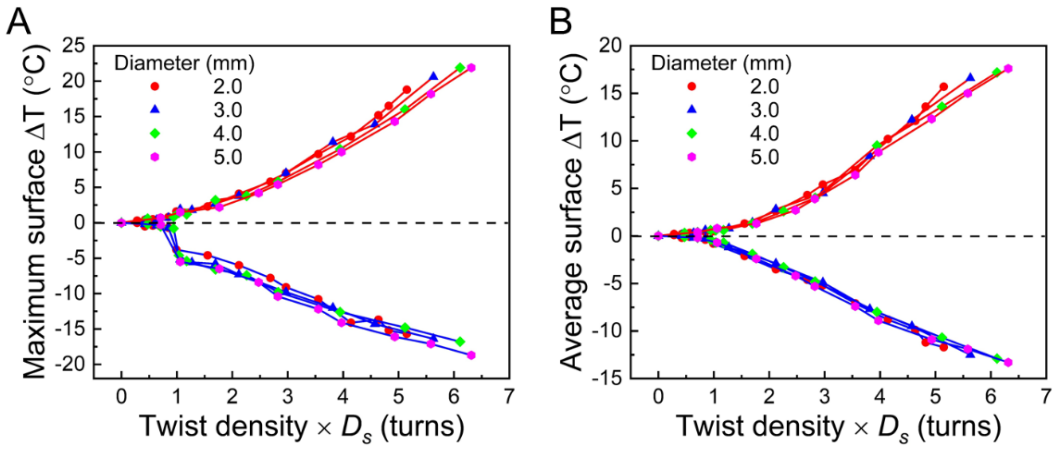

Fig. S17.

Maximum (**A**) and average (**B**) surface temperature changes on isometrically inserting and removing twist as a function of the product of twist density and stretched fiber diameter (D_s) for NR fibers having non-stretched diameters of between 2.0 and 5.0 mm. These measurements were conducted for an isometric stretch of 100%, but the twist density is normalized to the non-stretched length. The discontinuity in maximum surface cooling (A) for a twist density × D_s product of between 0.7 and 1.0 turns corresponds to the complete removal of coiling. The time required for twist insertion decreased from 1.8 s to 0.7 s as the fiber diameter increased from 2 to 5 mm.

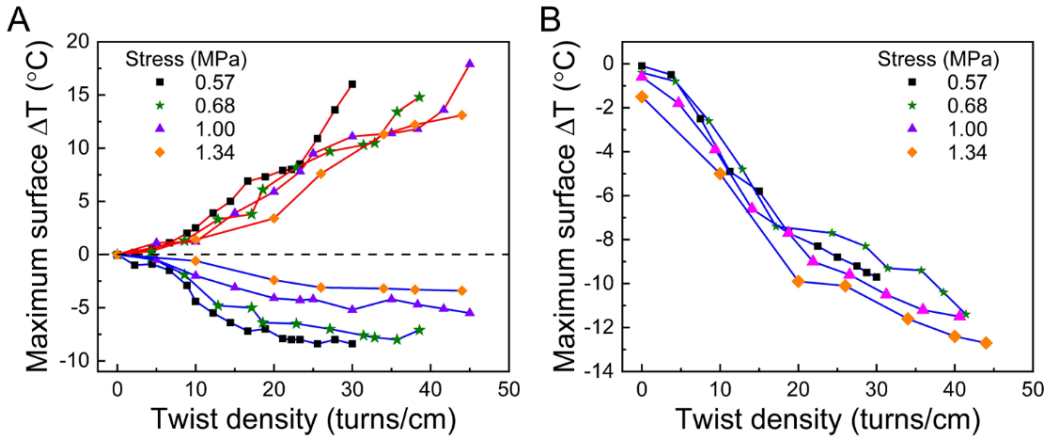

Fig. S18.

(**A**) The twist dependence of the maximum surface temperature changes of a NR fiber during isobaric twist and untwist for different applied stresses. (**B**) The twist dependence of maximum surface cooling of a NR fiber during combination of sequential isobaric untwist and then stretch release. The corresponding data for heating during sequential load application and the twist insertion is not provided because of the difficulty in attaching a load to the fiber without producing subsequent oscillations in fiber length. The NR fiber was 2.2 mm in diameter before stretch or twist insertion.

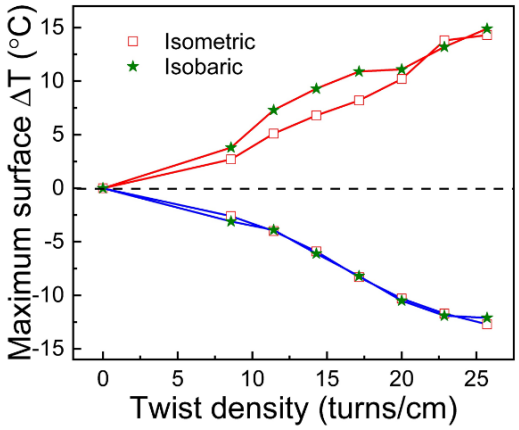

Fig. S19.

Comparison of the twist dependence of maximum surface temperature changes during twist insertion and twist removal for 2.0-mm-diameter NR fibers having the same length and the same inserted twist in the twisted/stretched states, using different twist insertion processes (isometric and isobaric), but the same twist removal process (isometric). The applied stress for the isobaric measurements was 0.70 MPa. Note that twistocaloric cooling was independent of whether twist was inserted isometrically or isobarically.

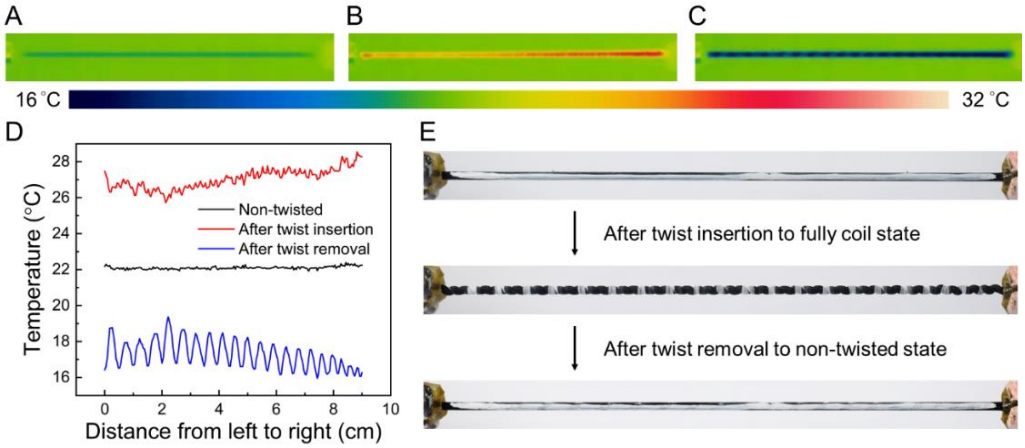

Fig. S20.

(**A**–**C**) Thermal camera images showing the temperature distribution along: (A) the non-twisted NR fiber equilibrated at room temperature, (B) the NR fiber immediately after twist insertion to form the fully coiled fiber, and (C) the NR fiber immediately after removing twist from the thermally equilibrated, fully-coiled fiber. (**D**) The temperature along the fiber length corresponding to (A, black curve), (B, red curve), and (C, blue curve). (**E**) Photographs of the non-twisted NR fiber (top), the fully coiled NR fiber (middle), and the twist-released NR fiber (bottom). A white line, which is apparent in the photographs of (E), was painted along the fiber length so that the effects of twisting and untwisting can be seen. The image for the coiled NR fiber shows there are 44 coils along the length of the coiled fiber, which is the same as the number of thermal fluctuations for the coiled fiber (which corresponds to a wavelength of 1.8 mm). The 2.0-mm-diameter NR fiber formed the fully coiled state at a twist density of 30 turns/cm. The time for twist insertion and twist removal processes for the NR fiber was 1.8 s.

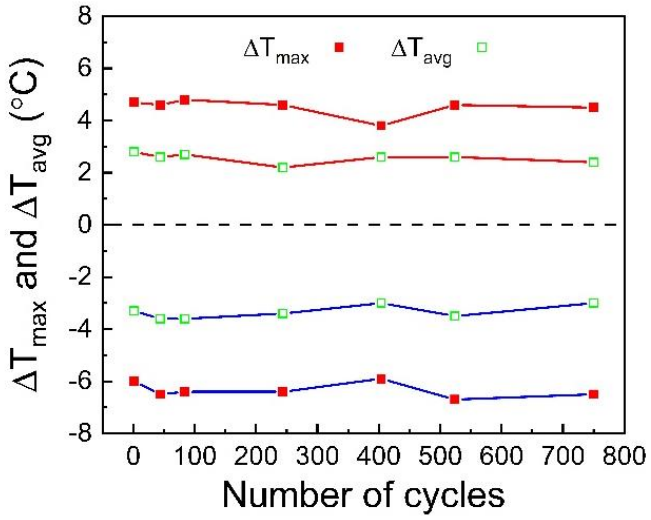

Fig. S21.

The maximum and average surface temperature changes during 750 cycles of isometric insertion and removal of 15 turns/cm of twist at 100% strain for a 2.2-mm-diameter parent NR fiber.

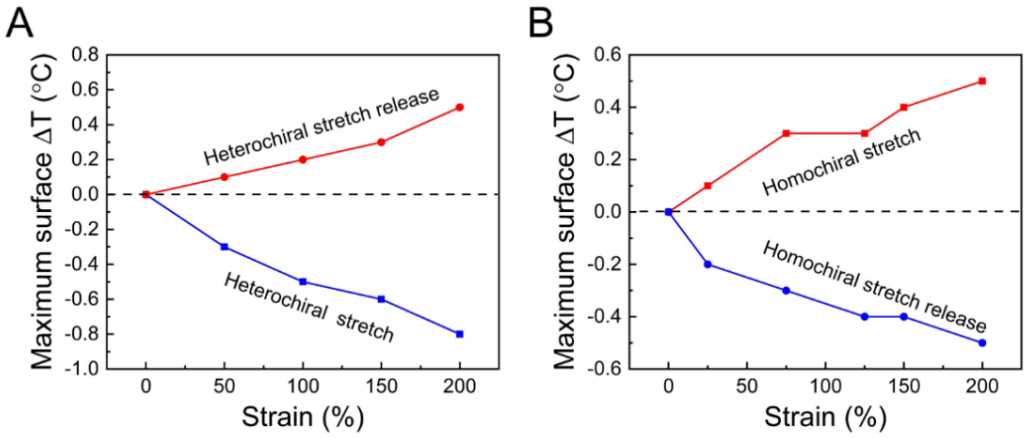

Fig. S22.

Comparison of the dependence of maximum twistocaloric surface temperature changes on the applied tensile strain for (**A**) a heterochiral and (**B**) a homochiral supercoiled NR fiber.

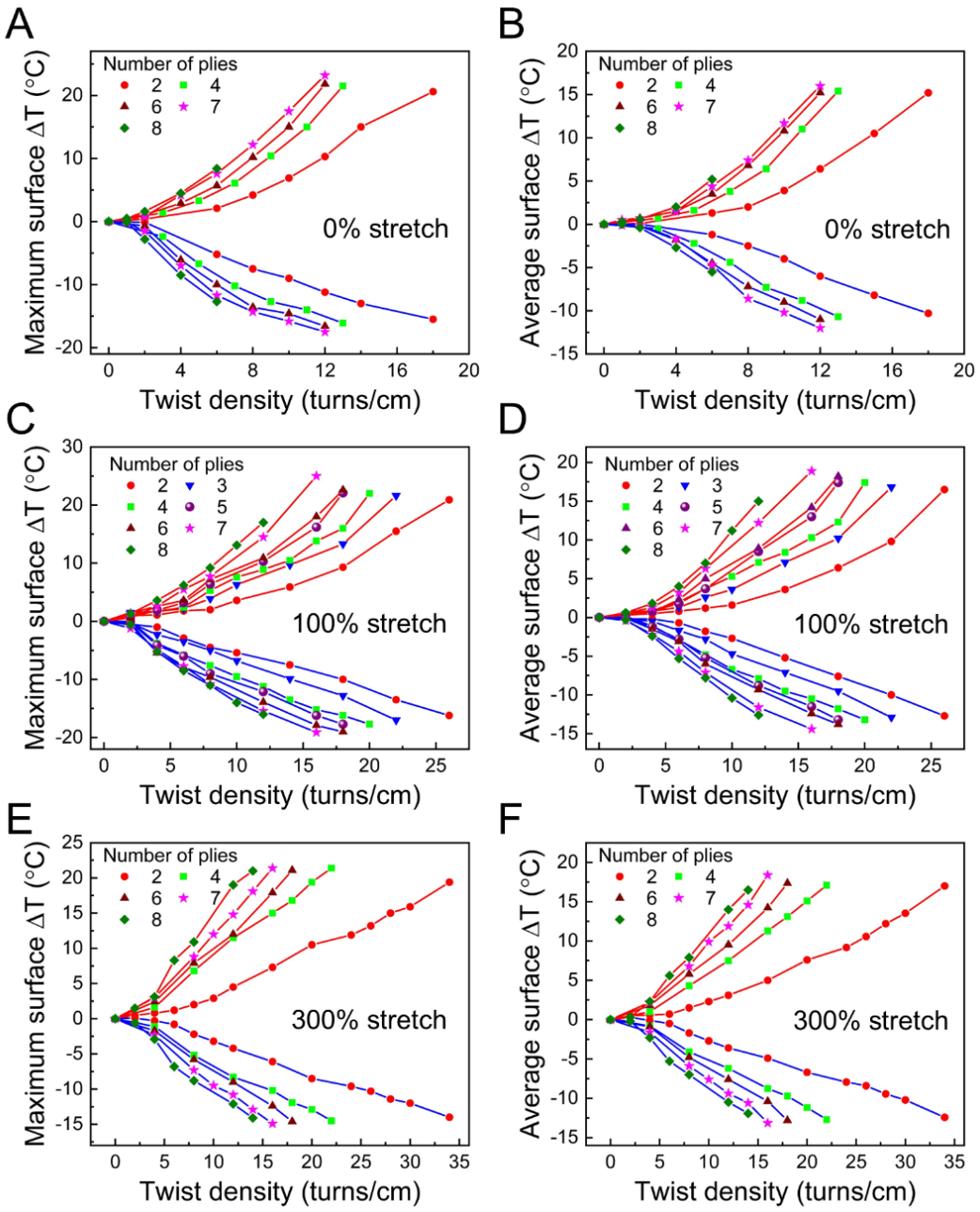

Fig. S23.

The dependences of twistocaloric surface temperature changes on the twist density used for plying at different isometric strains. For plying NR fibers, the twist dependence of the maximum and average temperature changes, respectively, for an isometric stretch of (**A**, **B**) 0%, (**C**, **D**) 100%, and (**E**, **F**) 300%. The diameter of the fibers that are being plied by inserted twist was 2.2 mm before twist or stretch.

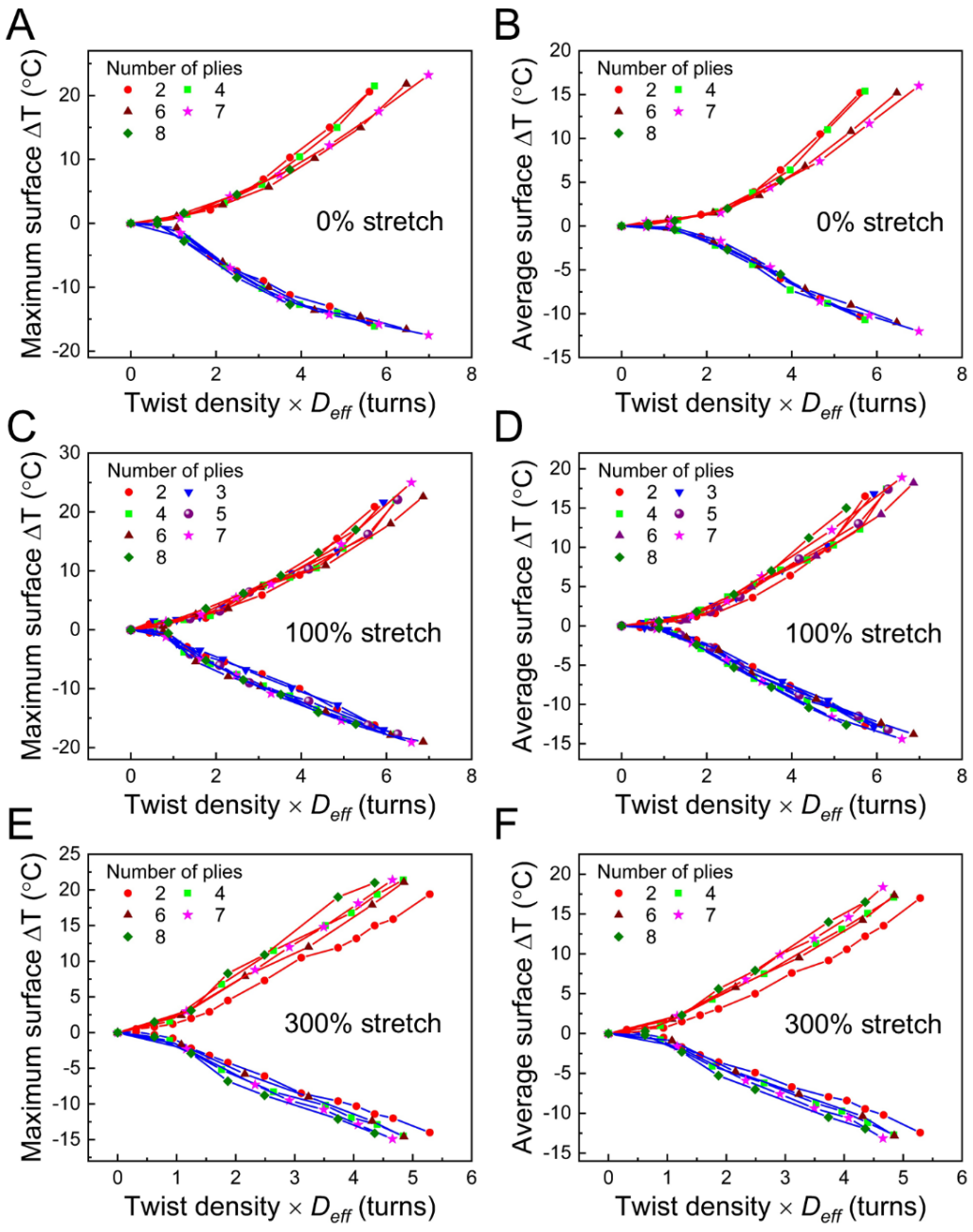

Fig. S24.

The dependences of twistocaloric surface temperature changes produced by plying NR fibers on the product of twist density and the effective diameter of the plied yarn, which are derived using the results of Fig. S23. (**A**, **B**) For NR fibers at 0% isometric strain, the dependences of maximum and average surface temperature changes, respectively, on the product of twist density and the effective diameter of the plied yarn. The effective fiber diameter is $D_{\text{eff}} = n^{0.5} \times D_{\text{s}}$, where n is number of plies and D_{s} is the diameter of each fiber after stretch. (**C**, **D**) The results of A and B, respectively, for NR fibers at 100% isometric strain. (**E**, **F**) The results of A and B, respectively, for NR fibers at 200% isometric strain.

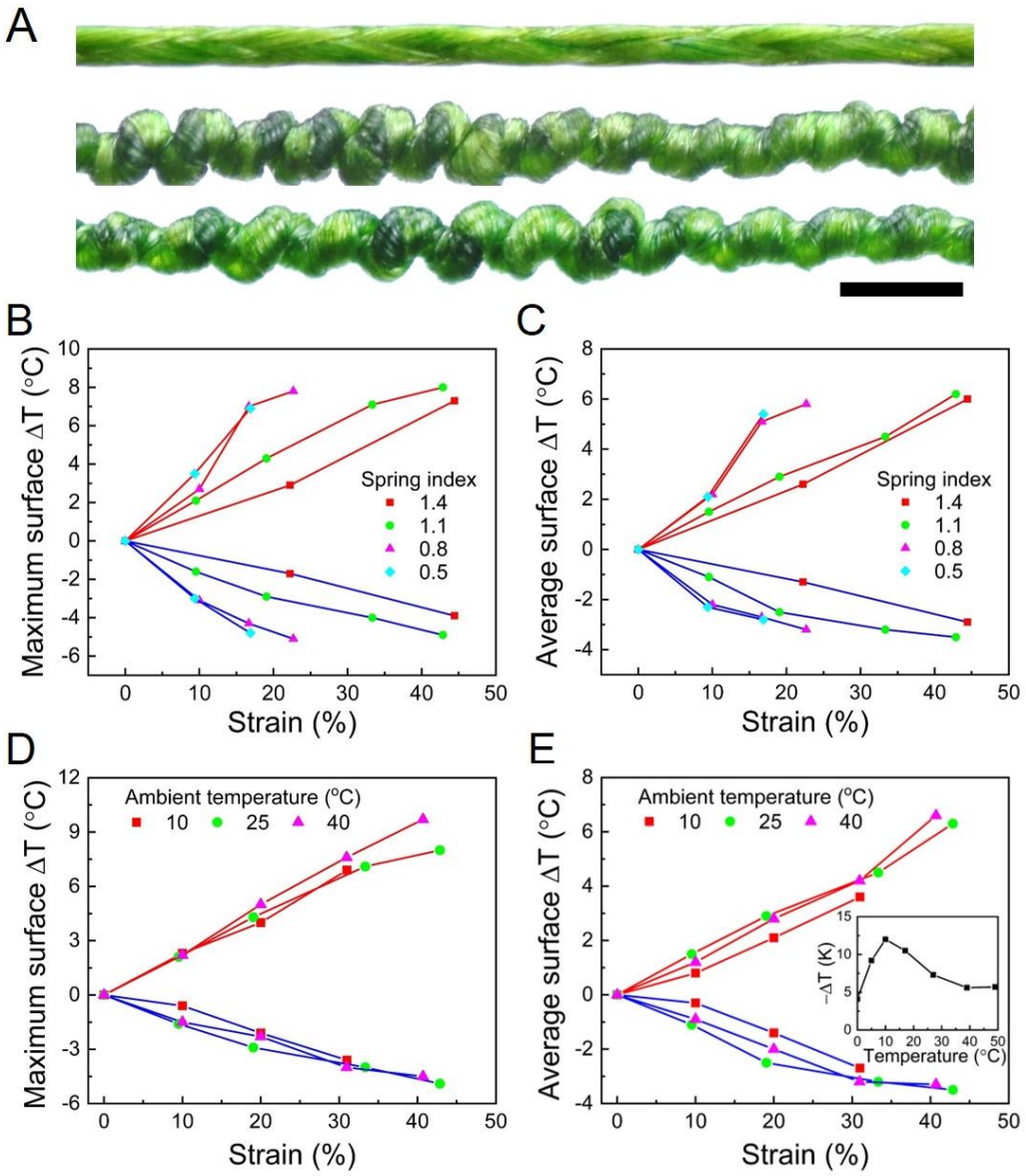

Fig. S25.

(**A**) Photographs of a 0.41-mm-diameter, high-strength, multi-filament polyethylene fishing line before twist insertion (top), after self-coiling (middle), and after stretching the coil by 20% (bottom). The scale bar is 1.0 mm. The fishing line was dyed green by the manufacturer in order to make it less visible to fish. The dependences of (**B**) maximum surface temperature changes and (**C**) average surface temperature changes on applied tensile strain for self-coiled, high-strength polyethylene yarn having different spring indices for an ambient temperature of 25°C. The strain dependences of (**D**) maximum surface temperature changes and (**E**) average surface temperature changes for a self-coiled, high-strength polyethylene yarn having a spring index of 1.1 that was elastically deformed at different ambient temperatures. The inset shows the measured temperature dependence of elastocaloric cooling for a stretched NR fiber (*22*).

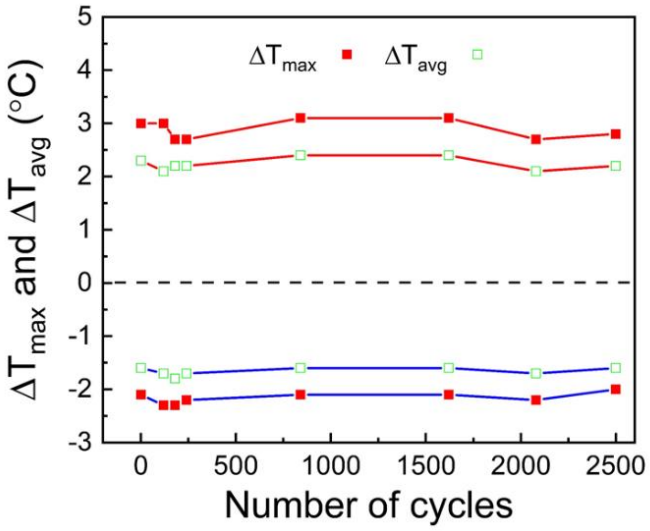

Fig. S26.

The maximum and average surface temperature changes during 2500 stretch and stretch release cycles up to 13% tensile strain for a self-coiled, high-strength polyethylene yarn having a spring index of 1.1.

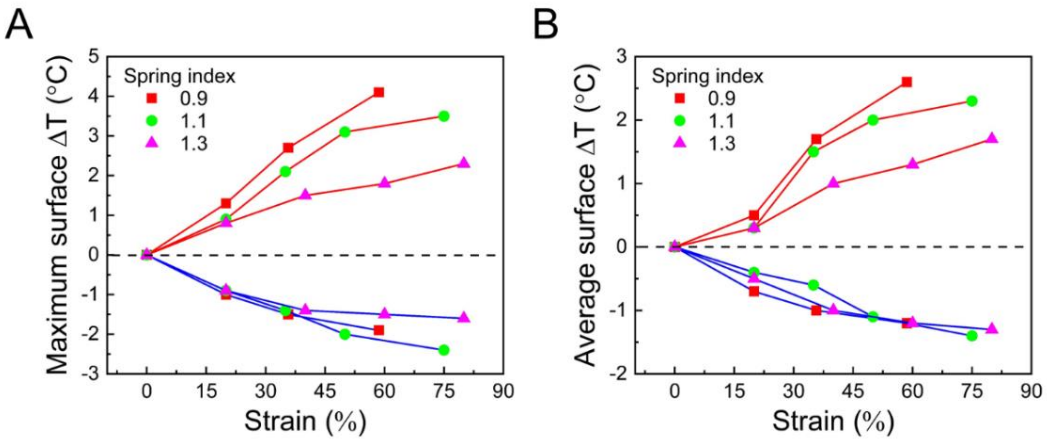

Fig. S27.

Twistocaloric temperature changes on stretch and stretch release for self-coiled, low-strength, low-modulus polyethylene fibers. The dependences of maximum (**A**) and average (**B**) surface temperature changes on stretch and stretch release for self-coiled polyethylene monofilament fiber having different spring indices. The diameter of the polyethylene fiber before twist or stretch was 0.40 mm.

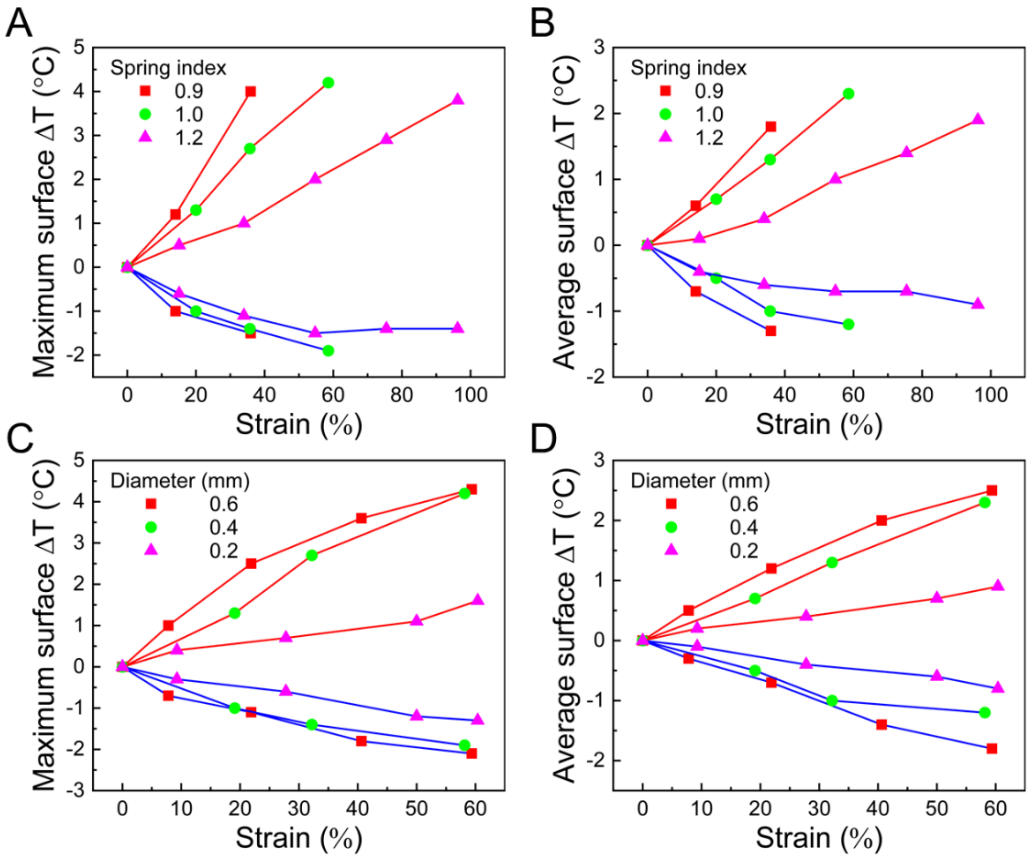

Fig. S28.

Twistocaloric temperature changes on stretch and stretch release for a self-coiled nylon 6 fiber. The dependence of (**A**) maximum surface temperature changes and (**B**) average surface temperature changes on stretch and stretch release for self-coiled nylon 6 fibers having different spring indices. The diameter of the nylon 6 fiber before twist or stretch was 0.4 mm. The dependence of (**C**) maximum surface temperature changes and (**D**) average surface temperature changes on stretch and stretch release for self-coiled nylon 6 fibers having different fiber diameters. The spring index of the different diameter nylon 6 fibers was 1.0.

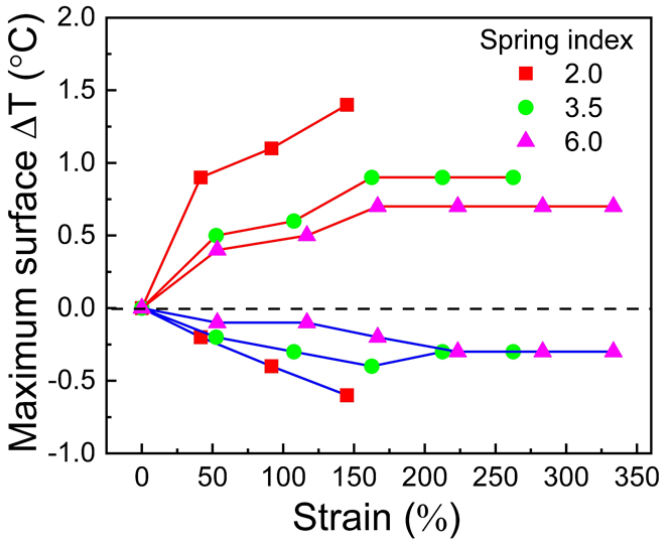

Fig. S29.

Comparison of the dependence of twistocaloric temperature changes on the applied tensile strain for homochiral, mandrel-coiled, low-strength PE fibers having different spring indices.

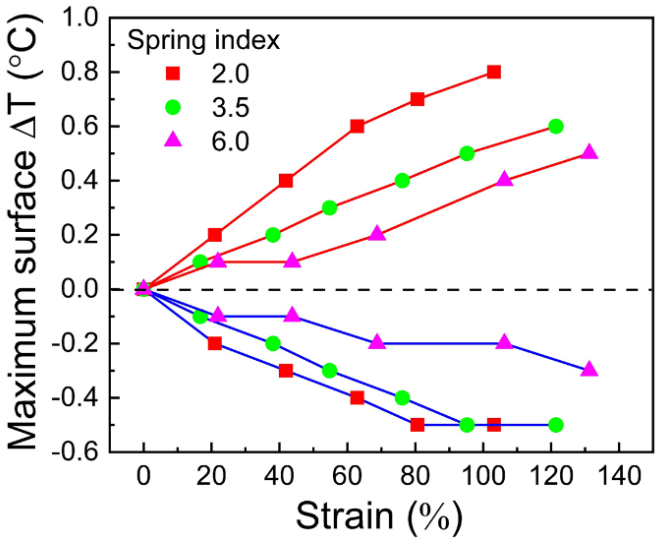

Fig. S30.

Comparison of the dependence of twistocaloric temperature changes on the applied tensile strain for homochiral, mandrel-coiled, thermally set nylon 6 fibers having different spring indices.

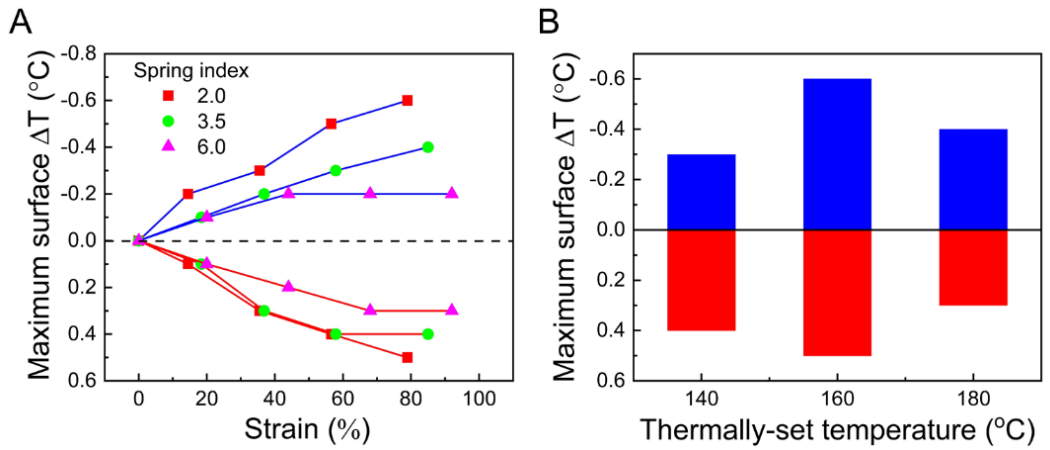

Fig. S31.

Twistocaloric temperature changes during stretch and stretch release of a heterochiral coiled nylon 6 monofilament fishing line. (**A**) Comparison of the dependence of twistocaloric temperature changes on the applied tensile strain for a heterochiral coiled nylon 6 fishing line having different spring indices. (**B**) The dependence of twistocaloric temperature changes on thermal setting temperature for a heterochiral coiled nylon 6 fishing line having a spring index of 2.0. The nylon 6 monofilament fishing line had an initial diameter of 0.40 mm and an initial length of 40 cm. The time for thermal setting was one hour.

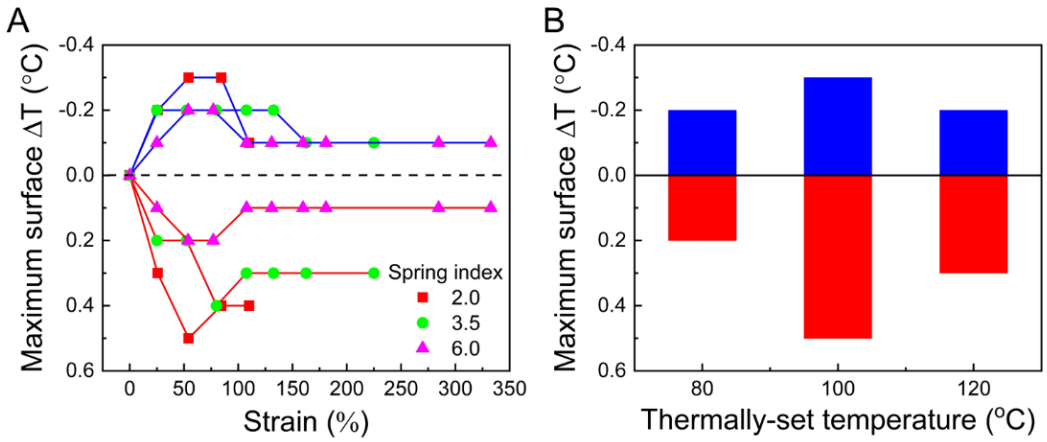

Fig. S32.

Twistocaloric temperature changes on stretch and stretch release for a heterochiral coiled polyethylene fiber. (**A**) Comparison of the dependence of twistocaloric temperature changes on applied tensile strain for heterochiral coiled PE fibers having different spring indices. (**B**) The dependence of twistocaloric temperature changes on thermal setting temperature for a heterochiral, coiled PE fiber having a spring index of 2.0.

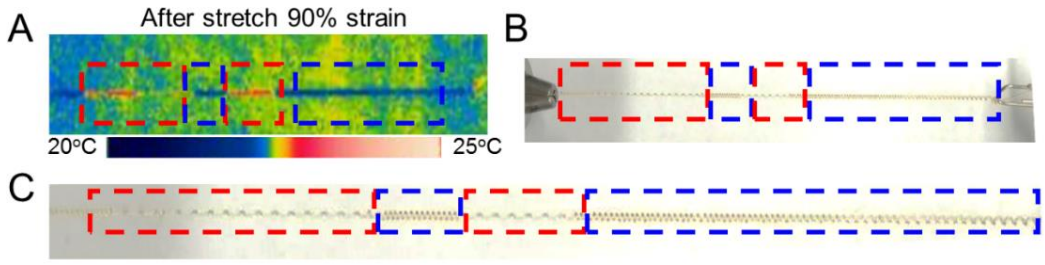

Fig. S33.

Simultaneous existence of heating and cooling for a heterochiral nylon 6 fiber that undergoes irreversible fiber stretch. (**A**) Thermal image and (**B** and **C**) optical photographs of a heterochiral, coiled nylon 6 fishing line immediately after stretch at 42 cm/s to 90% strain. The coiled, heterochiral fiber was made by inserting 6.3 turns/cm of twist in a 0.40-mm-diameter, 40-cm-long nylon fiber, coiling this fiber on a 0.4-mm-diameter steel wire, and then annealing the coiled structure at 160°C for one hour.

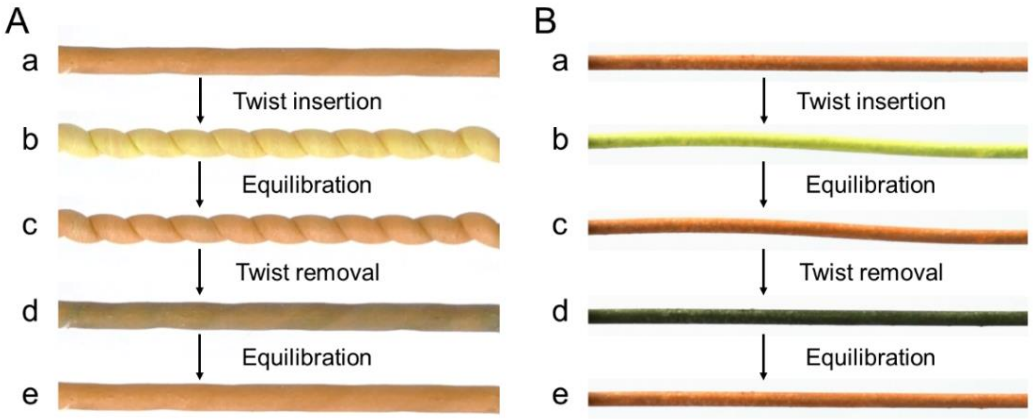

Fig. S34.

(A) Optical photographs showing the surface color changes during isometric twist insertion and twist removal for a 7.0-mm-diameter NR fiber that was stretched to 200% strain and then coated with thermochromic dyes. A 200% stretched NR fiber which is (**a**) non-twisted and at room temperature, (**b**) heated by twist insertion to a fully coiled state, (**c**) cooled by equilibration to room temperature in the fully coiled state, (**d**) cooled by twist removal to produce the non-twisted state, and (**e**) equilibrated to room temperature in the non-twisted state. **(B)** Optical photographs showing the surface color changes of a thermochromic-dye-coated single NiTi wire during quasi-isometric twist insertion and removal. A dye-coated NiTi wire which is (**a**) non-twisted and at room temperature, (**b**) heated by twist insertion to a twisted state, (**c**) cooled by equilibration to room temperature in the twisted state, (**d**) cooled by twist removal to produce the non-twisted state, and (**e**) equilibrated to room temperature in the non-twisted state.

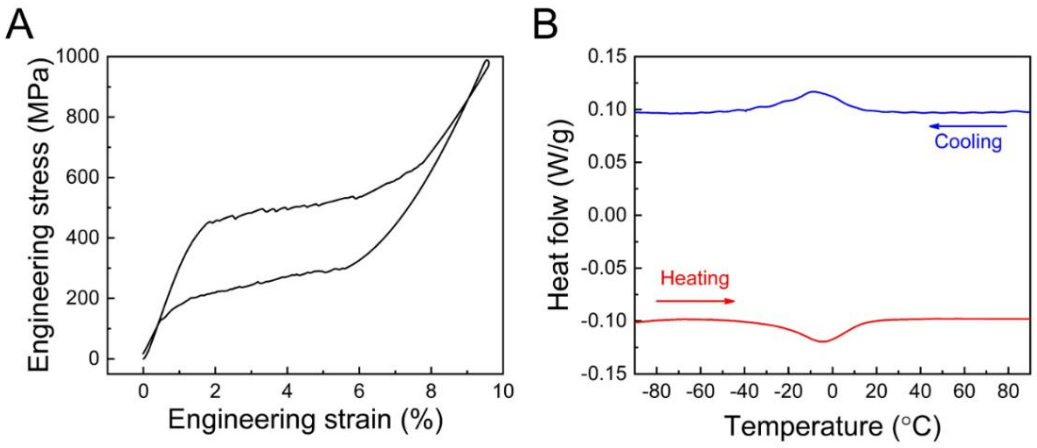

Fig. S35.

(**A**) The stress-strain curve for a 0.7-mm-diameter NiTi wire. (**B**) The DSC curve for a 0.7-mm-diameter NiTi wire measured at a heating rate of 10°C/min in N_2 atmosphere. The composition of the NiTi wire is $Ni_{52.6}Ti_{47.4}$.

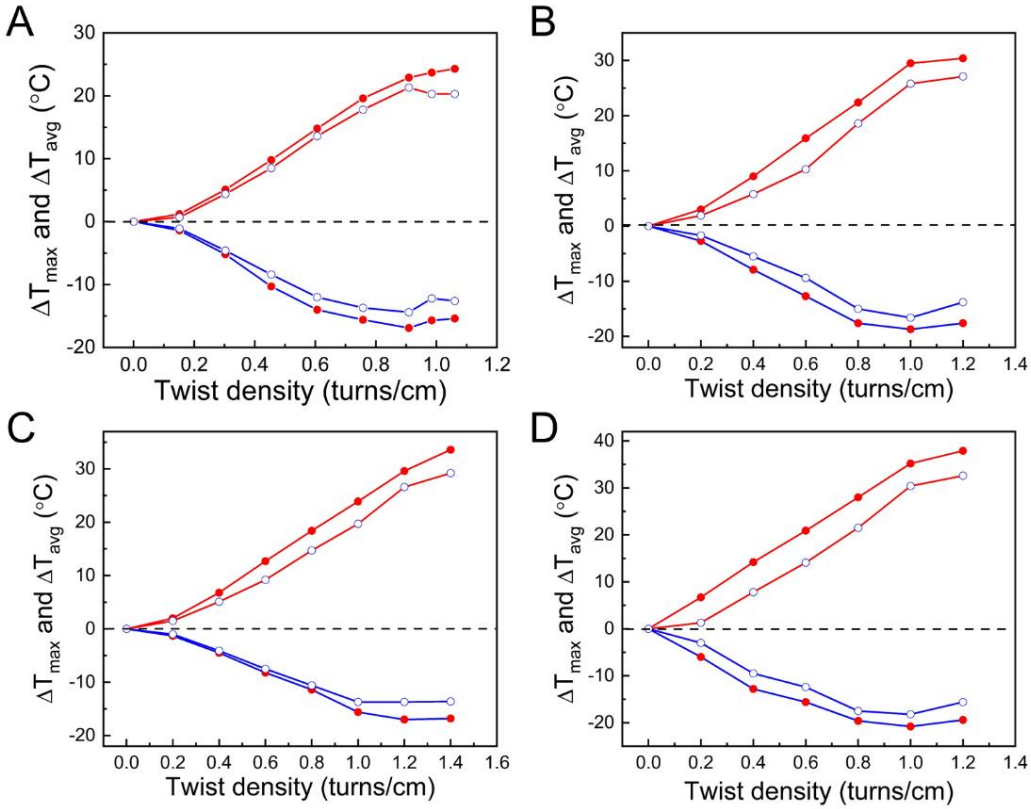

Fig. S36.

The maximum (filled symbols) and average (open symbols) surface temperature changes as a function of twist density for (**A**) quasi-isometric twisting and untwisting a single NiTi wire, and for quasi-isometric plying and unplying (**B**) two-ply NiTi wires, (**C**) three-ply NiTi wires, and (**D**) four-ply NiTi wires.

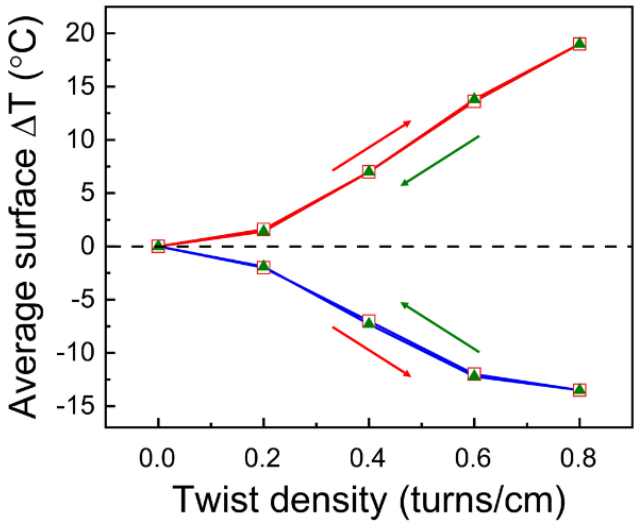

Fig. S37.

The dependence of average twistocaloric surface temperature changes on twist density for a 0.7-mm-diameter single NiTi wire. The open squares are for twist insertion and twist removal steps that progressively increase in twist level and the close triangles are for twist insertion and twist removal steps that progressively decrease in twist level.

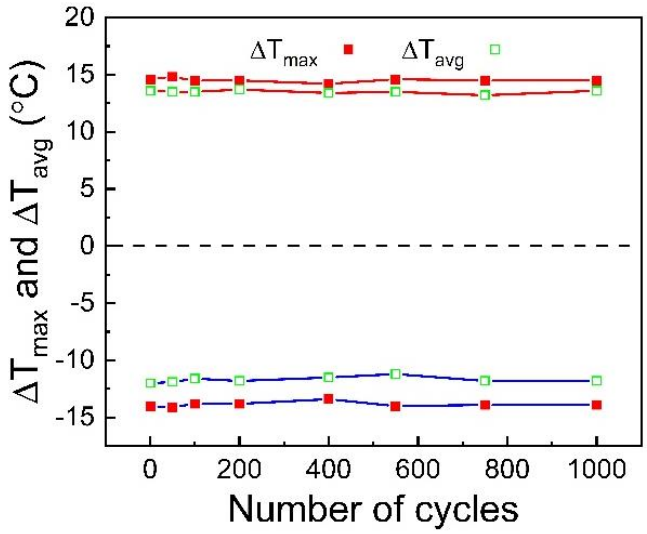

Fig. S38.

The maximum and average surface temperature changes during 1000 cycles of quasi-isometric twist insertion and twist removal up to 0.6 turns/cm of twist for a 0.7-mm-diameter NiTi wire. This experiment is quasi-isometric, even though the separation between wire ends was kept constant, since the length of the NiTi wire increases during twist insertion, causing wire buckling.

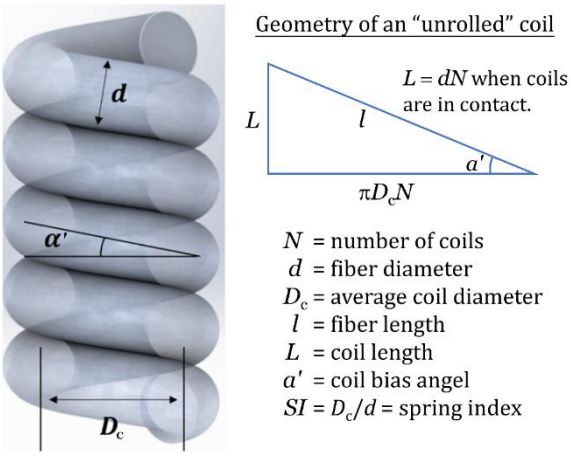

Fig. S39.

The geometry of a coiled fiber. The key geometric parameters for a coil are shown, as well as for the triangle that would be formed if the coil were unrolled. From these considerations, we can conclude that the twist change per fiber length resulting from an applied strain should have an inverse square dependence on coil spring index.

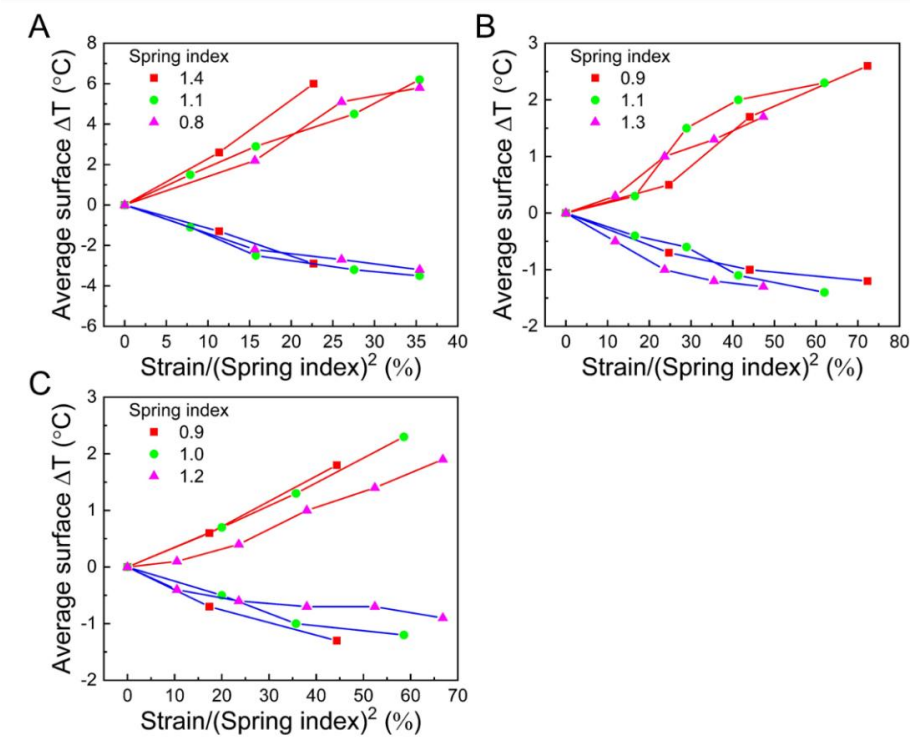

Fig. S40.

Twistocaloric temperature changes for self-coiled polyethylene and nylon fibers. The dependences of the average temperature changes on the ratio of tensile strain and the square of spring index for (**A**) high-strength polyethylene yarns, (**B**) low-strength polyethylene fibers, and (**C**) nylon 6 fibers.

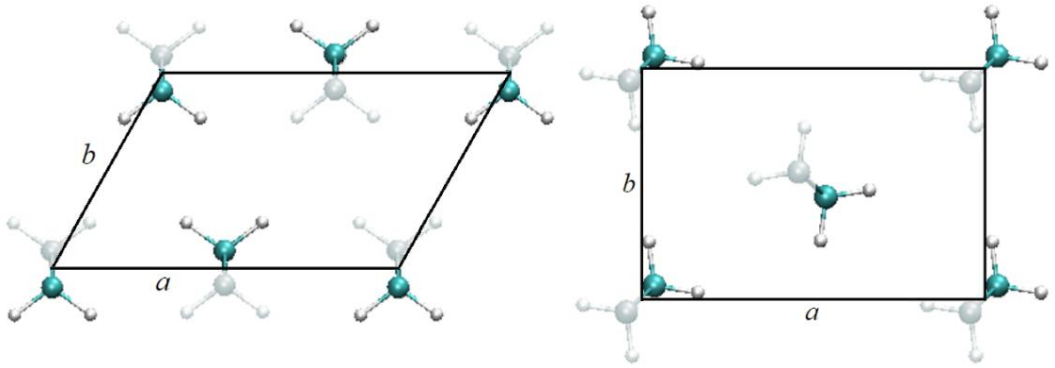

Fig. S41.

The structures for the monoclinic phase (left) and orthorhombic phase (right) of polyethylene. The unit cell parameters (*24*, *26*) are approximately: a = 8.09 Å, b = 4.79 Å, c = 2.53 Å, β = 108° (monoclinic) and a = 7.41 Å, b = 4.95 Å, c = 2.54 Å (orthorhombic).

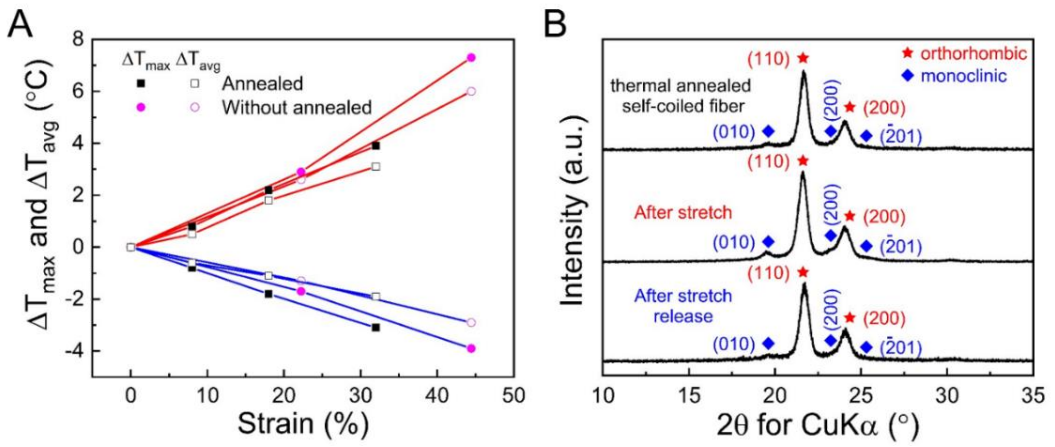

Fig. S42.

(**A**) The dependence of maximum and average twistocaloric surface temperature changes on applied tensile strain for a self-coiled, high-strength polyethylene fiber and for a self-coiled polyethylene fiber that has been annealed for 2 hours at 120°C. (**B**) X-ray diffraction scans for a non-strained, thermally-annealed, self-coiled, high-strength polyethylene fiber (top), for this fiber after 20% stretch (middle), and after release of this stretch (bottom).

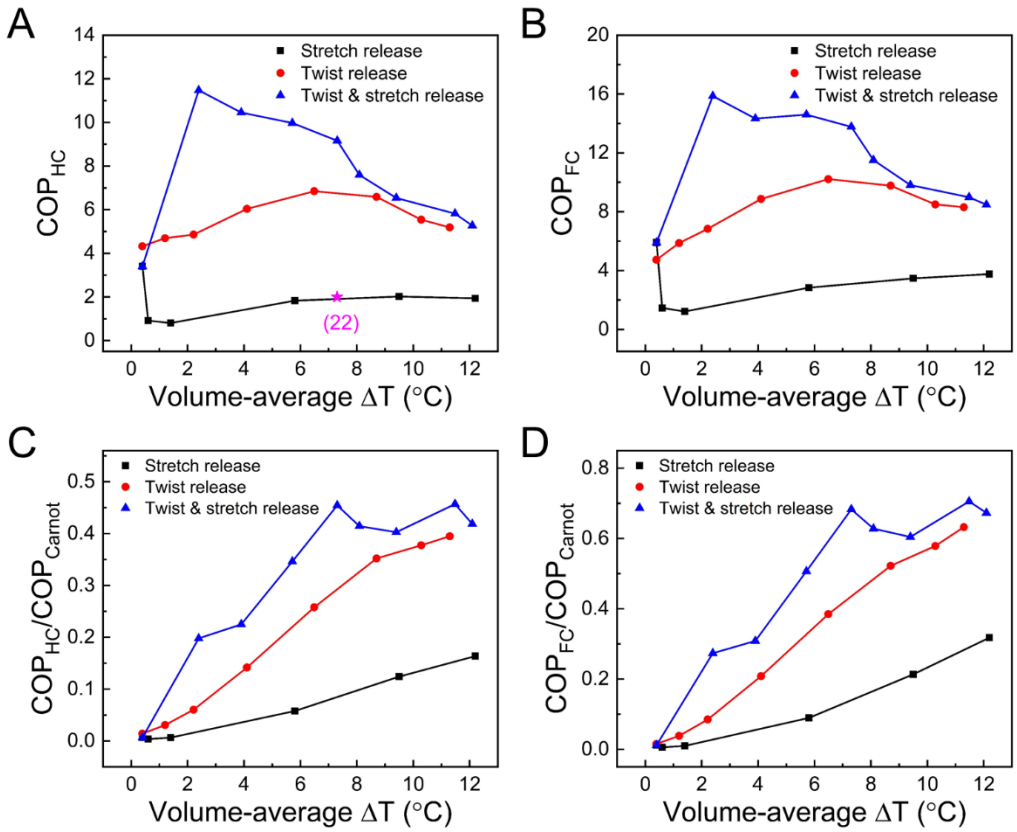

Fig. S43.

For 2.2-mm-diameter NR fibers, (**A**) the COP_{HC}, (**B**) the COP_{FC}, (**C**) the COP_{HC}/COP_{Carnot}, and (**D**) the COP_{FC}/COP_{Carnot}, as a function of the volume-average cooling for, respectively, twist release (red circles), the combination of twist and stretch release (blue triangles) for 100% strain, and for release of up to 600% strain for a non-twisted fiber (black squares). The pink asterisk in (A) is the COP_{HC} for a previously reported NR fiber (*22*) that has undergone release of 600% tensile strain.

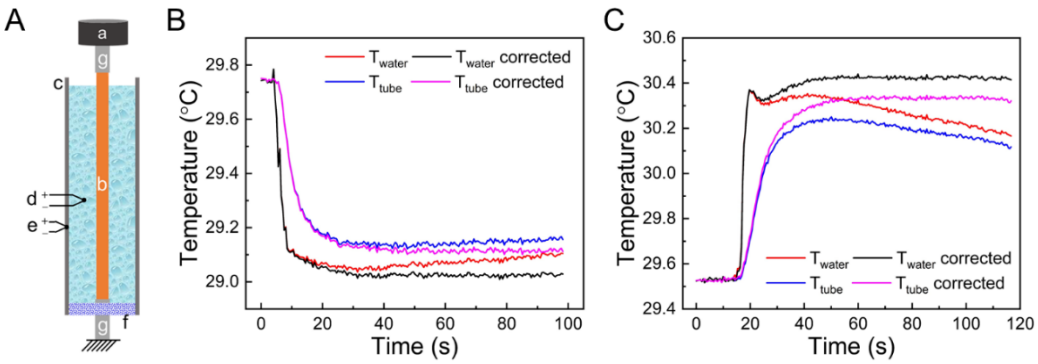

Fig. S44.

(**A**) Schematic illustration of the apparatus for measuring specific cooling energy for a NR fiber as a function of twist density during isometric twist removal by cooling of water. Twist insertion was isometric for a 100%-stretched, 2.2-mm-diameter parent fiber. The components were (a) a 80-step servo motor, (b) a NR fiber, (c) a PP tube filled with water, (d and e) thermocouples for measuring the temperatures of water and the PP tube, (f) epoxy resin for sealing the bottom-end of the PP tube, and (g) clamps for attaching the NR fiber to the motor and for torsional tethering. (**B**) The time dependence of the temperatures of the water and the PP tube during and after isometric twist removal of 30 turns/cm of twist from the NR fiber, as well as the corresponding loss-corrected curves. (**C**). The time dependence of the temperatures of the water and the PP tube during and after isometric insertion of 30 turns/cm of twist, as well as the corresponding loss-corrected curves.

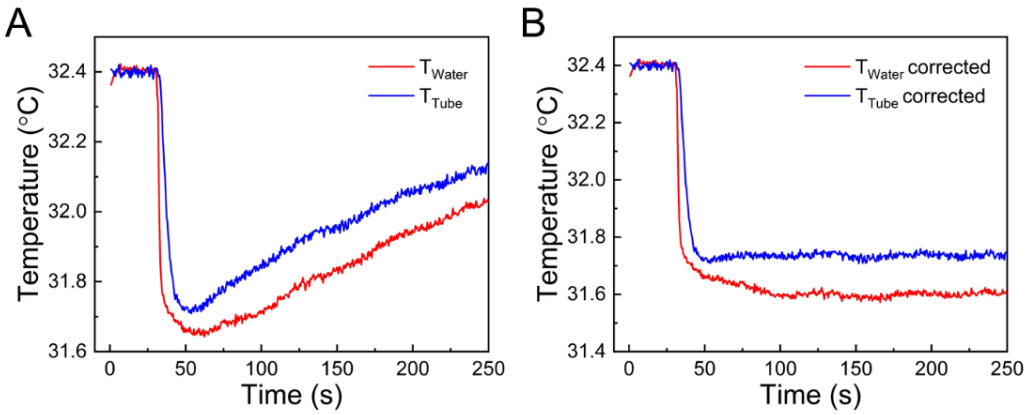

Fig. S45.

(**A**)The time dependences of temperatures of the water and the outer surface of the PP tube during isometric removal of 0.7 turns/cm of twist from a 0.7-mm-diameter, non-stretched NiTi wire, using an apparatus nearly identical to that shown in Fig. S44A. (**B**) Correction of the cooling curves of (A) for heat exchange with the environment.

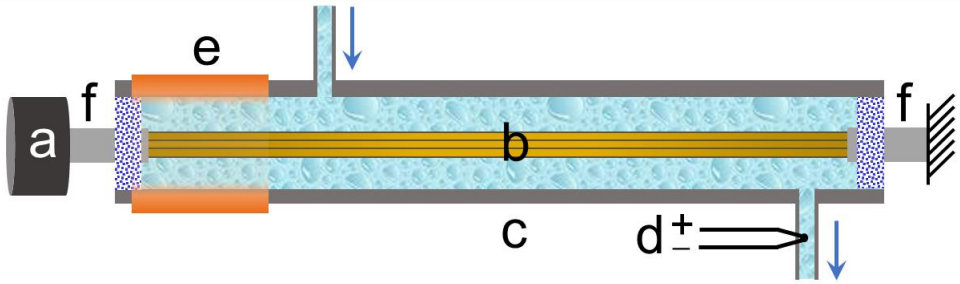

Fig. S46.

Schematic illustration of the apparatus for cooling flowing water by unplying NiTi wires. The components are (a) a 80-step servo motor, (b) plied NiTi wires, (c) a PP tube filled with flowing water, (d) a thermocouple for measuring the water temperature in the outlet pipe, (e) the rubber tube that seals the PP-tube water chamber, while still allowing twisting of the NiTi wires, and (f) the epoxy resin that seals both ends of the PP tube.

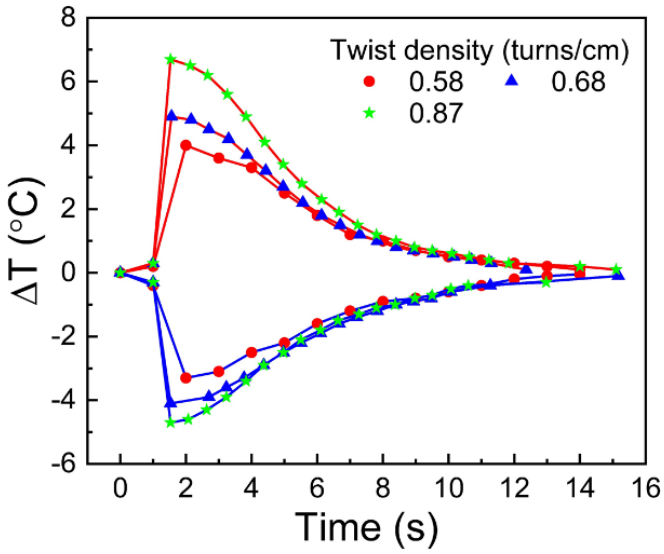

Fig. S47.

Time dependence of outlet water temperature for isometric twist insertion and twist removal of three-ply, 0.6-mm-diameter NiTi wires at a water flow rate of 0.04 mL/min using the apparatus in Fig. S46.

Table S1.

Comparison of the maximum and average mechanocaloric surface temperature changes during isometric twist insertion and twist removal at 0% strain and the temperature changes during stretch and stretch release of the non-twisted fibers. At the indicated twist densities, the natural rubber, Spandex, and SEBS rubber fibers are partially supercoiled, the EPDM rubber, TPU, and PDMS fibers are partially coiled, and the NiTi wire is non-coiled.

Fiber type	**Fiber diameter (mm)**	**Twist density (turns/cm)**	**Twist density × diameter (turns)**	**ΔT_{max} and ΔT_{avg} during twist (°C)**	**ΔT_{max} and ΔT_{avg} during untwist (°C)**	**Percent stretch**	**ΔT during stretch (°C)**	**ΔT during stretch release (°C)**
Natural rubber	2.2	26.0	5.72	+20.5 +15.3	−14.6 −10.5	600%	+11.9	−12.2
3-ply Spandex rubber	0.2	31.0	0.62	+22.1 +14.6	−11.4 −9.1	520%	+6.6	−7.1
EPDM rubber	2.0	24.1	4.82	+15.2 +12.0	−7.0 −5.2	200%	+2.3	−2.6
SEBS rubber	4.0	70.2	28.1	+5.1 +3.5	−2.2 −1.0	1000%	+0.2	−0.3
TPU	3.0	6.1	1.83	+11.3 +6.0	−3.5 −1.8	240%	+4.3	−1.2
PDMS	1.0	25.3	2.53	+2.7 +1.8	−0.9 −0.6	500%	+1.6	−0.6
Single-ply NiTi wire	0.7	0.9	0.063	+24.3 +21.3	−17.0 −14.4	6%	+21.0	−17.0
Four-ply NiTi wire	0.7	1.0 twist of plying	0.14	+35.2 +30.4	−20.8 −18.2	6%	+21.0	−17.0

Table S2.

Summary of CuKα XRD results for non-stretched, stretched, and stretch-released coiled yarns of high-strength polyethylene fishing line. The relative intensities of monoclinic (mono), orthorhombic (ortho), and amorphous peaks are indicated. These results are used to derive the weight percent of the crystalline phases that is in the monoclinic phase and in the orthorhombic phase (next-to-last column) and the ratio of amorphous scattering intensity to the total scattering intensity by both the amorphous and crystalline phases (last column) for the non-stretched, 10% stretched, 20% stretched, and stretch-released yarns.

Peak		1	2	3	4	5	Intensity of amorphous	Mono/Ortho	Amorphous /Crystalline
Non-stretched	Intensity (%)	0.707	45.98	1.056	17.54	1.624	33.09	5.03% mono 94.97% ortho	0.494
	(*hkl*) mono	010		200		$\bar{2}01$			
	(*hkl*) ortho		110		200				
10% stretched	Intensity (%)	0.886	45.09	2.143	17.29	1.688	33.16	6.80% mono 93.20 ortho 1.77% change	0.496
	(*hkl*) mono	010		200		$\bar{2}01$			
	(*hkl*) ortho		110		200				
20% stretched	Intensity (%)	1.802	42.01	3.867	16.96	1.945	33.48	11.43% mono 88.57% ortho 6.39% change	0.503
	(*hkl*) mono	010		200		$\bar{2}01$			
	(*hkl*) ortho		110		200				
Stretch-released	Intensity (%)	0.700	45.76	1.098	17.65	1.698	32.99	5.21% mono 94.79% ortho 0.18% change	0.492
	(*hkl*) mono	010		200		$\bar{2}01$			
	(*hkl*) ortho		110		200				

Table S3.

The effect of the ratio of water flow length (~5.5 cm) to total plied NiTi wire length for measurements conducted using constant flow length and flow rate.

NiTi wire length (cm)	15.8	10.3	9.0
Ratio of flow length to wire length (%)	35.4	58.2	61.6
Ratio of water length in tube to wire length (%)	72	73	78
Maximum cooling of water (°C)	4.7	4.7	4.1
Mass ratio of water in tube to NiTi alloy	0.0375	0.0345	0.0401
Specific cooling energy of NiTi wire (J/g)	6.88	6.75	6.60
Volume average cooling of NiTi wire calculated from cooling energy (°C)	12.5	12.3	12.0

Movie S1.

The temperature changes of a 2.0-mm-diameter, 3-cm-long natural rubber fiber during isometric twist insertion and twist removal at 200% strain at a twist rate of 50 turns/s. A twist of 30 turns/cm was isometrically inserted to produce a fully coiled fiber and the same twist was isometrically removed to produce a non-twisted fiber. The maximum and minimum surface temperatures of the natural rubber fiber were recorded using a thermal camera (FLIR T440) during isometric twist insertion and twist removal. The movie segments during twist insertion and twist removal are slowed-down to 4X real time. The times required for equilibration for this 2.0-mm-diameter NR fiber are not shown.

Movie S2.

The color changes of a 7.0-mm-diameter natural rubber fiber coated with a thermochromic dye during isometric twist insertion and twist removal at 200% strain. A twist of 6.4 turns/cm was isometrically inserted to produce a fully coiled fiber and the same twist was isometrically removed to produce a non-twisted fiber. The color changes are from orange to yellow after twist insertion, to orange after equilibration to room temperature, to dark green after twist removal, and then to orange after equilibration to room temperature. The movie segments during twist insertion and twist removal are slowed-down to 4X real time and the movie segments during resulting color changes are sped-up to 1/4 real time. The times required for equilibration for this very large diameter NR fiber are not shown.

Movie S3.

The color changes during 13% stretch and stretch release for a 0.41-mm-diameter, 6.8-cm-long, self-coiled polyethylene fishing line that was coated with a cholesteric liquid crystal. The color changes are from green to purple during stretch, to green after equilibration at room temperature, to orange after stretch release, and then to green after equilibration to room temperature. The movie segments during stretch and stretch release are slowed down to 4X real time. The times required for thermal equilibration are not shown.

Movie S4.

The color changes of a 0.7-mm-diameter, 2.4-cm-long NiTi wire coated with a thermochromic dye, during quasi-isometric twist insertion and twist removal. A twist of 0.8 turns/cm was quasi-isometrically inserted and the same twist was removed to form a non-twisted wire at a twist rate of 50 turns/s. The color changes are from orange to yellow after twist insertion, to orange after equilibration to room temperature, to dark green after twist removal, and then to orange after equilibration to room temperature. The movie segments during twist insertion and twist removal are slowed-down to 8X real time. The times required for equilibration for this 0.7-mm-diameter NiTi wire are not shown.

References and Notes

1. J. Gough, A description of a property of caoutchouc or Indian rubber; with some reflections on the cause of the elasticity of this substance. *Mem. Lit. Phil. Soc. Manchester 1 (2nd Series)* **288**, 288–295 (1805).

2. R. Ma, Z. Zhang, K. Tong, D. Huber, R. Kornbluh, Y. S. Ju, Q. Pei, Highly efficient electrocaloric cooling with electrostatic actuation. *Science* **357**, 1130–1134 (2017). doi:10.1126/science.aan5980 Medline

3. B. Neese, B. Chu, S. G. Lu, Y. Wang, E. Furman, Q. M. Zhang, Large electrocaloric effect in ferroelectric polymers near room temperature. *Science* **321**, 821–823 (2008). doi:10.1126/science.1159655 Medline

4. E. Defay, R. Faye, G. Despesse, H. Strozyk, D. Sette, S. Crossley, X. Moya, N. D. Mathur, Enhanced electrocaloric efficiency via energy recovery. *Nat. Commun.* **9**, 1827 (2018). doi:10.1038/s41467-018-04027-9 Medline

5. M. Trček, M. Lavrič, G. Cordoyiannis, B. Zalar, B. Rožič, S. Kralj, V. Tzitzios, G. Nounesis, Z. Kutnjak, Electrocaloric and elastocaloric effects in soft materials. *Philos. Trans. R. Soc. London Ser. A* **374**, 20150301 (2016). doi:10.1098/rsta.2015.0301 Medline

6. X. Moya, S. Kar-Narayan, N. D. Mathur, Caloric materials near ferroic phase transitions. *Nat. Mater.* **13**, 439–450 (2014). doi:10.1038/nmat3951 Medline

7. T. Gottschall, A. Gràcia-Condal, M. Fries, A. Taubel, L. Pfeuffer, L. Mañosa, A. Planes, K. P. Skokov, O. Gutfleisch, A multicaloric cooling cycle that exploits thermal hysteresis. *Nat. Mater.* **17**, 929–934 (2018). doi:10.1038/s41563-018-0166-6 Medline

8. A. Chauhan, S. Patel, R. Vaish, C. R. Bowen, A review and analysis of the elasto-caloric effect for solid-state refrigeration devices: Challenges and opportunities. *MRS Energy Sustain.* **2**, E16 (2015). doi:10.1557/mre.2015.17

9. J. Cui, Y. Wu, J. Muehlbauer, Y. Hwang, R. Radermacher, S. Fackler, M. Wuttig, I. Takeuchi, Demonstration of high efficiency elastocaloric cooling with large ΔT using NiTi wires. *Appl. Phys. Lett.* **101**, 073904 (2012). doi:10.1063/1.4746257

10. J. Tušek, K. Engelbrecht, L. P. Mikkelsen, N. Pryds, Elastocaloric effect of Ni-Ti wire for application in a cooling device. *J. Appl. Phys.* **117**, 124901 (2015). doi:10.1063/1.4913878

11. J. Tušek, K. Engelbrecht, D. Eriksen, S. Dall'Olio, J. Tušek, N. Pryds, A regenerative elastocaloric heat pump. *Nat. Energy* **1**, 16134 (2016). doi:10.1038/nenergy.2016.134

12. Y. Liu, I. C. Infante, X. Lou, L. Bellaiche, J. F. Scott, B. Dkhil, Giant room-temperature elastocaloric effect in ferroelectric ultrathin films. *Adv. Mater.* **26**, 6132–6137 (2014). doi:10.1002/adma.201401935 Medline

13. Y. Li, D. Zhao, J. Liu, S. Qian, Z. Li, W. Gan, X. Chen, Energy-efficient elastocaloric cooling by flexibly and reversibly transferring interface in magnetic shape-memory alloys. *ACS Appl. Mater. Interfaces* **10**, 25438–25445 (2018). doi:10.1021/acsami.8b07703 Medline

14. S. Qian, Y. Geng, Y. Wang, T. E. Pillsbury, Y. Hada, Y. Yamaguchi, K. Fujimoto, Y. Hwang, R. Radermacher, J. Cui, Y. Yuki, K. Toyotake, I. Takeuchi, Elastocaloric effect in CuAlZn and CuAlMn shape memory alloys under compression. *Philos. Trans. R. Soc. London Ser. A* **374**, 20150309 (2016). doi:10.1098/rsta.2015.0309 Medline

15. Y. Yoshida, K. Yuse, D. Guyomar, J. F. Capsal, G. Sebald, Elastocaloric effect in poly(vinylidene fluoride-trifluoroethylenechlorotrifluoroethylene) terpolymer. *Appl. Phys. Lett.* **108**, 242904 (2016). doi:10.1063/1.4953770

16. I. Takeuchi, K. Sandeman, Solid-state cooling with caloric materials. *Phys. Today* **68**, 48–54 (2015). doi:10.1063/PT.3.3022

17. A. M. G. Carvalho, W. Imamura, E. O. Usuda, N. M. Bom, Giant room-temperature barocaloric effects in PDMS rubber at low pressures. *Eur. Polym. J.* **99**, 212–221 (2018). doi:10.1016/j.eurpolymj.2017.12.007

18. Materials and methods are available as supplementary materials.

19. T. L. Bergman, F. P. Incropera, D. P. DeWitt, A. S. Lavine, *Fundamentals of Heat and Mass Transfer* (Wiley, ed. 7, 2011).

20. S. L. Dart, R. L. Anthony, E. Guth, Rise of temperature on fast stretching of synthetics and natural rubbers. *Ind. Eng. Chem.* **34**, 1340–1342 (1942). doi:10.1021/ie50395a020

21. C. S. Haines, M. D. Lima, N. Li, G. M. Spinks, J. Foroughi, J. D. W. Madden, S. H. Kim, S. Fang, M. Jung de Andrade, F. Göktepe, Ö. Göktepe, S. M. Mirvakili, S. Naficy, X. Lepró, J. Oh, M. E. Kozlov, S. J. Kim, X. Xu, B. J. Swedlove, G. G. Wallace, R. H. Baughman, Artificial muscles from fishing line and sewing thread. *Science* **343**, 868–872 (2014). doi:10.1126/science.1246906 Medline

22. Z. Xie, G. Sebald, D. Guyomar, Temperature dependence of the elastocaloric effect in natural rubber. *Phys. Lett. A* **381**, 2112–2116 (2017). doi:10.1016/j.physleta.2017.02.014

23. R. J. Young, P. B. Bowden, Twinning and martensitic transformations in oriented high-density polyethylene. *Philos. Mag.* **29**, 1061–1073 (1974). doi:10.1080/14786437408226591

24. P. A. T. Olsson, P. Hyldgaard, E. Schröder, E. P. Jutemar, E. Andreasson, M. Kroon, *Ab initio* investigation of monoclinic phase stability and martensitic transformation in crystalline polyethylene. *Phys. Rev. Mater.* **2**, 075602 (2018). doi:10.1103/PhysRevMaterials.2.075602

25. R. Androsch, M. L. Di Lorenzo, C. Schick, B. Wunderlich, Mesophases in polyethylene, polypropylene, and poly(1-butene). *Polymer* **51**, 4639–4662 (2010). doi:10.1016/j.polymer.2010.07.033

26. H. Tadokoro, Structure and properties of crystalline polymers. *Polymer* **25**, 147–164 (1984). doi:10.1016/0032-3861(84)90321-5

27. Y. Jin, B. Wunderlich, Heat capacities of paraffins and polyethylene. *J. Phys. Chem.* **95**, 9000–9007 (1991). doi:10.1021/j100175a105

28. C. T. Ratnam, M. Nasir, A. Baharin, K. Zaman, Electron beam irradiation of epoxidized natural rubber: FTIR studies. *Polym. Int.* **49**, 1693–1701 (2000). doi:10.1002/1097-0126(200012)49:12<1693:AID-PI595>3.0.CO;2-K

29. S. Gunasekaran, R. K. Natarajan, A. Kala, FTIR spectra and mechanical strength analysis of some selected rubber derivatives. *Spectrochim. Acta A Mol. Biomol. Spectrosc.* **68**, 323–330 (2007). doi:10.1016/j.saa.2006.11.039 Medline

30. N. Candau, L. Chazeau, J.-M. Chenal, C. Gauthier, J. Ferreira, E. Munch, D. Thiaudière, Strain induced crystallization and melting of natural rubber during dynamic cycles. *Phys. Chem. Chem. Phys.* **17**, 15331–15338 (2015). doi:10.1039/C5CP00384A Medline

31. R. Kirschbaum, J. L. J. van Dingenen, "Advances in gel-spinning technology and Dyneema fiber applications" in *Integration of Fundamental Polymer Science and Technology—3*, P. Lemstra, L. A. Kleintjens, Eds. (Springer, 1989), pp. 178–198.

32. S. Plimpton, Fast parallel algorithms for short-range molecular dynamics. *J. Comput. Phys.* **117**, 1–19 (1995). doi:10.1006/jcph.1995.1039

33. P. M. Piaggi, M. Parrinello, Entropy based fingerprint for local crystalline order. *J. Chem. Phys.* **147**, 114112 (2017). doi:10.1063/1.4998408 Medline

34. D. Hands, F. Horsfall, The thermal diffusivity and conductivity of natural rubber compounds. *Rubber Chem. Technol.* **50**, 253–265 (1977). doi:10.5254/1.3535140

35. U. Gaur, B. Wunderlich, Heat capacity and other thermodynamic properties of linear macromolecules. IV. Polypropylene. *J. Phys. Chem. Ref. Data* **10**, 1051–1064 (1981). doi:10.1063/1.555650

36. C. Zanotti, P. Giuliani, G. Riva, A. Tuissi, A. Chrysanthou, Thermal diffusivity of Ni-Ti SMAs. *J. Alloys Compd.* **473**, 231–237 (2009). doi:10.1016/j.jallcom.2008.05.040

37. L. Mañosa, A. Planes, Materials with giant mechanocaloric effects: Cooling by strength. *Adv. Mater.* **29**, 1603607 (2017). doi:10.1002/adma.201603607 Medline

38. J. Quarini, A. Prince, Solid state refrigeration: Cooling and refrigeration using crystalline phase changes in metal alloys. *Proc. Inst. Mech. Eng. C. J. Mech. Eng. Sci.* **218**, 1175–1179 (2004). doi:10.1243/0954406042369062

39. E. A. Pieczyska, S. P. Gadaj, W. K. Nowacki, H. Tobushi, Phase-transformation fronts evolution for stress-and strain-controlled tension tests in TiNi shape memory alloy. *Exp. Mech.* **46**, 531–542 (2006). doi:10.1007/s11340-006-8351-y

40. H. Ossmer, C. Chluba, B. Krevet, E. Quandt, M. Rohde, M. Kohl, Elastocaloric cooling using shape memory alloy films. *J. Phys. Conf. Ser.* **476**, 012138 (2013). doi:10.1088/1742-6596/476/1/012138

41. J. Tušek, K. Engelbrecht, N. Pryds, Elastocaloric effect of a Ni-Ti plate to be applied in a regenerator-based cooling device. *Sci. Technol. Built Environ.* **22**, 489–499 (2016). doi:10.1080/23744731.2016.1176809